CONTENTS

		Page	
1.0	SUMMARY	1	1/A6
2.0	INTRODUCTION	3	1/A8
3.0	SYMBOLS	5	1/A10
4.0	DISCUSSION	9	1/A14
	4.1 Skin Friction Drag	12	1/B4
	4.2 Far-Field Wave Drag	13	1/B5
	4.3 Near-Field Wave Drag	15	1/B7
	4.4 Drag-Due-to-Lift	34	1/D3
5.0	INTERACTIVE GRAPHICS	83	2/A7
	APPENDIX (General Slender Body Theory)	85	2/A10
	REFERENCES	97	2/B8

JAN 2 1 1981

NAS 1.26:3351

NASA Contractor Report 3351

ORIGINAL

COMPLETED

A System for Aerodynamic Design and Analysis of Supersonic Aircraft

Part 1 - General Description and Theoretical Development

W. D. Middleton and J. L. Lundry

CONTRACT NAS1-15534
DECEMBER 1980

NASA

NASA Contractor Report 3351

A System for Aerodynamic Design and Analysis of Supersonic Aircraft

Part 1 - General Description and Theoretical Development

W. D. Middleton and J. L. Lundry
Boeing Commercial Airplane Company
Seattle, Washington

Prepared for
Langley Research Center
under Contract NAS1-15534

National Aeronautics
and Space Administration

**Scientific and Technical
Information Branch**

1980

CONTENTS

		Page
1.0	SUMMARY	1
2.0	INTRODUCTION	3
3.0	SYMBOLS	5
4.0	DISCUSSION	9
	4.1 Skin Friction Drag	12
	4.2 Far-Field Wave Drag	13
	4.3 Near-Field Wave Drag	15
	4.4 Drag-Due-to-Lift	34
5.0	INTERACTIVE GRAPHICS	83
	APPENDIX (General Slender Body Theory)	85
	REFERENCES	97

1.0 SUMMARY

An improved integrated system of computer programs has been developed for the design and analysis of supersonic configurations. The system uses linearized theory methods for the calculation of surface pressures and supersonic area rule concepts in combination with linearized theory for calculation of aerodynamic force coefficients. Interactive graphics are optional at the user's request.

The integrated system consists of an executive driver and eight basic computer programs including a geometry input module, which are used to build up the force coefficients of a selected configuration.

The description of the design and analysis system is covered in four separate documents with the following subtitles:

Part 1 - General Description and Theoretical Development (CR-3351)
Part 2 - User's Manual (CR-3352)
Part 3 - Computer Program Description (CR-3353)
Part 4 - Test Cases (CR-3354).

These documents supersede NASA Contractor Reports CR-2715, CR-2716, and CR-2717, which described an earlier version of the system.

This document (Part 1) presents a general description of the system and describes the theoretical methods used.

BLANK PAGE

BLANK PAGE

2.0 INTRODUCTION

Over a period of years, NASA-Langley has developed a basic computerized series of supersonic design and analysis methods for aerodynamic configuration studies (reference 1). The methods are characterized by their reliability in use and input simplicity.

The Boeing Company has extended this basic series of methods and combined them into an integrated system of computer programs. The extensions to the methods provide several new features:

- Addition of a near-field (thickness pressure) wave drag program, to complement the existing supersonic area rule program.
- Improved modeling of fuselage in lifting surface design and analysis programs.
- Addition of configuration-dependent loadings in the wing design program, so that the wing design is performed in the presence of fuselage and nacelle effects.
- Addition of pressure limiting terms in the lifting pressure programs, to constrain the linear theory solution.
- Optional CRT displays of selected program input and output data and provisions for limited user editing and intervention.

A plot module is included in the system to produce configuration drawings, and a common geometry module is used to permit a single geometry input for all programs. A wing pressure module permits summaries of wing pressures at desired conditions.

The basis of the system is supersonic linearized theory, modified in two respects:

- The "Whitham" correction to disturbance positioning is used in the propagation of body pressure fields.
- The wing lifting pressure modules contain an optional limiting pressure feature to control the permissible level of upper surface pressure coefficient. In addition, the wing design module contains a further constraint feature to limit the upper surface streamwise pressure gradient.

Superposition is used to build up the theoretical force coefficients of a selected configuration.

The goals of the integrated system have been to develop an easily used supersonic design and analysis capability, with recognition of the need for

constraints on linear theory methods to provide physical realism, and with inclusion of interactive display for increased design control over optimization cycles.

The description of the design and analysis system is broken into four documents:

Part 1 - General Description and Theoretical Development (CR-3351)
Part 2 - User's Manual (CR-3352)
Part 3 - Computer Program Description (CR-3353)
Part 4 - Test Cases (CR-3354).

This report (Part 1) presents a general description of the system and the theoretical methods used.

These four documents supersede NASA contractor reports CR-2715, CR-2716, and CR-2717, which described an earlier version of the system.

3.0 SYMBOLS

A	element fraction
A_i	load strength factor
$A(x)$	cross-sectional area at x
B	trailing-edge element fraction
$\bar{c}$	pitching moment reference length
C	wing tip element fraction
c	chord
c_a	section axial force coefficient
c_d	section drag coefficient
C_D	drag coefficient, D/qS
$C_{D_{Sym}}$	minimum drag coefficient
C_F	skin friction coefficient
c_l	section lift coefficient
C_L	lift coefficient, lift/qS
C_{L_α}	lift coefficient per degree angle of attack
C_m	pitching moment coefficient, pitching moment/qS$\bar{c}$
C_{mo}	pitching moment coefficient at zero lift
c_n	section normal force coefficient
C_p	local pressure coefficient, $(p - p_\infty)/q_\infty$
$C_{p,\ lim}$	limiting pressure coefficient used in definition of attainable thrust

ΔC_p	lifting pressure coefficient (lower surface pressure coefficient minus upper surface pressure coefficient)
$\Delta C_p \sqrt{x'}$	leading-edge singularity parameter
$(\Delta C_p \sqrt{x'})_o$	limiting value of leading edge singularity parameter at $x' = 0$
c_t	section thrust coefficient
c_t^*	attainable section thrust coefficient
C_T	theoretical wing thrust coefficient
D	drag force
F(y)	Whitham function
h(Z)	decay function for F(y) calculation
k	Mach number parameter
K_1, K_2, K_3	constants used in curve-fitting
K_T	attainable thrust factor, c_t^*/c_t
L	grid element variable in x (lengthwise) direction
M	Mach number
N	grid element variable in spanwise direction
p	pressure
p_∞	freestream static pressure
q	dynamic pressure, $0.7\ p_\infty M^2$
R	body radius
$\bar{R}$	influence function
r	radial distance to point in flow field
S	reference area or cross-sectional area (figure 4.3-3)

T	temperature
t	variable of integration (figure 4.3-4)
U	freestream velocity
u	x perturbation velocity
v	y perturbation velocity
V	freestream velocity vector
W(Z)	body pressure decay function
w	upwash, w perturbation velocity
x	lengthwise variable
x'	distance behind local wing leading edge
y	span station or distance variable
z	vertical variable
Z	decay function parameter
α	angle of attack
ϵ	local fuselage camber angle
β	Mach number parameter = $\sqrt{M^2 - 1}$
ξ	x variable of integration
λ	surface shape (equation 13) or Lagrange multiplier (figure 4.4-4)
η	spanwise variable of integration or semispan fraction
ρ	density
Φ	velocity potential
θ	radial angle variable
Λ	leading-edge sweepback angle

δ	angle at a cambered-wing leading edge between tangent to surface and wing reference plane
τ	region of influence
μ	dynamic viscosity coefficient

Subscripts:

∞	freestream conditions
i	incompressible condition (equation (5))
i,j	loading numbers (equation (31))
t	tilted lengthwise variable (figure 4.3-5)

Superscripts:

'	reference temperature condition (equation (2)) or first derivative with respect to x
''	second derivative with respect to x
*	field point grid element

4.0 DISCUSSION

The integrated supersonic design and analysis system is shown schematically in figure 4.0-1. It consists of an executive "driver" and eight basic computer programs. The individual programs, or modules, provide data for configuration design or analysis as follows:

- Skin friction is computed using turbulent flat plate theory.
- Wave drag is calculated from either far-field (supersonic area rule) or near-field (surface pressure integration) methods. The far-field method is used for wave drag coefficient calculations and for fuselage optimization according to area rule concepts. The near-field method is used primarily as an analysis tool, where detailed pressure distributions are of interest.
- Lifting pressures, drag-due-to-lift, pitching moment and trim drag are computed from the lift analysis program, which breaks arbitrary wing/fuselage/ canard/nacelles/horizontal tail configurations into a mosaic of "Mach-box" rectilinear elements which are employed in linear theory solutions. A complementary wing design and optimization program solves for the wing shape required to support an optimized pressure distribution at a specified flight condition.
- The plot module draws configuration pictures according to size and view inputs.
- The geometry module handles configuration geometry for the system.
- The wing pressure module summarizes and tabulates wing surface pressure data for input conditions.
- Interactive graphics, for data display or editing, are optional in the system at user's request.

Operating in the analysis mode, the force coefficients of a selected configuration are built up through superposition as shown in figure 4.0-2.

The entire design and analysis system is a single overlaid program. The executive level of the system controls module execution by means of special identification cards in the input data. Transfer of data in the system between modules is handled by disk storage and common blocks.

All configuration geometry is read (or updated) in the geometry module. Geometry inputs are patterned after those of the NASA- LRC configuration plotting program. All "paneling" of the configuration for theoretical analyses is accomplished within the programs, and the user prepares only "drawing-type" geometry.

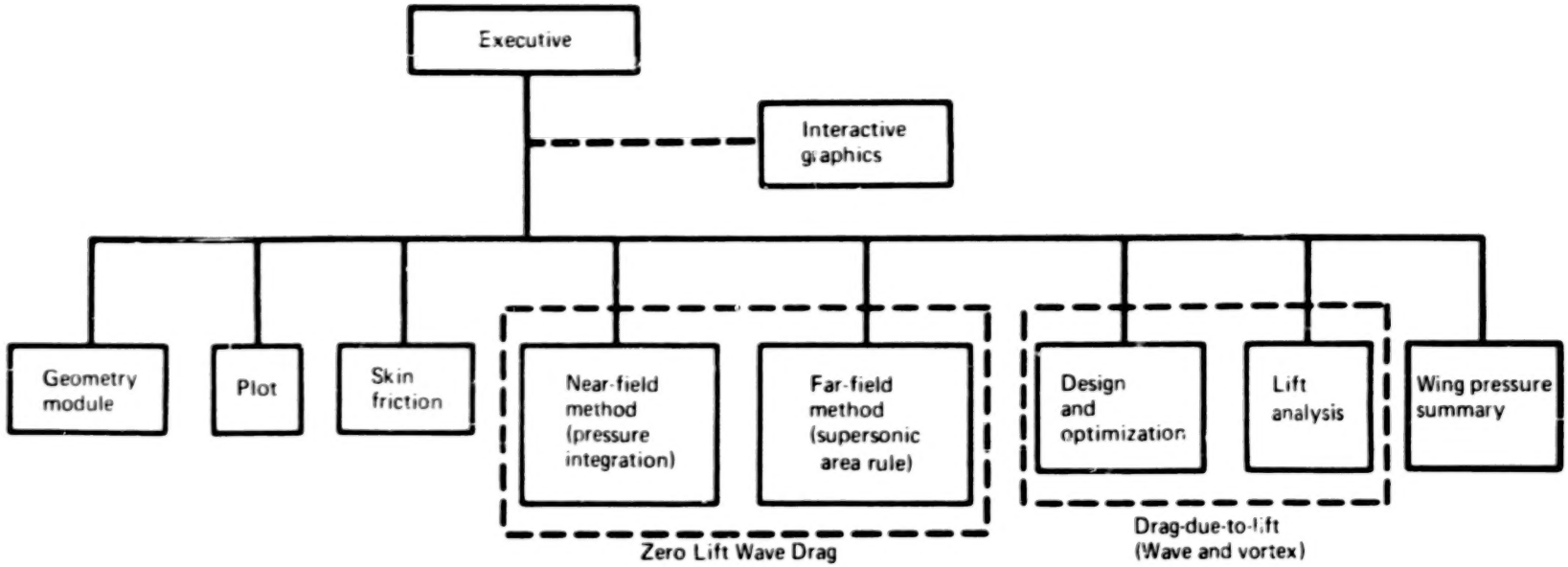

FIGURE 4.0-1.—INTEGRATED SUPERSONIC DESIGN AND ANALYSIS SYSTEM

SUPERPOSITION METHOD OF DRAG ANALYSIS

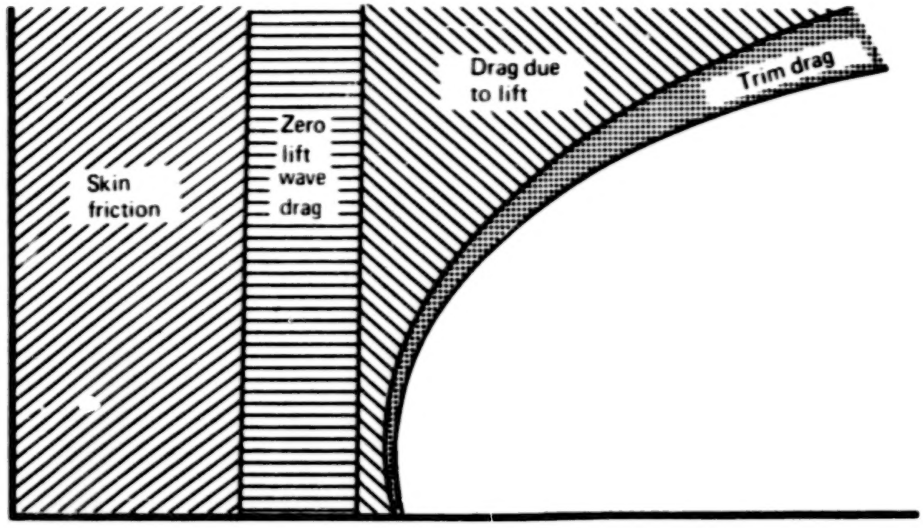

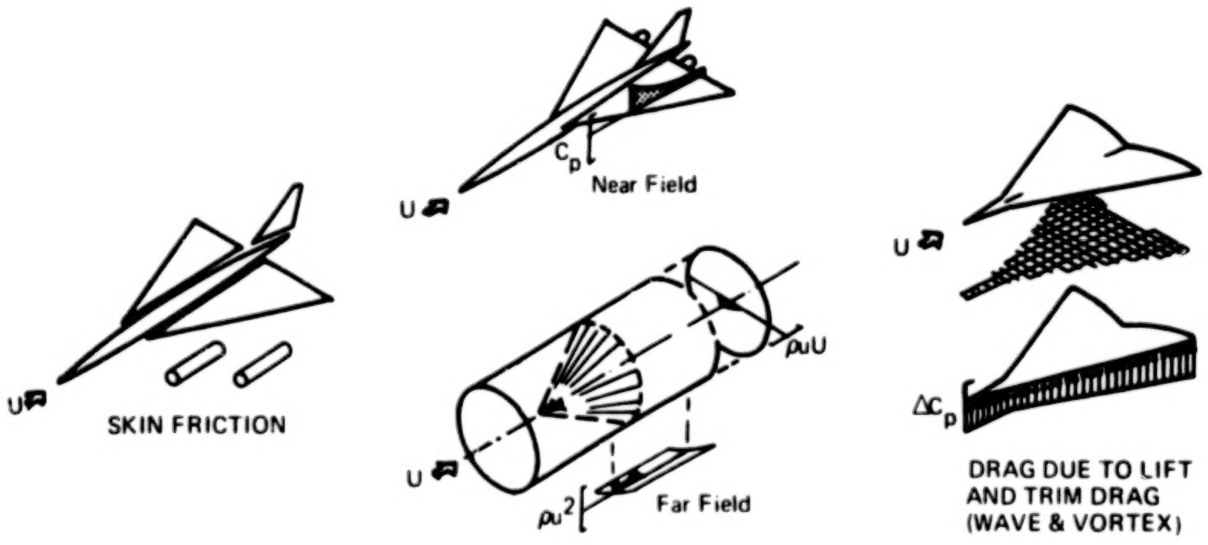

FIGURE 4.0-2. – DRAG BUILDUP

Additional data on system structure and input and output formats are presented in Parts 2, 3, and 4. The theoretical methods used in the modules are in the remainder of this document.

4.1 Skin Friction Drag

The skin friction drag of an arbitrary configuration is calculated from the T' method of reference 2. Smooth flat-plate, adiabatic-wall, and turbulent boundary layer conditions are assumed, with transition assumed to occur at the leading edge of each configuration component.

The theory and experimental verification of the T' method are given in detail in reference 2. The essential elements of the method are presented in Appendix C of the reference, and are summarized here for completeness.

The T' method is based on the calculation of a compressible skin friction coefficient, C_F, from a reference skin friction coefficient, C'_F, for a selected Mach number, M_∞, Reynolds number, R_∞, and adiabatic wall temperature, T_W. (The subscript ∞ is used throughout to denote free stream conditions).

The wall temperature ratio, T_W/T_∞, is calculated from one-dimensional relationships assuming a wall recovery factor of .89.

$$\frac{T_W}{T_\infty} = 1 + 0.178\, M_\infty^2 \tag{1}$$

The prime superscript (T', R', etc.,) refers to conditions at which incompressible flow relations must be evaluated in order to represent compressible flow. Sommer and Short in reference 2 obtained the key relationship

$$\frac{T'}{T_\infty} = 1 + 0.035\, M_\infty^2 + 0.45\left(\frac{T_W}{T_\infty} - 1\right) \tag{2}$$

The Reynolds number relationship is

$$\frac{R'}{R_\infty} = \frac{1}{\left(\frac{T'}{T_\infty}\right)\left(\frac{\mu'}{\mu_\infty}\right)} \tag{3}$$

where the viscosity ratio is given by the Sutherland equation

$$\frac{\mu'}{\mu_\infty} = \left(\frac{T'}{T_\infty}\right)^{1.5} \left(\frac{T_\infty + 216}{T' + 216}\right) \tag{4}$$

with T in degrees Rankine.

The incompressible skin friction coefficient is given by the Karman-Schoenherr

equation

$$\frac{0.242}{\sqrt{C_{F_i}}} = \log_{10}\left(C_{F_i} R_i\right) \tag{5}$$

which gives the corresponding relationship based on the T' analogy:

$$\frac{0.242}{\sqrt{C_F'}} = \log_{10}\left(C_F' R'\right) \tag{6}$$

This equation is solved iteratively for C_F'. The desired compressible skin friction coefficient is obtained from C_F' by

$$C_F = C_F'\left(T_\infty/T'\right) \tag{7}$$

Most of the skin friction program is involved with computing wetted areas and reference lengths for the configuration. Components which may exhibit large variations in reference length (such as the wing, tail, canard etc.) are broken into strips in order to calculate C_F accurately.

4.2 Far-Field Wave Drag

The far-field wave drag program computes the zero lift wave drag of an arbitrary configuration by means of the supersonic area rule. A description of the program has been given in reference 3, and is summarized here. The method assumes not only an integrated total lift of zero, but local lift everywhere zero, and thus includes none of the wave drag contribution associated with the generation of lift.

The supersonic area rule is a generalization of the transonic area rule, which states that the transonic wave drag of an aircraft is essentially the same as the wave drag of an equivalent body of revolution having the same cross-sectional area distribution. In the supersonic area rule procedure, several equivalent bodies of revolution are produced by passing a series of parallel cutting planes through the configuration, as shown below.

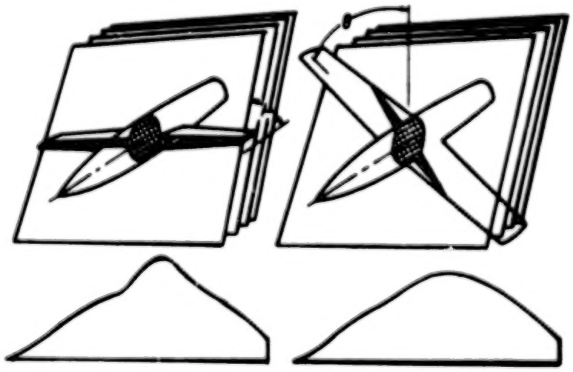

The cutting planes are inclined with respect to the aircraft axis at the Mach angle μ , and a single equivalent body is produced for the series of cutting planes at a constant azimuthal angle, θ. The area of the equivalent body at each station is the projection of the area intercepted by the cutting plane onto a plane normal to the aircraft axis.

The wave drag of each equivalent body is calculated from the Von Kármán slender-body formula (reference 4), which gives the drag as a function of the free stream conditions and equivalent-body area distribution.

$$D(\theta) = -\frac{\rho U_\infty^2}{4\pi} \int_0^\ell \int_0^\ell A''(x_1)\, A''(x_2) \log |x_1 - x_2|\, dx_1\, dx_2 \tag{8}$$

where x_1 and x_2 are lengthwise variables of integration and
A" is the second derivative of the body area distribution.

The wave drag of the aircraft at a given Mach number is calculated from the integrated average of the equivalent-body wave drags.

$$D = \frac{1}{2\pi} \int_0^{2\pi} D(\theta)\, d\theta \tag{9}$$

A useful feature of the supersonic area rule occurs in the optimization of a fuselage area distribution to minimize the wave drag of a wing-fuselage combination. According to Sheppard (reference 5), the wave drag of a wing-fuselage can be written as:

$$\frac{D}{q} = \left(\frac{D}{q}\right)_{\text{wing}} + \left(\frac{D}{q}\right)_{\substack{\text{wing eq. body} \\ \text{+ body}}} - \left(\frac{D}{q}\right)_{\substack{\text{wing eq.} \\ \text{body}}} \tag{10}$$

where the wing equivalent body is a body of revolution obtained by averaging from $\theta = 0$ to 2π all the projected areas intercepted by cutting planes passing through the wing for each X station.

Considering a wing-fuselage, then, and assuming that the wing geometry is fixed, both the first and third terms of equation (10) are fixed. This leaves optimization of the second term only, so that to design the minimum drag configuration, the fuselage must be contoured to produce a wing-equivalent-body-plus-fuselage having the shape of a minimum drag body of revolution.

The wave drag program uses the Eminton-Lord fairing through a discrete set of points, which defines the shape of a minimum drag body through the points.

Using this fairing, and identifying a few "control-points" on the fuselage area definition, an optimized fuselage area definition may be obtained as the difference between the wing equivalent body and the combined wing-equivalent -body-plus-fuselage.

The wave drag program has mechanized this solution, and also includes the effects of nacelles, tail, etc., which are included similarly. The shape of the minimum drag fuselage area distribution, and the drag of the complete configuration including the minimum drag fuselage, may be calculated for each configuration input.

Because of the configuration generality that can be handled, the far-field program is the primary source of zero-lift wave drag coefficients in the design and analysis system. A complementary near-field program, more restricted in scope but which computes detailed thickness pressures, is described in the following section.

4.3 Near-Field Wave Drag

Isolated Component Pressures

The near-field wave drag program computes zero-lift thickness pressure distributions for wing-body-nacelle-empennage configurations in supersonic flow. The pressure distributions are integrated over the cross-sectional areas of the configuration to obtain the resultant drag force. Three basic calculations are performed to obtain the required pressure fields:

- Thickness pressure distribution for a wing or tail of arbitrary section and planform.
- Thickness pressure distribution on surface of fuselage or nacelles.
- "Whitham" near-field calculations to define pressure distributions propagating from fuselage or nacelles.

Superposition is used to calculate the interference drag terms associated with the pressure field of a given component acting on the surfaces of the other components.

The surface pressure distributions calculated include some (from the nacelles) which contribute lift due to a non-symmetrical distribution of volume, so that the drag calculations which include these loadings contain wave drag due to lift contributions. However, by selection of program options and subtraction of certain drag contributions, a zero lift wave drag comparable to the far-field wave drag value may be obtained, as described on page 34.

Wing or empennage thickness pressures. - The surface pressure coefficient on the upper (or lower) surface of a flat mean-line wing of symmetrical surface shape is obtained by first calculating the corresponding velocity potential, differentiating with respect to x (to get u), and then computing the pressure coefficient from the linear theory approximation, $C_p = -2u/U_\infty$.

The velocity potential computation, from reference 13, is

$$\phi(x,y) = -\frac{1}{\pi}\iint_{\tau}\frac{\lambda\, d\eta\, d\xi}{\sqrt{(x-\xi)^2 - \beta^2(y-\eta)^2}} \qquad (11)$$

where $\phi(x,y)$ = velocity potential at a defined wing field point (x,y)
λ = surface slope (dz/dx) of wing section at a wing integration point
β = $\sqrt{M^2 - 1}$
ξ = x variable of integration
η = y variable of integration
τ = subscript denoting interval of integration (surface of the wing planform within the Mach forecone from x,y)

The wing thickness pressure coefficient is

$$C_p(x,y) = \frac{p-p_\infty}{q_\infty} = -2\,\frac{u}{U_\infty} = -2\,\frac{\partial\phi(x,y)}{\partial x} \qquad (12)$$

where p = local pressure at x,y
p_∞ = free stream static pressure
u_∞ = x perturbation velocity
U_∞, q_∞ = free stream velocity and dynamic pressure

Integration of the velocity potential equation is performed by representing the wing as a grid of rectangular elements, and substituting a numerical summation for the integration. The wing element "Mach-box" system exactly follows the arrangement described in Section 4.4 (for the lifting pressure case) and is summarized in figure 4.3-1. The grid elements, identified by L and N, are defined such that L is numerically equal to x and N is numerically equal to βy, where x and βy take on only integer values. Partial grid elements along the wing leading and trailing edges are used to permit a closer approximation to the actual wing planform. The grid system of figure 4.3-1 is rather coarse for illustrative purposes; in actual usage, many more grid elements are employed.

With respect to a specified field point x,y, the upstream region of influence τ is approximated by the shaded grid elements in figure 4.3-1. Each of the shaded elements has associated with it an influence factor, $\bar{R}$, which relates the effect of the element and its surface slope to the total velocity potential at the field point.

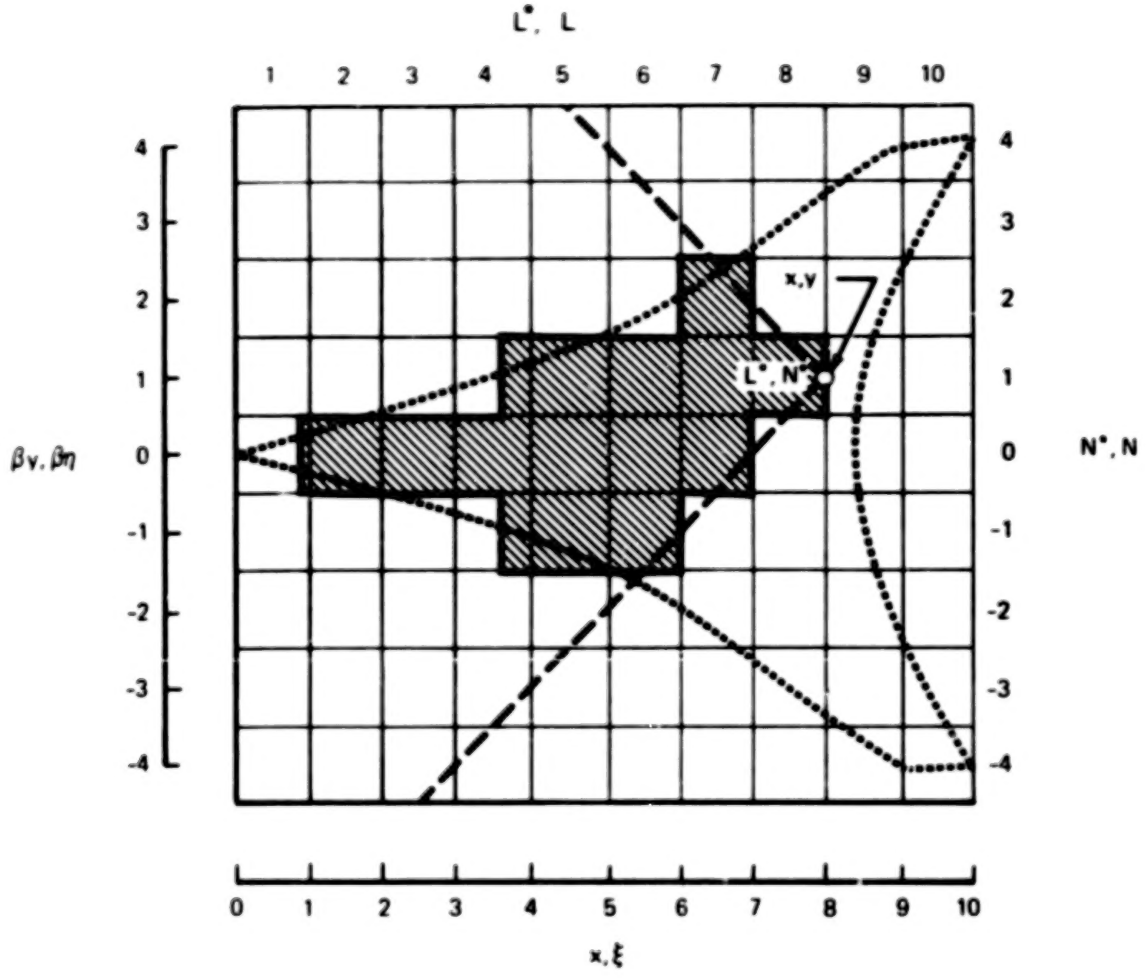

FIGURE 4.3-1.–WING COORDINATE SYSTEM

The factor $\bar{R}$ is obtained by an approximate solution to Equation (11) as follows:

Let $y-\eta = u$ so that $du = -d\eta$

$$\phi(x,y) = \frac{1}{\pi}\iint_{\tau}\frac{\lambda\, du\, d\xi}{\sqrt{(x-\xi)^2 - \beta^2 u^2}} \tag{13}$$

Substituting an average value of $(x-\xi) = (x-\xi)$ and integrating with respect to u,

$$\phi(x,y) = \frac{1}{\pi}\left[\frac{\lambda}{\beta}\sin^{-1}\frac{\beta u}{(\overline{x-\xi})}\right]_{u_1}^{u_2} \tag{14}$$

Restoring $y - \eta = u$

$$\phi(x,y) = \frac{1}{\pi\beta}\left[\lambda \sin^{-1}\frac{\beta(y-\eta)}{(\overline{x-\xi})}\right]_{\eta_1}^{\eta_2} \tag{15}$$

For a given grid element in the Mach forecone, the integration interval η_1 to η_2 gives

$$\beta(v-\eta_1) = N^* - N + 0.5$$
$$\beta(v-\eta_2) = N^* - N - 0.5$$

Also, $\overline{X-\xi} = L^* - L + .05$

L^* and N^* define the field point grid element and L and N define an element in the forecone. The numerical summation then becomes

$$\phi(x,y) = \frac{1}{\pi\beta}\sum_{\tau}\lambda_{L,N}\left[\sin^{-1}\frac{N^* - N - 0.5}{L^* - L + 0.5} - \sin^{-1}\frac{N^* - N + 0.5}{L^* - L + 0.5}\right] \tag{16}$$

with $\bar{R}$ being the quantity between the brackets for the element (L,N).

The character of the R function is such that the sum of $\bar{R}$ for all elements across the Mach forecone at a constant L value is equal to $-\pi$. In considering the case of an infinite rectangular wing of constant thickness shape (wedge section), it is seen that the $-\pi$ summation must be the case, since the ϕ function for successive L^* rows is increased by

$$\frac{\lambda}{\pi\beta}\left[\Sigma\bar{R}\right]_{L=\text{const.}}$$

so that

$$\frac{\Delta\phi}{\Delta x} = \frac{\lambda}{\pi\beta}(-\pi) = -\frac{\lambda}{\beta}$$

and

$$C_p = -2\frac{\Delta\phi}{\Delta x} = 2\frac{\lambda}{\beta}$$

which is the established linear theory result. Values of $\bar{R}$ within the Mach forecone from a typical field element are presented in figure 4.3-2.

The computer program for the wing thickness pressure calculations sets up the wing grid system, defines the surface slope λ for each grid element, performs the summation for ϕ at selected field elements, and differentiates ϕ numerically to obtain C_p. Wave drag is obtained by summing the pressure coefficients times the corresponding surface slopes of the wing.

In the wing surface slope definition, slopes of the elements occupying space covered by the fuselage (if there is one) are set equal to zero to eliminate their drag contribution. Partial elements are used at the wing-body intersection to improve the geometry definition.

As was found to be the case in lifting surface programs involving the grid system used in the wing calculations, some oscillation in computed pressure coefficient values occurs. This has been suppressed by a smoothing of the calculated pressure coefficient values, using a 5 term equation of the form;

$$C_p = \frac{.333\,A_{L^*-2}\,C_{P_{L^*-2}} + .667\,A_{L^*-1}\,C_{P_{L^*-1}} + A_{L^*}C_{P_{L^*}} + .667\,C_{P_{L^*+1}} + .333\,C_{P_{L^*+2}}}{.333\,A_{L^*-2} + .667\,A_{L^*-1} + A_{L^*} + 1.0} \quad (17)$$

where A = factor defining size of associated element (1 if whole element, fraction if not).

Fuselage and nacelle thickness pressures. - The pressure distribution on the surface of fuselage or nacelles is obtained from a method developed at the Boeing Company by R. M. Kulfan, based on the Lighthill theory of reference 6. The method is applicable to bodies having either smooth area distributions or bodies with slope discontinuities. As used in the near-field program, smooth area distributions are assumed except (if required) at the nose or aft end of the body. Open-nose bodies, such as nacelles, are permissible.

The solution technique is summarized in figure 4.3-3. An axial perturbation velocity is calculated which is a function of the body cross-sectional area

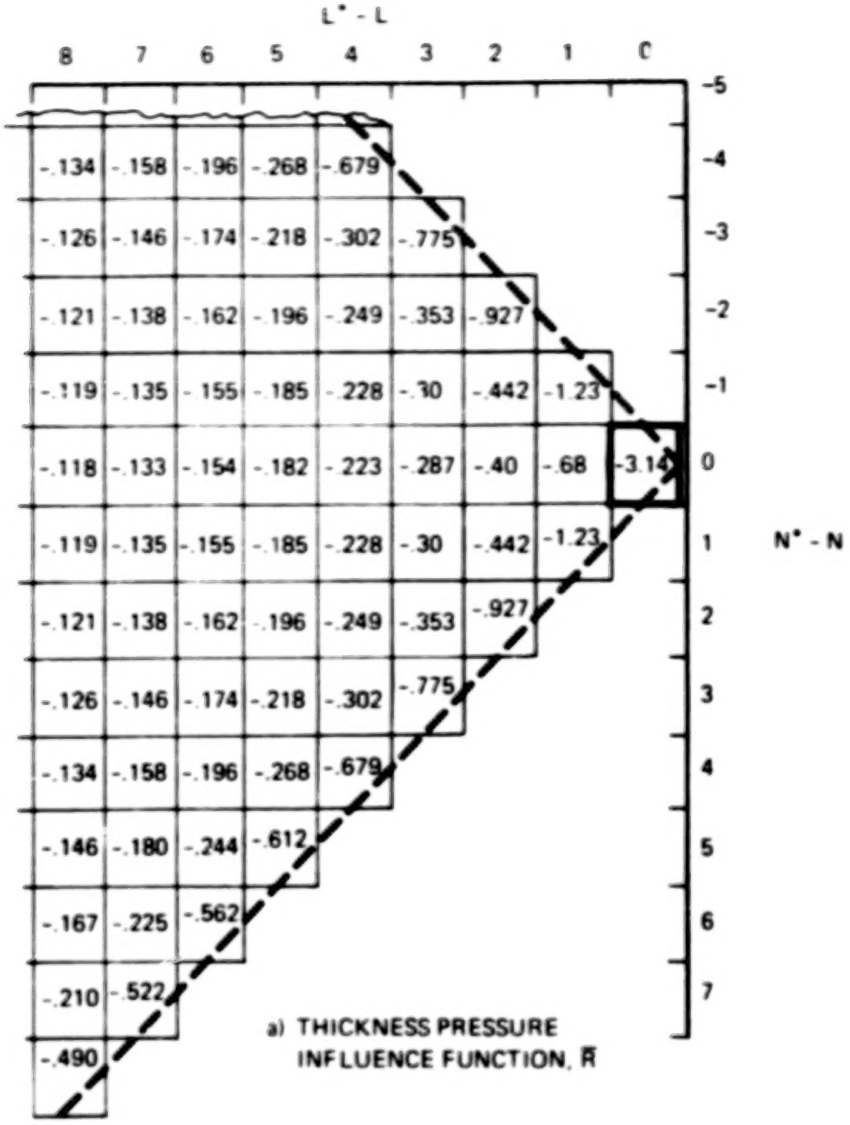

a) THICKNESS PRESSURE INFLUENCE FUNCTION, $\bar{R}$

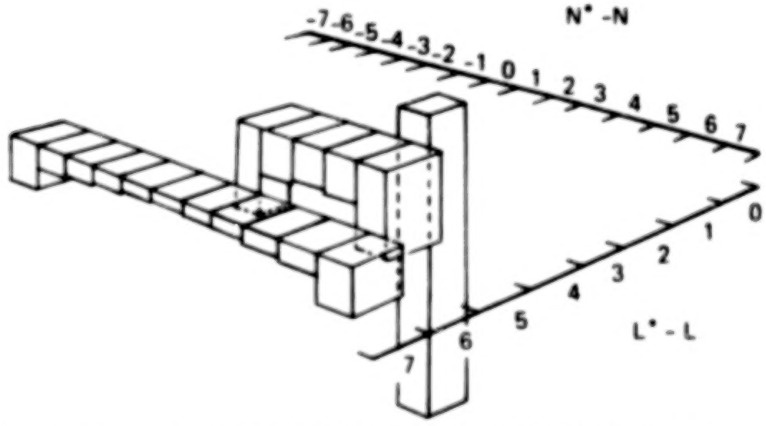

b) REPRESENTATIVE INFLUENCE FACTOR CHARACTERISTICS

FIGURE 4.3-2.–THICKNESS PRESSURE INFLUENCE FUNCTION

growth (and radius distribution) and a decay function which relates area growth to its effect on a given field point.

The axial perturbation velocity, u, is given by

$$u(x) = -\frac{1}{2\pi}\int_{o}^{x} \frac{W(Z)}{\beta R_{(\xi)}}\, d S'_{(\xi)} \tag{18}$$

where

x = body field station
$W(Z)$ = decay function
ξ = x variable of integration
Z = position function = $\frac{x-\xi}{\beta R_{(\xi)}}$
$R_{(\xi)}$ = body radius at ξ
$S'_{(\xi)}$ = first derivative of body cross-sectional area (S) at ξ

The pressure coefficient is calculated from one-dimensional flow relationships (rather than the simpler linear theory approximation), as shown in figure 4.3-3. The decay function, W(Z), is tabulated on page 23.

Fuselage and nacelle flow-field pressures. - The pressure field propagated by the fuselage or nacelles is calculated using the Whitham solution of reference 7. This solution, which is converted to a method amenable to the digital computer in reference 8, calculates shock wave positions and strengths through a modification of linear theory results.

The Whitham solution begins with the calculation of a function, F(y), which is dependent on body geometry:

$$F(y) = \frac{1}{2\pi}\int_{o}^{y_{end}} \left[\frac{2}{\beta R_{(t)}}\right]^{\frac{1}{2}} h(Z)\, d S'_{(t)} \tag{19}$$

where

y = body field station
$h(Z)$ = decay function (similar to body pressure calculation)
t = y variable of integration
Z = t position function
$S'(t)$ = first derivative of body cross-sectional area (S) at t
y_{end} = y at end of integration (see figure 4.3-4).

The solution for F(y) is very much like that of the body thickness pressure solution, with the exception that the integration is carried out to the point (y_{end}) at which the aft-running Mach line from the body centerline at y

BLANK PAGE

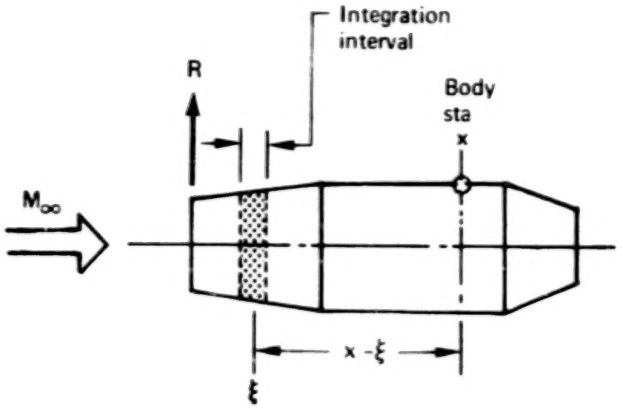

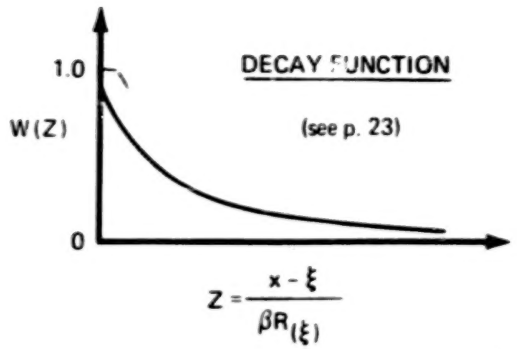

PERTURBATION VELOCITY

$$u(x) = -\frac{1}{2\pi}\int_0^x \frac{W(Z)}{\beta R_{(\xi)}}\, dS'_{(\xi)} \quad , \quad S = \text{cross-sectional area}$$

where

dS' may include dS'_{smooth} and dS' discontinuous

$$u(x) = \Delta u_{(x)_{smooth}} + \Sigma\ \Delta u_{(x)_{disc}}$$

$$u(x)_{smooth} = -\frac{1}{2\pi}\int_0^x \frac{W(Z)}{\beta R_{(\xi)}}\left[\frac{dS'}{dx}\right] d\xi$$

Where integration excludes ds'_{disc}

$$\Delta u_{i(x)_{disc}} = -\left[\frac{\Delta R'(x_i)}{\beta}\right] W(Z_i)$$

PRESSURE COEFFICIENT

$$C_p(x) \quad \frac{1}{0.7\, M_\infty^2}\left\{\left[1.0 - 0.2\, M_\infty^2\left(\left(1.0 + R'_{(x)}{}^2\right)\left(1.0 + u_{(x)}\right)^2 - 1.0\right)\right]^{3.5} - 1.0\right\}$$

FIGURE 4.3-3.–BODY SURFACE PRESSURES (LIGHTHILL THEORY)

DECAY FUNCTION

For body surface pressures. $Z = \frac{x - \xi}{\beta R_{(\xi)}}$, see fig. 4.3-3.

Z	W(Z)
0	1.0
.1	.9518
.2	.907
.3	.8653
.4	.8265
.5	.7902
.6	.7562
.7	.7244
.8	.6946
.9	.6666
1.0	.6403
1.2	.5923
1.4	.5496
1.6	.5115
1.8	.4774
2.0	.4467
2.4	.3941
2.8	.3508
3.2	.3148
3.6	.2846
4.0	.2591
4.8	.2184
5.4	.1947
6.0	.1753
7.0	.1499
8.0	.1307
9.0	.1157
10.	.1037
12.	.0858
14.	.0731
16.	.0637
18.	.0564
20.	.0507
> 20.	$1.0/\sqrt{1.0+Z^2}$

emerges from the body contour. The F(y) calculation is summarized in figure 4.3- 4, and the decay function h(Z) is tabulated on page 27.

Development of the near-field pressure signature at a radial distance (r) from the body centerline is summarized in figure 4.3-5. The F(y) function is tilted, as shown, by displacing the F(y) function according to

$$\Delta y = k\sqrt{r}\, F(y) \tag{20}$$

where

$$k = \frac{1.6973\, M^4}{\beta^{1.5}}$$

This process results in a double-valued pressure signature where shock waves are present, a situation which is corrected by an area-balancing technique. The area-balancing (shaded lobes are equal in area) defines shock wave locations and strengths. The resultant tilted/area-balanced signature is then converted to pressure coefficient by

$$C_p = \frac{p - p_\infty}{q_\infty} = \frac{2\, F(y)}{\sqrt{2\beta r}} \tag{21}$$

The position of the pressure signature at radius (r) is then given by

$$x = y_t + \beta r \tag{22}$$

where x is the longitudinal distance from the body nose. The "tilting" thus produces a correction in pressure signature positioning, relative to simple translation along a Mach line, which is the result of the remarkable theory of reference 7.

Interference Calculations

The previous sections summarized the basic pressure calculations performed by the near-field wave drag program. Integration of the wing and fuselage or nacelle pressure distributions over their respective surfaces gives the "isolated" wave drags of the components. Interference drags are obtained by superposition, i.e., the pressure field of each component is imposed upon the surfaces of the other components to calculate the resultant interference forces. Interference terms between empennage surfaces and the rest of the configuration have been considered small, however, and are neglected.

The computer solution allows for up to 3 pairs of nacelles located external to the wing-fuselage (or 2 pairs plus a single nacelle at y = 0). The nacelles may be either above or below the wing (or both).

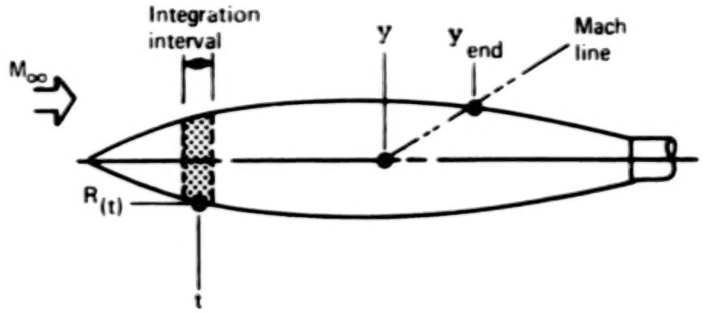

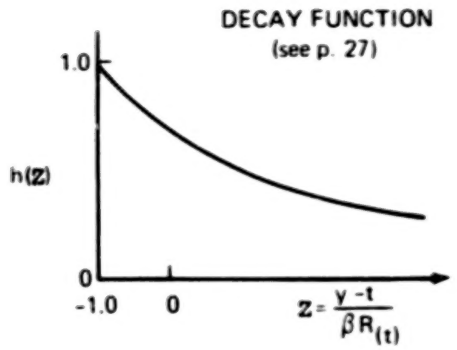

$$F(y) = \frac{1}{2\pi} \int_0^{y_{end}} \left[\frac{2}{\beta R_{(t)}} \right] h(Z)\, dS'_{(t)}$$

S = Cross-sectional area

PRESSURE COEFFICIENT

$$C_p = \frac{p - p_\infty}{q_\infty} = \frac{2F(y)}{\sqrt{2\beta r}}$$

where:

r = radial distance from body

F(y) function displaced, shock waves located as shown in fig. 4.3-5

FIGURE 4.3-4. – WHITHAM F(y) FUNCTION (NEAR-FIELD PRESSURE BASIS)

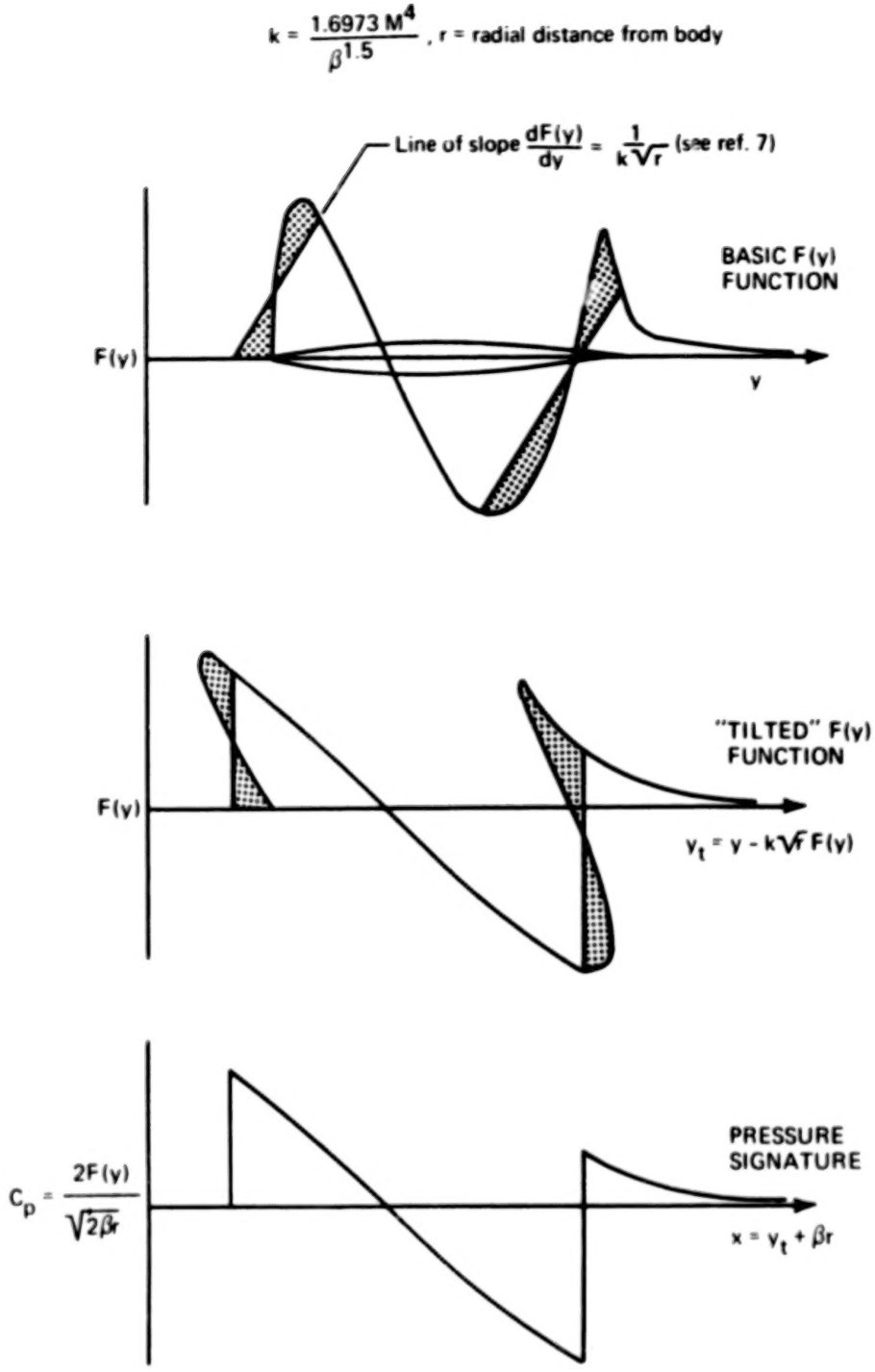
$k = \frac{1.6973\,M^4}{\beta^{1.5}}$, r = radial distance from body
Line of slope $\frac{dF(y)}{dy} = \frac{1}{k\sqrt{r}}$ (see ref. 7)
BASIC F(y) FUNCTION
F(y)
y
"TILTED" F(y) FUNCTION
F(y)
$y_t = y - k\sqrt{r}\,F(y)$
PRESSURE SIGNATURE
$C_p = \frac{2F(y)}{\sqrt{2\beta r}}$
$x = y_t + \beta r$

FIGURE 4.3-5.–DEVELOPMENT OF NEAR-FIELD PRESSURE SIGNATURE

DECAY FUNCTION

For F(y) calculation. $Z = \frac{y - t}{\beta R_{(t)}}$, see fig. 4.3-4.

Z	h(Z)
-1.0	1.0
-.9	.964
-.8	.929
-.7	.897
-.6	.868
-.5	.84
-.4	.814
-.3	.789
-.2	.766
-.1	.742
0	.72
.25	.674
.50	.633
.75	.597
1.0	.565
1.5	.511
2.0	.467
2.5	.431
3.0	.401
3.5	.375
4.0	.353
>4.0	$1.0/\sqrt{2Z}$

Wing-fuselage interference. - Fuselage-on-wing interference is obtained by calculating the near-field pressure signature from the fuselage at selected spanwise stations, and imposing them upon the corresponding wing sections as a buoyancy field. The spanwise stations are the same as those used in the isolated wing thickness pressure calculations.

Wing-on-fuselage interference is obtained from wing thickness pressures computed in the area occupied by the fuselage, after the wing surface slopes in the fuselage area have been set equal to zero. The thickness pressures thus calculated are "carry-over" pressures, and are imposed upon the fuselage surface slopes by transposing them aft along Mach lines to the fuselage. The fuselage area covered by the wing root is deleted from the interference term.

Typical results from wing-body calculations are presented in figure 4.3-6. The wing data, both isolated and fuselage-on-wing interference, are converted to section drag form.

Nacelle interference terms are calculated like the wing-body interference terms, with the provision that two alternative solutions may be specified for the nacelle-on-wing interference term. Available experimental data do not make it clear whether a "wrap" or "glance" solution, as shown in figure 4.3-7, is more correct. Since the nacelle-on-wing interference term is substantial, both solutions are available in the program (controlled by an input code).

The nacelle interference terms are calculated as follows:

Nacelle-on-wing term. - The nacelle pressure field acting on the wing is obtained by calculating nacelle pressure signatures at the same spanwise stations used for the wing thickness pressures (plus extra stations immediately adjacent to the nacelle centerlines), then defining a composite signature by summing the contributions from all nacelles. The nacelle pressure coefficients are doubled to account for reflection from the wing surface.

In the case of nacelles both above and below the wing, separate nacelle pressure fields for nacelles below, and then above, the wing are calculated and then summed.

A unique feature of the near-field approach lies in the solution choices available, since the pressure signatures generated by a nacelle to act on the wing surface may be terminated on encountering another nacelle or may be allowed to pass undiminished around (or through) it. In the first case, the "glance" solution, the nacelle pressure field is assumed to reflect from other nacelles in such a way that the reflected field exerts no further influence upon the wing surface. In the second case, the "wrap" solution, the nacelle pressure field is assumed to propagate around the other nacelles as if no obstruction were offered; i.e., as if they were transparent to the pressure field.

$C_{D_{wing}} = 0.00113$ $C_{D_{wing\text{-}on\text{-}body}} = 0.00008$ $\Sigma C_{D_{wing\text{-}body}} = 0.00153$

$C_{D_{body}} = 0.00032$ $C_{D_{body\text{-}on\text{-}wing}} = -.000003$

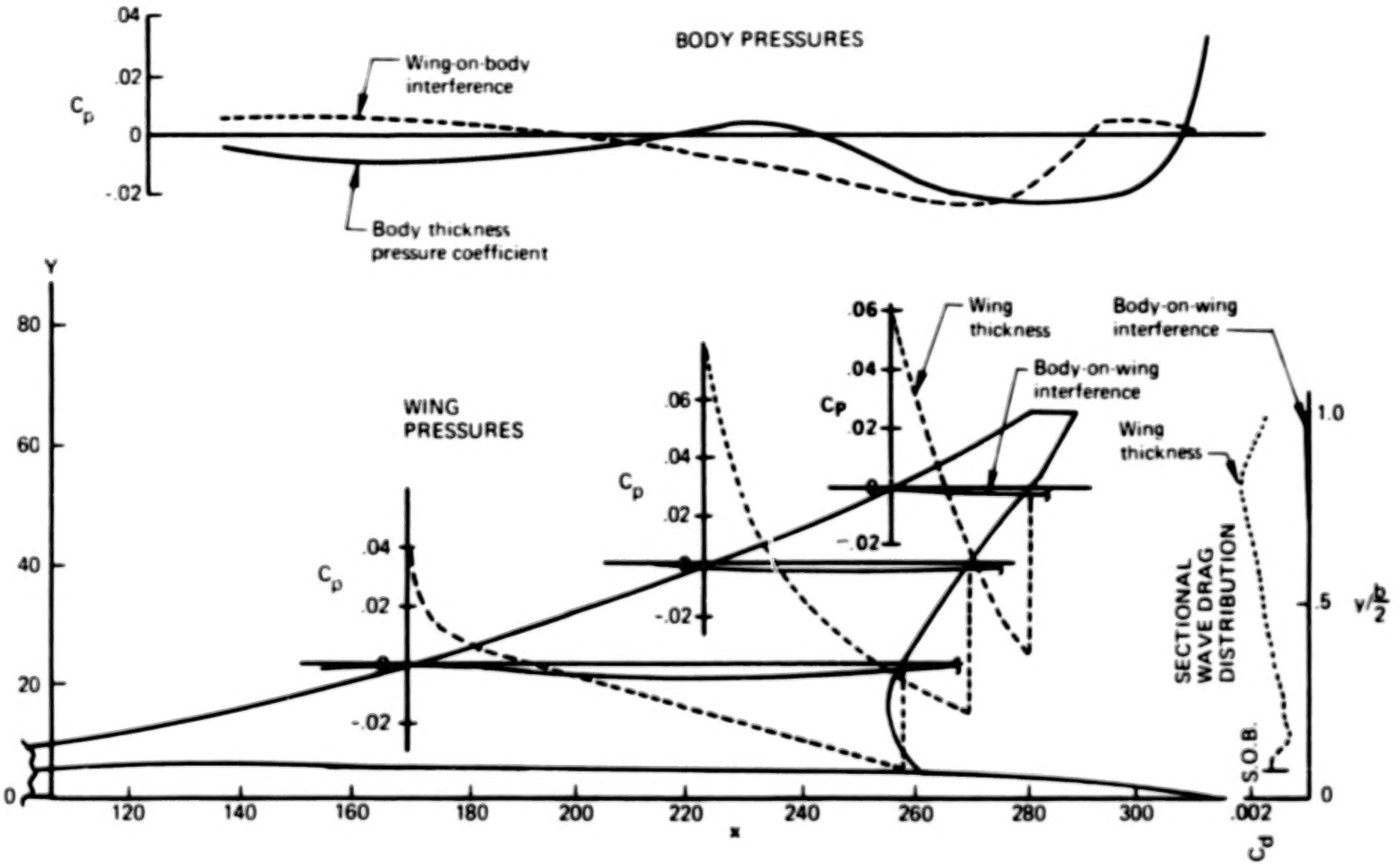

FIGURE 4.3-6.– WING-BODY SOLUTION, M = 2.6

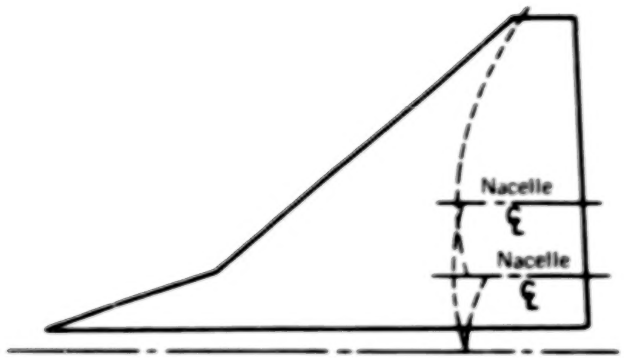

PRESSURES "GLANCE" AWAY FROM WING AT ADJACENT NACELLES

The nacelle pressure field and accompanying shock waves "glance" away from the wing when encountering adjacent nacelles. In application, the nacelle generated pressure field is terminated on encountering another nacelle.

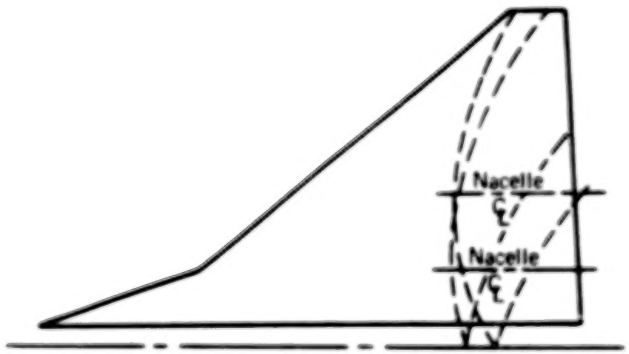

PRESSURES "WRAP" AROUND ADJACENT NACELLE

The nacelle pressure fields and accompanying shock waves "wrap" around adjacent nacelles. In application, the nacelle generated pressure field is allowed to pass through another nacelle as if it were transparent.

FIGURE 4.3-7.–NACELLE GENERATED WING PRESSURE FIELD CONCEPTS

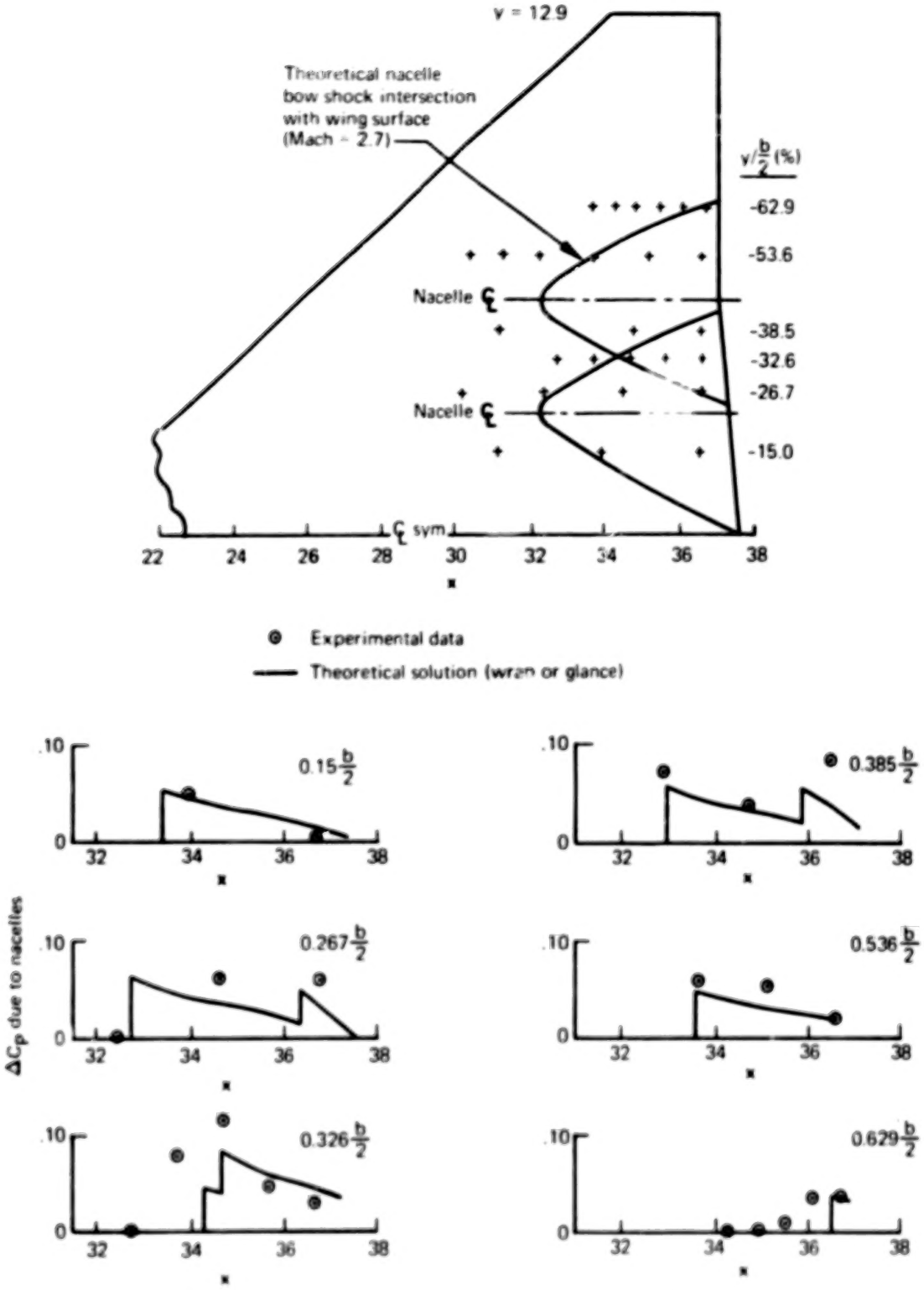

FIGURE 4.3-8.–NACELLE PRESSURE FIELD DATA, M = 2.7

A comparison of the theoretical nacelle pressure field with experimental data is presented in figures 4.3-8 and 4.3-9 at Mach numbers of 2.7 and 1.1. At M = 2.7, there is no difference between wrap and glance solutions. At M = 1.1, the solution choice appears to favor the glance approach except on the outboard wing. However, the experimental pressure points are too sparse to permit firm conclusions.

Nacelle-on-fuselage term. - The effect of the nacelles on the fuselage area distribution is built up by integrating each nacelle's pressure signature upon the fuselage area growth, with the provision that nacelles below the wing affect only the fuselage area below the wing in the region of the wing (and vice-versa for above-wing nacelles). In the fuselage region below the wing, or above the wing, the nacelle pressures are doubled to account for reflection (as is done for the nacelle pressures acting on the wing).

Fuselage-on-nacelle term. - The fuselage pressure signature is imposed on each nacelle surface as a buoyancy force.

Wing-on-nacelle term. - Wing thickness pressures at span stations where nacelles are located are transferred aft along Mach lines from the wing surface to the nacelle centerline to obtain the buoyancy field acting on each nacelle.

Nacelle-on-nacelle term. - The interference term of other nacelles acting on a selected nacelle is calculated by building up the composite buoyancy field, and then imposing it upon the nacelle surface. In the case of nacelles on opposite sides of the wing (i.e., above and below wing), the pressure signatures are cut off where intercepted by the wing.

The nacelle-generated pressure field is assumed to pass undiminished around or through other nacelles that may be present when a particular nacelle pair interference term is being calculated much as in the "wrap" solution employed for nacelle on wing terms. The "wrap" or "glance" option is not provided in this case because of the generally negligible difference in results.

Nacelle image effects. - If the nacelle is located next to the wing (or body), an "image" nacelle is used to create the reflected buoyancy field. The reflected field is cut off forward or aft of the wing if the nacelle is not entirely under the wing.

The principal image effect is caused by the nacelle pressure field reflecting off the wing back onto itself. However, the reflected nacelle pressure field acting on other nacelles is also computed. This solution also utilizes an image nacelle representation, and the reflected signature is restricted to whatever part of the "real" signature encountered a reflecting surface.

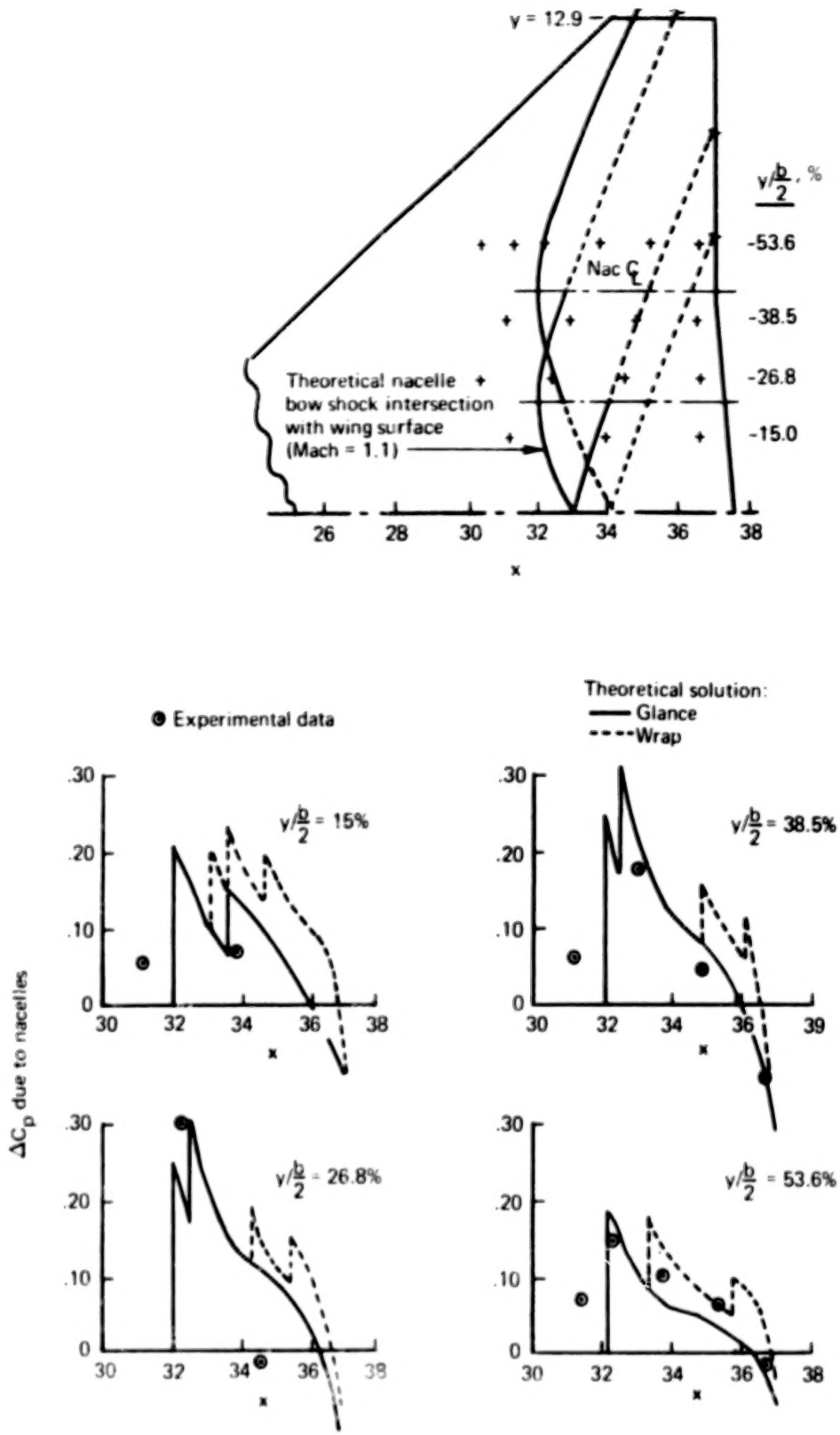

FIGURE 4.3-9.—NACELLE PRESSURE FIELD DATA, M = 1.1

Composite Thickness Pressure Signatures and Configuration Drag

Typical theoretical thickness pressure distributions acting on the configuration components are presented in figure 4.3-10. The net effect of these pressure signatures on drag is obtained by summing the various inputs and integrating them over the surface of the configuration. The corresponding drag terms are summarized in the data of figure 4.3-11.

The near-field wave drag program has three calculation features that have no direct counterpart in the far-field wave drag program. These are:

1) Wrap or glance solution for nacelle pressure field acting on wing. The wrap solution is nominally the same as the far-field solution.

2) Nacelle image effects. Because of the transparency assumption of the far-field program pressure propagation, nacelle pressures do not reflect off adjacent surfaces. (Through addition and subtraction of separate calculations involving "image" nacelles, however, comparable drag data can be generated using the far-field program.)

3) Above- or below-wing fuselage area separation in the nacelle-on-fuselage term. Directly comparable results are obtained only for mid-wing configurations.

Using the "wrap" solution, a mid-wing arrangement, and subtracting the nacelle image drag terms, a direct comparison between near-field and far-field program drag calculations can be made.

4.4 Drag-Due-to-Lift (Design and Analysis)

The wing design and lift analysis modules are separate lifting surface methods which solve the direct or inverse problems of:

- Design - to define the wing camber surface shape required to produce a selected lifting pressure distribution. The wing design program includes methods for defining an optimum (least drag) pressure distribution.

- Lift analysis - to define the lifting pressure distribution acting on a given wing camber surface, and calculate the associated force coefficients.

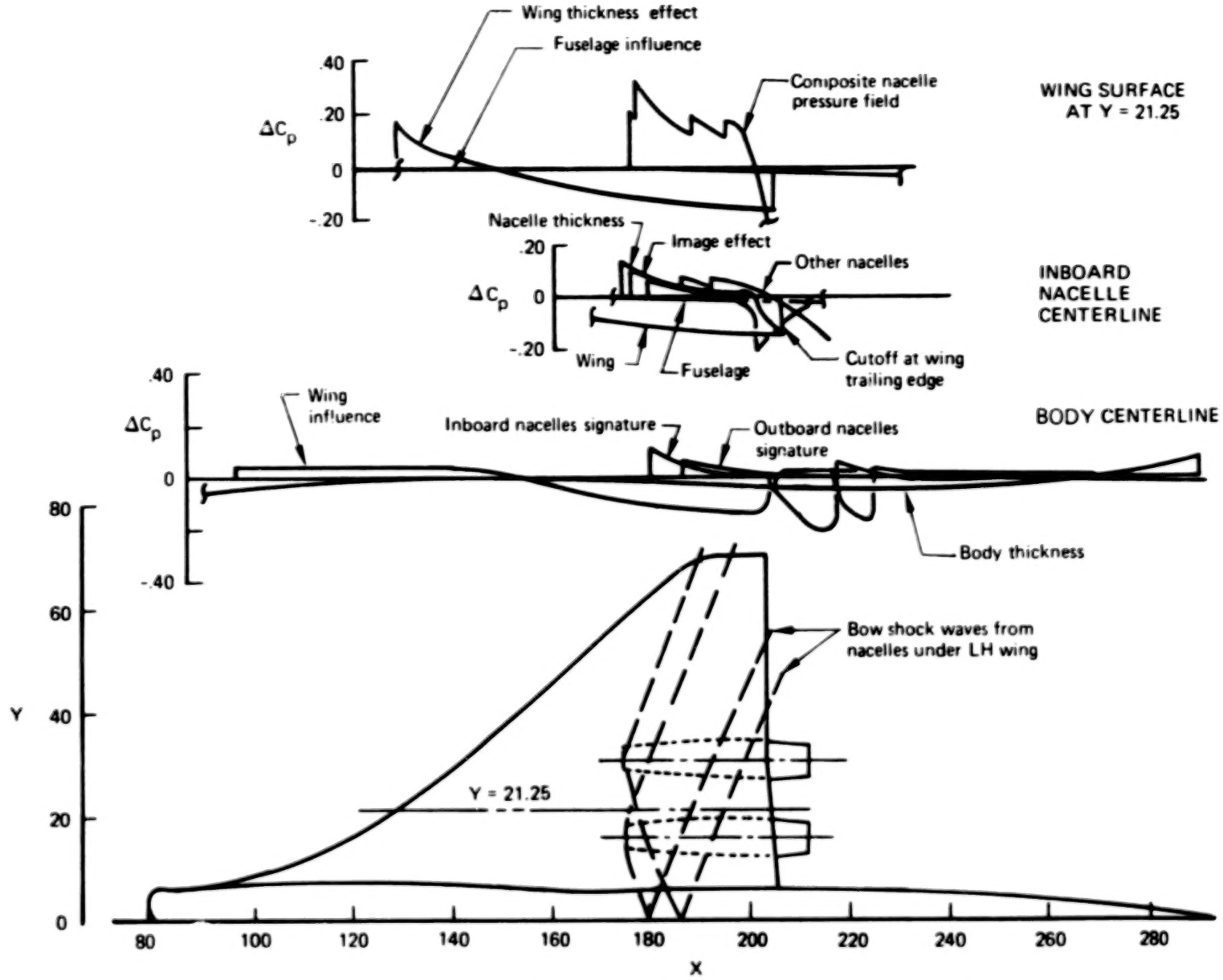

FIGURE 4.3-10.– NEAR-FIELD PRESSURE SIGNATURES, M = 1.1 "WRAP" SOLUTION

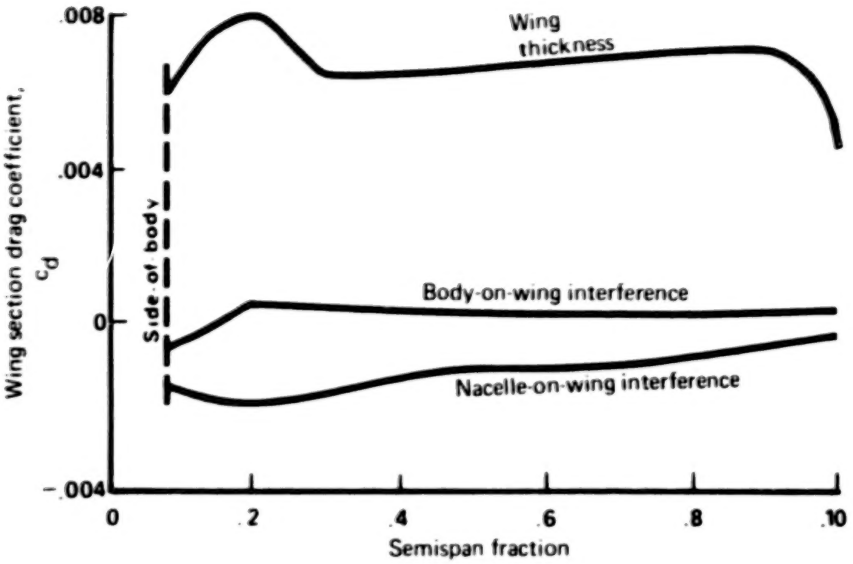

Wing-Body Terms

$C_{D_{wing}} = 0.00639$	$C_{D_{wing\text{-}on\text{-}body\ interference}} = -0.00013$	$\Sigma = 0.00711$
$C_{D_{body}} = 0.00072$	$C_{D_{body\text{-}on\text{-}wing\ interference}} = 0.00013$	

Nacelle Terms

Isolated $C_{D_{wave}}$	0.00075	0.00075
Body-on-nacelle interference	-0.00002	0.00000
Nacelle-on-body interference	0.00005	0.00010
Nacelle-on-nacelle interference		
Direct	0.00034	0.00023
Image	0.00054	0.00046
Wing-on-nacelle interference	-0.00043	-0.00058
	-0.00156	
	$\Sigma C_{D_{nac}} = 0.00064$	

Σ Wing-body-nacelle $C_{D_{wave}} = 0.00775$

FIGURE 4.3-11.–TYPICAL WAVE DRAG COEFFICIENT SUMMARY NEAR-FIELD PROGRAM, M = 1.1

Originally, these programs were developed to utilize the "Mach-box" method of wing representation and evaluation of linear theory integral equations (references 9 through 11). In the Mach-box method, the wing is replaced by a grid of small rectilinear elements. Since many elements (in the thousands) can be used, a detailed description of complicated surface shapes, with associated computational accuracy, is possible.

The wing design and lift analysis programs have been expanded several times to add features (e.g., reference 10) and have been reviewed in reference 12. The discussion of the aerodynamic theory of the Mach-box method in reference 12 is quite detailed, and is summarized here for completeness. The numerical method for the "direct" case of wing design and optimization is given first, followed by the inverse case of lift analysis on page 53.

Design Case

Camber surface for a given loading. - A typical wing planform described by a rectangular Cartesian coordinate system is illustrated in figure 4.4-1. The y coordinate has been multiplied by the Mach number parameter $\beta = \sqrt{M^2 - 1}$ for convenience in mathematical manipulations.

For a wing of zero thickness lying essentially in the z=0 plane, linearized theory for supersonic flow defines the wing surface shape necessary to support a specified lift distribution by the integral equation

$$\frac{\partial z_c}{\partial x}(x,y) = \frac{-\beta}{4}\Delta C_p(x,y) + \frac{1}{4\pi}\int d\xi \int_{\tau} \frac{(x-\xi)\,\Delta C_p(\xi,\eta)\,d\eta}{(y-\eta)^2\sqrt{(x-\xi)^2 - \beta^2(y-\eta)^2}} \tag{23}$$

which is a slightly modified form of equation (77a) of reference 13. With respect to a specified field point x, y, the upstream region of influence, τ, enclosed by the Mach forecone is shown by the shaded area.

Equation (23) may be rewritten into an influence function form by introducing the factor R, such that

$$\frac{\partial z_c}{\partial x}(x,y) = \frac{-\beta}{4}\Delta C_p(x,y) + \frac{\beta}{4\pi}\int d\xi \int_{\tau} \bar{R}(x-\xi,y-\eta)\,\Delta C_p(\xi,\eta)\,d\beta\eta \tag{24}$$

where $\bar{R}$ is defined as

$$\bar{R}(x-\xi,y-\eta) = \frac{x-\xi}{\beta^2(y-\eta)^2\sqrt{(x-\xi)^2 - \beta^2(y-\eta)^2}} \tag{25}$$

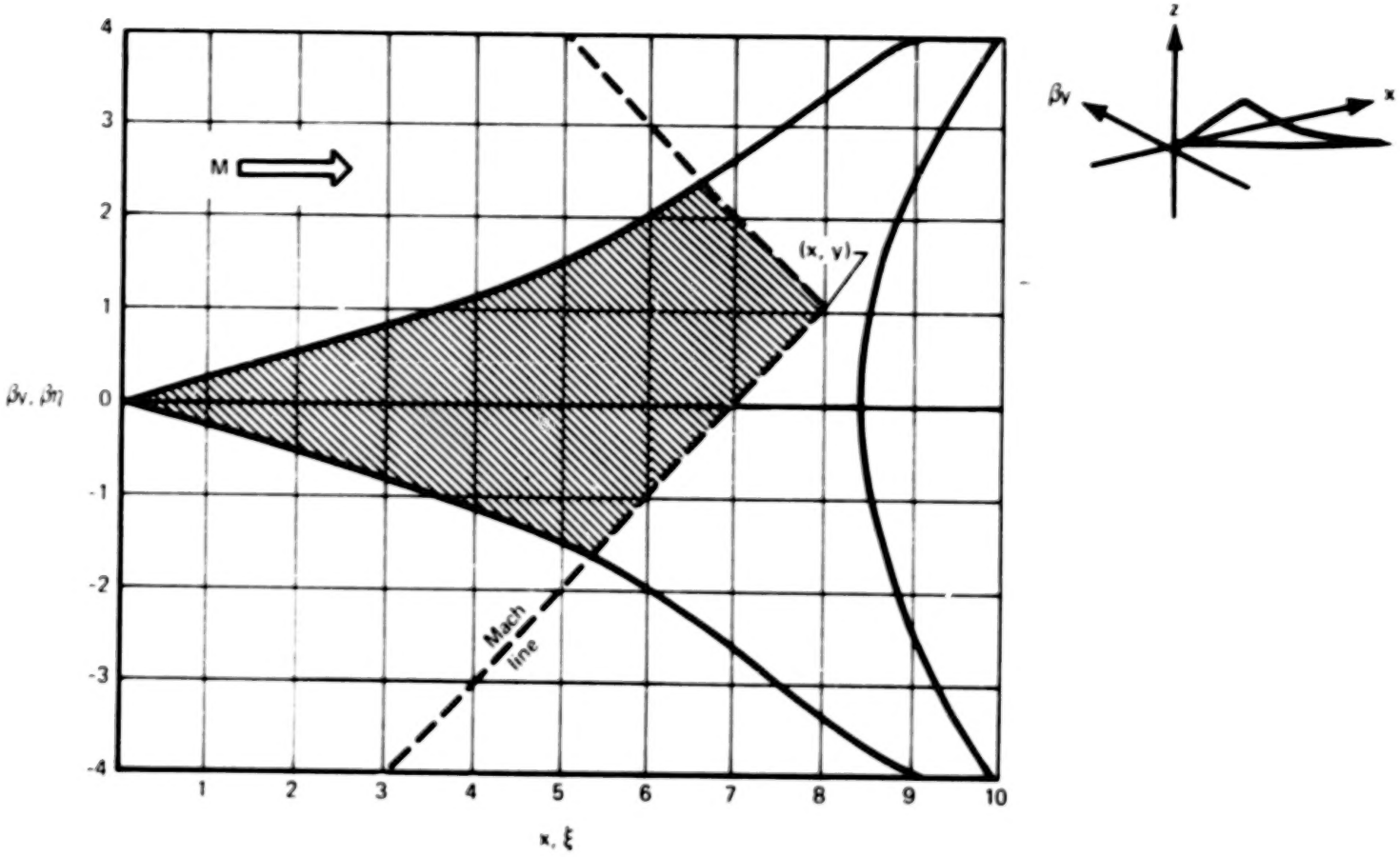

FIGURE 4.4-1.–CARTESIAN COORDINATE SYSTEM

$\bar{R}$ is a function relating the local loading at point ξ, to its influence in determining the downwash (or upwash) at the field point.

For the numerical evaluation of this integral, the wing is replaced by the grid system of figure 4.4-2. The grid elements, identified by L and N, are defined such that L is equal to X and N is equal to βy, where X and βy take on only integer values. Partial grid elements along the wing leading and trailing edges are used to permit a closer approximation to the actual wing planform. The grid system of figure 4.4-2 is rather coarse for illustrative purposes. In actual usage, many grid elements are employed.

In the grid system, the field point x, y is located at the aft midpoint of a field point element L*, N*, and the region of integration, τ, is approximated by the shaded grid elements.

The integration required by equation (24) is performed for each element within the Mach forecone, considering ΔC_p constant over the element and using an average value of $X-\xi = L^*-L+0.5$. The resulting expression, derived in reference 9, is the factor $\bar{R}$ which is the value of the influence function for an element L, N:

$$\bar{R}(L^*-L,N^*-N) = \frac{\sqrt{(L^* - L + 0.5)^2 - (N^* - N - 0.5)^2}}{(L^* - L + 0.5)(N^* - N - 0.5)} - \frac{\sqrt{(L^* - L + 0.5)^2 - (N^* - N + 0.5)^2}}{(L^* - L + 0.5)(N^* - N + 0.5)} \tag{26}$$

The integral equation (23) may then be replaced by the summation given below, where the summation includes all elements within the forecone and on the wing planform. The factors A, B, and C are element fractions for the wing leading edge, trailing edge, and wing tip, respectively, to allow for partial elements at those locations.

$$\frac{\partial z_c}{\partial x}(L^*,N^*) = \frac{-\beta}{4}\Delta C_p(L^*,N^*) + \frac{\beta}{4\pi}\sum_{\tau}\bar{R}(L^*-L,N^*-N)\,A(L,N)\,B(L,N)\,C(L,N)\,\Delta C_p(L,N) \tag{27}$$

The character of the $\bar{R}$ function is such that, for a given L*-L set of elements within the forecone, the sum of the $\bar{R}$ values is zero, the single negative value at N* - N = 0 balancing all the others (see figure 4.4-3). At L* = L, where there is only one element in the summation, the $\bar{R}$ value is zero.

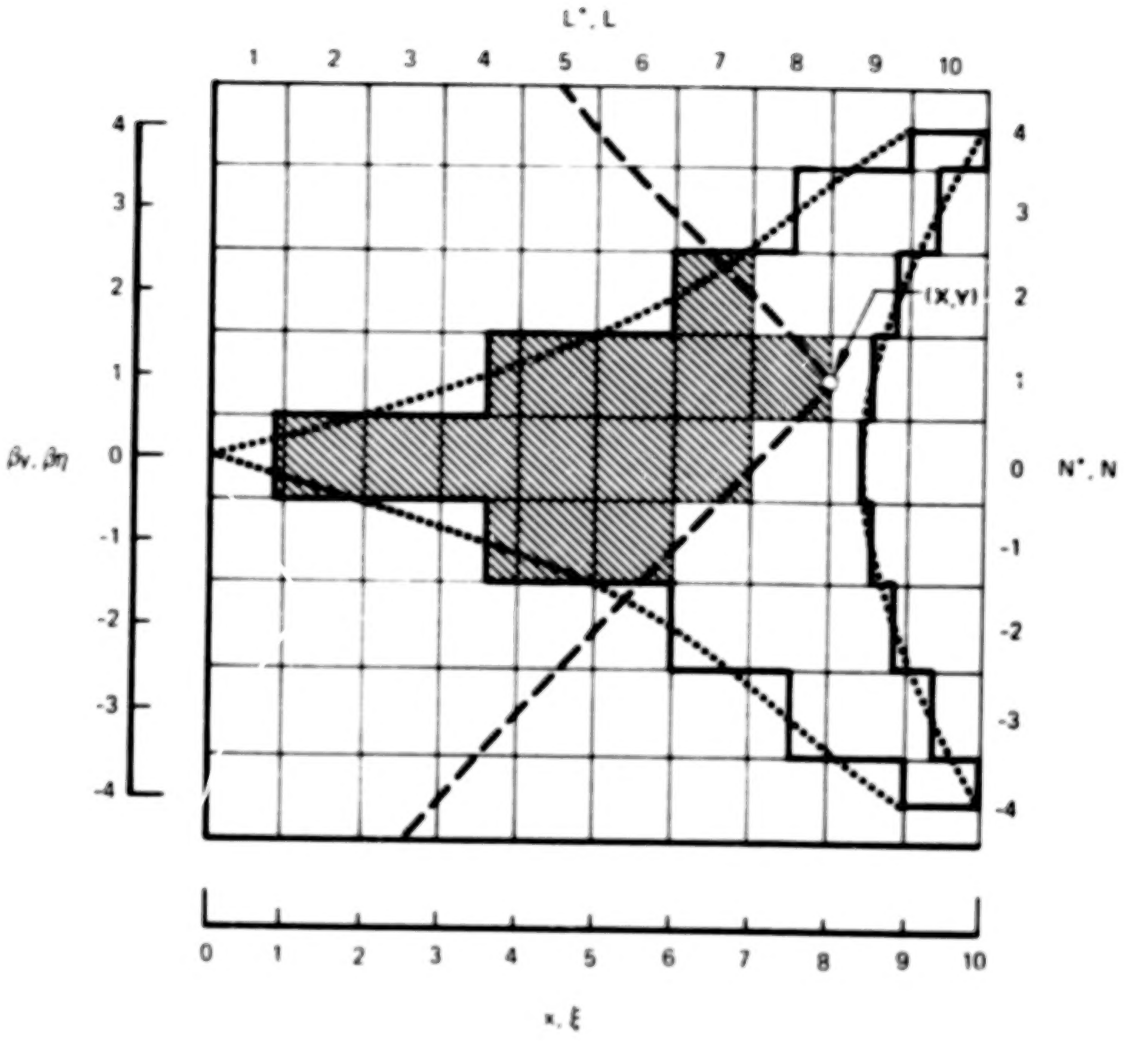

FIGURE 4.4-2. – GRID SYSTEM USED IN NUMERICAL SOLUTION

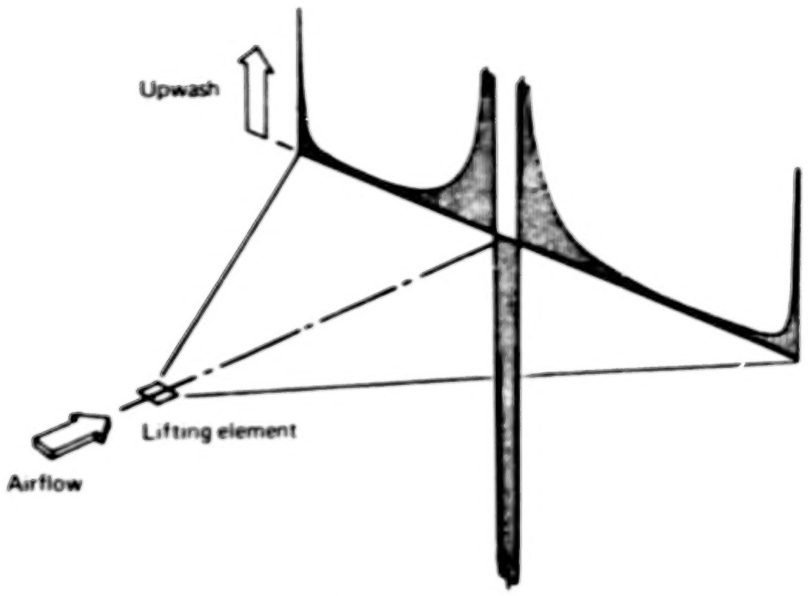

(a) UPWASH PRODUCED BY LIFTING ELEMENT

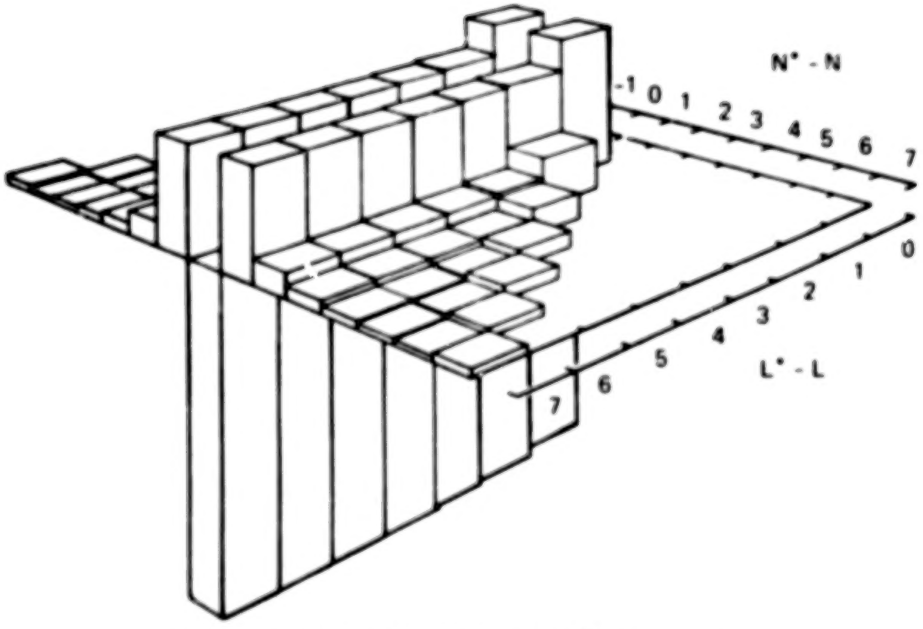

(b) NUMERICAL REPRESENTATION OF $\bar{R}$ FUNCTION

FIGURE 4.4-3. – INFLUENCE FACTOR CHARACTERISTICS

The physical significance of this $\bar{R}$ variation is that (for positive lift), all elements directly ahead of the field point element contribute only downwash and all other elements contribute upwash. An element at the leading edge near the wing tip of a subsonic leading-edge wing, therefore, sees a concentrated upwash field. It is this upwash field that makes the subsonic leading edge twisted and cambered wing attractive from the standpoint of drag-due-to-lift, since a local element may be inclined forward to produce both lift and thrust.

Conversely, an element located at the trailing edge and centerline of a diamond planform produces lift inefficiently, since the element sees an influencing region that contributes downwash.

In computing the local surface slope required to obtain a specified lifting pressure coefficient, the Cp value is known everywhere on the wing from loading formulas. In the wing design computer program, the wing camber surface shape is found by integrating the surface slopes for all chordwise elements at selected span stations. Section values of drag (Cp times slope), lift and pitching moment are then integrated spanwise to obtain wing force coefficients.

Optimum combination of loadings. - Equation (27), which defines the surface slope to support a specified lifting distribution, requires a description of the design pressure distribution. This is obtained from Lagrange's method of undetermined multipliers, which provides a means of selecting an optimum combination of component loadings, yielding minimum drag subject to various imposed constraints on the allowable pressure distribution.

A number of design point options are provided in the wing design program, involving the selection of loadings to be combined and the constraints desired. (The options are controlled by input codes, as described in the User's Manual, part 2).

The usual design conditions specified are:

- Drag-due-to-lift of the wing be minimized at a given design lift coefficient, subject to an optional pitching moment constraint.
- Effects of fuselage and nacelles be included in the design solution.
- Constraints be applied to the design pressure distribution and/or local camber surface shape to provide physical realism.

The design point options are discussed on page 49.

The optimum loading selection is an extension of the methods used in references 9 and 11, through the addition of the configuration-dependent

loadings (due to fuselage and nacelles) and the addition of the pressure and ordinate constraint formulation. Also, more component loadings were added to provide flexibility in rearranging pressure distributions at the design point in order to meet the pressure constraint condition. The maximum number of loadings is 17, defined in the table on page 44.

The wing design method actually consists of four solution steps:

- Flat wing solution
- Calculation of aerodynamic characteristics of selected component loadings.
- Optimization of loading combination
- Camber shape calculation

Flat wing solution. - The first step in the wing design process is to obtain the flat wing solution for the given wing planform and Mach number, using the analysis form of the lifting pressure calculation described on page 53 . This solution is obtained to locate the wing aerodynamic center for use in computing the pitching moment at zero lift for the individual loadings; and also, because its drag-due-to-lift factor is an often-used reference point in judging twisted and cambered wing designs.

Component loadings characteristics. - For each selected component loading, section lift, drag, and pitching moment coefficients are evaluated at a series of span stations and integrated spanwise to obtain overall lift, drag, and pitching moment. In addition, the interference drag coefficients between loadings are computed, where the drag interference between loadings i and j is given by

$$C_{D,ij} = C_{D,ji} = \frac{1}{\beta S} \sum \Delta C_{p,i}(L^*,N^*)\left(\frac{\partial z}{\partial x}\right)_j (L^*,N^*)\, A(L^*,N^*)\, B(L^*,N^*) \qquad (28)$$

$$+ \frac{1}{\beta S} \sum \Delta C_{p,j}(L^*,N^*)\left(\frac{\partial z}{\partial x}\right)_i (L^*,N^*)\, A(L^*,N^*)\, B(L^*,N^*)$$

where the summations are carried out over the wing planform. For the component loadings defined over the planform by analytical expressions, the loading is scaled by the appropriate power of either semispan or average wing chord, so that the resultant component loading lift coefficient is approximately 1.0.

TABLE 1.

DESCRIPTION OF WING LOADING TERMS

Loading Number	Definition
1.	Uniform
2.	Proportional to x, the distance from the leading edge
3.	Proportional to y, the distance from the wing centerline
4.	Proportional to y^2
5.	Proportional to x^2
6.	Proportional to x(c - x), where c is local chord
7.	Proportional to x^2 (1.5 c -x)
8.	Proportional to $2\,(1 + 15\,\frac{x}{c})^{-0.5}$
9.	Proportional to $\eta^2\,(\eta - 1)^2$
10.	Elliptical spanwise, proportional to $\sqrt{(1 - \eta)}$
11.	Proportional to x, the distance from the leading edge of an arbitrarily defined region
12.	A camber-induced loading proportional to the body buoyancy loading
13.	A camber-induced loading proportional to the body upwash loading
14.	A camber-induced loading proportional to the nacelle buoyancy loading
15.	The body buoyancy loading
16.	The body upwash loading
17.	The nacelle buoyancy loading

Interference drag coefficients associated with the configuration- dependent loadings are special cases. The configuration-dependent loadings are those produced by fuselage upwash, fuselage volume asymmetry, and nacelles, as described on page 62. They are calculated at discrete points over the wing planform, and interpolated linearly for a complete definition where needed . Since there is no camber surface associated with the configuration-dependent loadings, the interference drag coefficient between the "regular" loadings and the configuration dependent loadings has only one term. To ease the computational task of evaluating component and interference characteristics, the configuration-dependent loadings are assigned a corresponding wing slope definition of zero.

The nacelle configuration-dependent loading has yet another difference, since the flow fields of the "regular" loadings act on the fixed geometry of the nacelles, producing an appreciable axial force. The lifting pressure acting on the wing lower surface is assumed to propagate along Mach lines from the wing to the nacelle and the associated buoyancy force is computed.

If Z constraints are used, the camber surface Z values of all loadings are interpolated at the planform locations where Z constraints are to be applied.

These are used to constrain the optimum loading combination by requiring the specified Z value to occur at the constraint locations.

If a fuselage is present, the wing solution proceeds outboard from the side-of-fuselage station, and carry-over lift and fuselage camber is used to define the force coefficients of the wing inboard of the side-of-fuselage.

Fuselage contribution and "carry-over" lift. - If a fuselage is present in the solution, the lifting pressure distribution of the component loadings inboard of the side-of-fuselage station is of the "carry-over" type, rather than the analytically defined loading. I.e., the loading on the wing area occupied by the fuselage is a dependent function of the loading defined outboard of the side-of-fuselage station.

The carry-over pressure distributions are calculated for each component loading (excluding the configuration - dependent loadings) using the analysis form of the lifting pressure solution described on page 54. The carry-over pressure distributions are applied to the fuselage camberline to obtain the corresponding drag terms.

In addition, the fuselage contribution to configuration lift, drag, and pitching moment is included in the design point force coefficients. The fuselage coefficients are calculated in the lift analysis program for the input fuselage geometry as described on page 68 and transferred to the wing design program.

Optimization of loading combination. - Given the component loadings and their interference drag terms, the aerodynamic characteristics of a wing supporting any combination of these component loadings can be calculated in terms of load strength factors A_i assigned to each. The total lift coefficient for n loadings is

$$C_L = \sum_{i=1}^{i=n} C_{L,i} A_i \tag{29}$$

where $C_{L,i}$ denotes the loading and A_i its load strength factor. The total pitching moment coefficient at zero lift is C_{mo}

$$C_{mo} = \sum_{i=1}^{i=n} C_{mo_i} A_i \tag{30}$$

where

$$C_{mo,i} = C_{M,i} - \frac{dC_M}{dC_L} C_{L,i}$$

and the total drag coefficient is

$$C_D = \frac{1}{2} \sum_{i=1}^{i=n} \sum_{j=1}^{j=n} C_{D,i,j} A_i A_j + \sum_{i=1}^{i=n} C_{DWN,i} A_i \tag{31}$$

where the terms $C_{DWN,i}$ are the axial nacelle force coefficients for the component loadings. The contribution of each loading to the lifting pressure coefficient, to the wing upper surface longitudinal pressure gradient, and to the camber ordinate at point j can be summed to give

$$C_{p,j} = \sum_{i=1}^{i=n} C_{p,i,j} \tag{32}$$

The load strength factors of the configuration-dependent loadings are 1.0, since those loadings are not variable.

Hence, from the component loadings data, the drag, lift, and pitching moment characteristics of an infinite number of wing designs can be immediately calculated in terms of the A_i factors. The formal optimization of the wing loading involves the specification of the set of A_i's which gives least drag subject to the imposed constraints.

According to the Lagrangian method, the solution for the optimum A_i values involves the system of linear equations shown in figure 4.4-4, where matrix notation is used for compactness. The term $*C_{p,i}$ is the allowable lifting pressure coefficient corresponding to the ith pressure limiting constraint on the wing upper surface pressure.

Partitions in the square matrix of the solution have been identified by number and letter in figure 4.4-4. The left, uppermost partition of this matrix (zone A1) and the adjacent row and column correspond to Grant's original design solution (reference 14). The next m rows (zones C1-C7) and columns (zones A3-G3) are introduced by m local constraints on the lifting pressure coefficient, which are added (if necessary) in applying the pressure level constraint, as described on page 50. The next q rows (zones D1-D7) and columns (zones A4-G4) are introduced by q constraints on the longitudinal gradient of wing upper surface pressure coefficient; these terms are added in applying the pressure gradient limiting condition.

The next three rows (zones E1-E7) and columns (zones A5-G5) correspond to the constraints which set the loading factors A_i to 1.0 for the body buoyancy, body upwash, and nacelle buoyancy loadings. Each of these three rows and columns is present only if the corresponding configuration dependent loading is used. Zones F1-F7 and A6-F6 correspond to r constraints on ordinate, and appear only if ordinate constraints are actually specified by the user. The right-hand column (zones A7-G7) and bottom row (zones G1-G6) correspond to the constraint on pitching moment coefficient at zero lift; this constraint is also optional.

The unknowns of the design solution are the n values of the loading factors Ai and the (m+q+r+5) Lagrange multipliers (λ_i). These are contained in the left-hand-side column matrix.

The seven partitions of the right-hand-side column matrix contain: either the negative sum of the nacelle interference drag produced by wing lift and fuselage carry-over drag, or zero if not used; the design lift coefficient less fuselage lift coefficient; the pressure level constraint values applied to the lifting pressure coefficient (these are generated automatically by the design computer program, if they are necessary); the pressure gradient constraint values (also applied automatically if they are necessary); the values of A_i for the three configuration-dependent loadings; the constrained values of camber-line ordinate; and the design pitching moment coefficient at zero lift less fuselage pitching moment at zero lift.

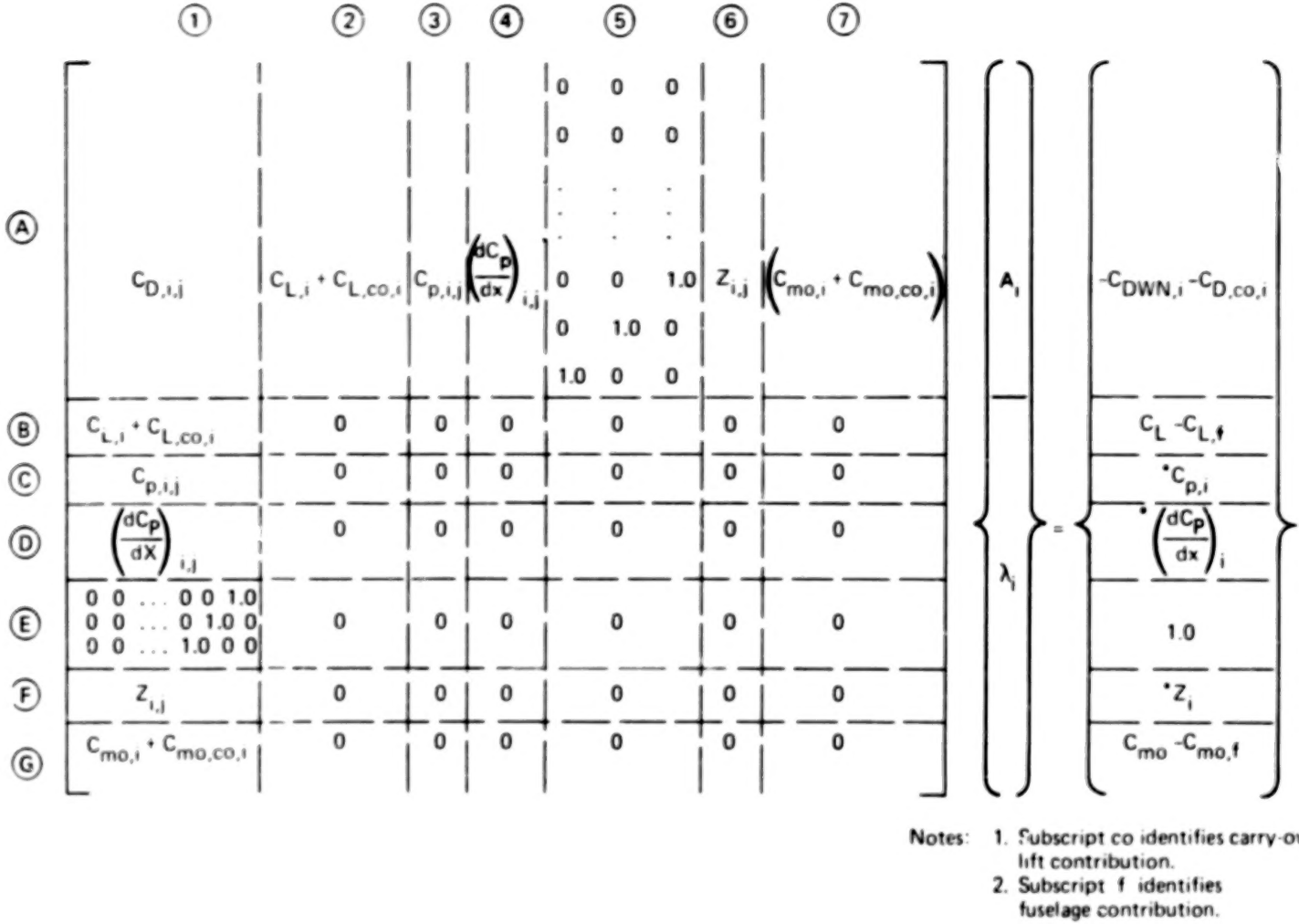
① ② ③ ④ ⑤ ⑥ ⑦
Ⓐ $C_{D,i,j}$ | $C_{L,i} + C_{L,co,i}$ | $C_{p,i,j}\left(\frac{dC_p}{dx}\right)_{i,j}$ | 0 0 0 / 0 0 0 / . . . / 0 0 1.0 / 0 1.0 0 / 1.0 0 0 | $Z_{i,j}$ | $\left(C_{mo,i} + C_{mo,co,i}\right)$
Ⓑ $C_{L,i} + C_{L,co,i}$ | 0 | 0 | 0 | 0 | 0 | 0
Ⓒ $C_{p,i,j}$ | 0 | 0 | 0 | 0 | 0 | 0
Ⓓ $\left(\frac{dC_p}{dX}\right)_{i,j}$ | 0 | 0 | 0 | 0 | 0 | 0
Ⓔ 0 0 ... 0 0 1.0 / 0 0 ... 0 1.0 0 / 0 0 ... 1.0 0 0 | 0 | 0 | 0 | 0 | 0 | 0
Ⓕ $Z_{i,j}$ | 0 | 0 | 0 | 0 | 0 | 0
Ⓖ $C_{mo,i} + C_{mo,co,i}$ | 0 | 0 | 0 | 0 | 0 | 0
A_i / λ_i = $-C_{DWN,i} - C_{D,co,i}$ / $C_L - C_{L,f}$ / $^*C_{p,i}$ / $^*\left(\frac{dC_p}{dx}\right)_i$ / 1.0 / $^*Z_i$ / $C_{mo} - C_{mo,f}$

Notes: 1. Subscript co identifies carry-over lift contribution.
2. Subscript f identifies fuselage contribution.

FIGURE 4.4-4.–OPTIMIZATION MATRIX

The maximum number of equations in figure 4.4-4 is 34. This number of equations can be reached if 17 loadings are combined, a pitching moment constraint is used, and the maximum number of constraints on lifting pressure coefficient are required.

Design camber surface. - Given the set of A_i factors, the design pressure distribution is known and the resulting camber surface is calculated using equation (27) on page 39.

Design point options. - Due to options in the wing design program to limit the solution extent (e.g., no C_{mo} constraint or no ordinate constraints or no pressure constraints), some parts of the solution matrix on page 49 may not be used. However, for purposes of describing the solution options, it is assumed that all options are chosen. In that case, the wing loading solution proceeds as follows, using repeated applications of the corresponding matrix:

(1) The wing loading having minimum lift-dependent drag with a constraint on design lift coefficient is defined. This solution will include ordinate constraints if any have been specified.

(2) A family of wing loadings having minimum lift-dependent drag with a constraint on design lift coefficient and a series of constraints on pitching moment coefficient at zero lift are defined. This series of solutions is presented in the form of drag due to lift factor, K_E, versus C_{mo}, and is referred to as the "bucket" plot. Ordinate constraints are not included.

(3) The wing loading having minimum lift-dependent drag with constraints on design lift coefficient wing upper surface pressure and camberline ordinates is found. This solution may require a cyclic process for the pressure constraints that begins with (1) above. If (1) satisfies the pressure criteria on both gradient and level everywhere on the planform, then this loading is set equal to (1). If (1) does not satisfy the pressure limits everywhere, then a pressure constraint is applied at the wing planform location where the pressure gradient is most strongly violated, and a new solution for wing loading is found. Its pressure distribution is tested against the gradient limit, and another constraint is imposed if the limit is violated. Each cycle adds another pressure gradient constraint to the solution in addition to the lift coefficient constraint. When pressure gradient is satisfied, then pressure level is similarly tested against its limit. Constraints on pressure level are also added cyclically until solution pressure level satisfies the level limit everywhere. Cycling continues until either the solution load

distribution everywhere satisfies the pressure gradient and level limit or until the number of solution constraints equals the maximum allowable number. In the latter case the limit level for pressure gradient is increased by 20%, and the cycle is started again.

It has been found that pressure gradient and pressure level constraints imposed early in this cyclic solution can subsequently become unnecessary as other pressure constraints are imposed. Constraints unnecessary for satisfying pressure gradient and level criteria penalize the wing design unnecessarily by increasing drag. Such constraints can be detected by the algebraic signs of their solution Lagrange multipliers. Accordingly, a test for unnecessary pressure constraints has been added to the solution cycle. Such constraints are removed when detected and cycling continues.

(4) The wing loading having minimum lift-dependent drag with constraints on design lift coefficient, camberline ordinates, and zero-lift pitching moment coefficient is defined.

(5) The wing loading having minimum lift-dependent drag with constraints on design lift coefficient, pitching moment coefficient at zero lift, camberline ordinates, and wing upper surface pressure is found. The latter type of constraints are imposed, if necessary, in the cyclic fashion of (3).

Examples of loading solutions (1), (2), (4), and (5) are shown in figure 4.4-5. For this case, loading solution (1) satisfies the wing upper surface pressure constraint, and is therefore identical to loading solution (3).

The effect of the number of loadings on the "bucket" plot and on loading solution (5) is illustrated in figure 4.4-6. Increasing the number of loadings from 3 to 11 results in a substantial theoretical drag decrease; however, this decrease is reduced substantially when pressure gradient constraints are added.

Experience with the wing design program has shown an occasional "endless loop" fault in the process of adding and deleting pressure constraints under the constraint cycling described in paragraph (3). I.e., a given constraint will be successively added and then deleted and then added again. The problem occurs due to an improper solution matrix formulation caused by imprecise interference drag calculations between loadings. Imprecision in the interference drag calculations is inherent in the panel type approach, and it is not possible to predict when it will cause an endless loop in the optimization. It is possible, however, to detect the presence of the mathematically improper matrix formulation through an eigenvalue check and thereby avoid entering an endless loop.

The test for a probable endless loop situation is to calculate the number of zero and negative eigenvalues of the solution matrix. The matrix solution is

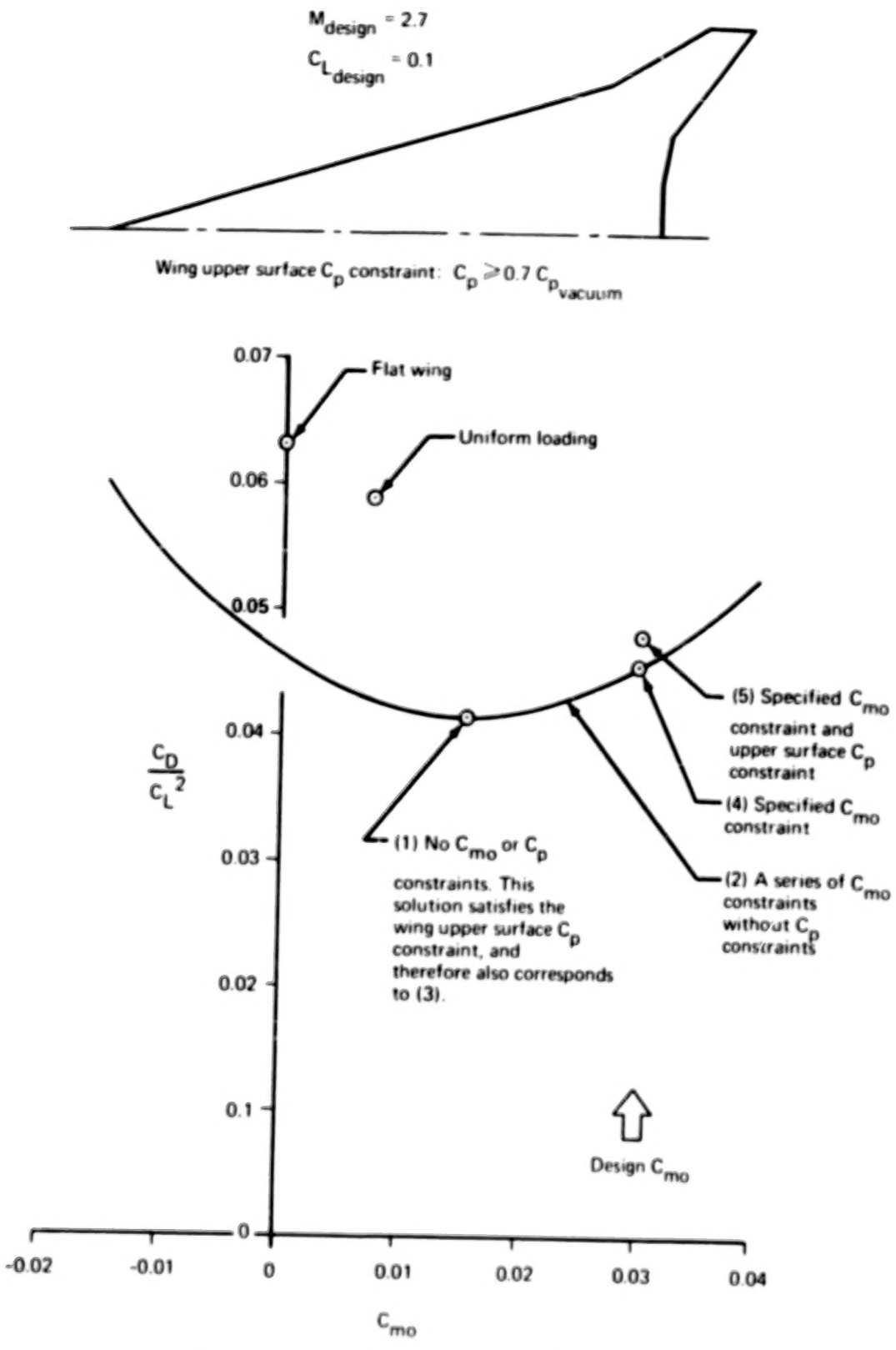

FIGURE 4.4-5.–TYPES OF LOADING SOLUTIONS

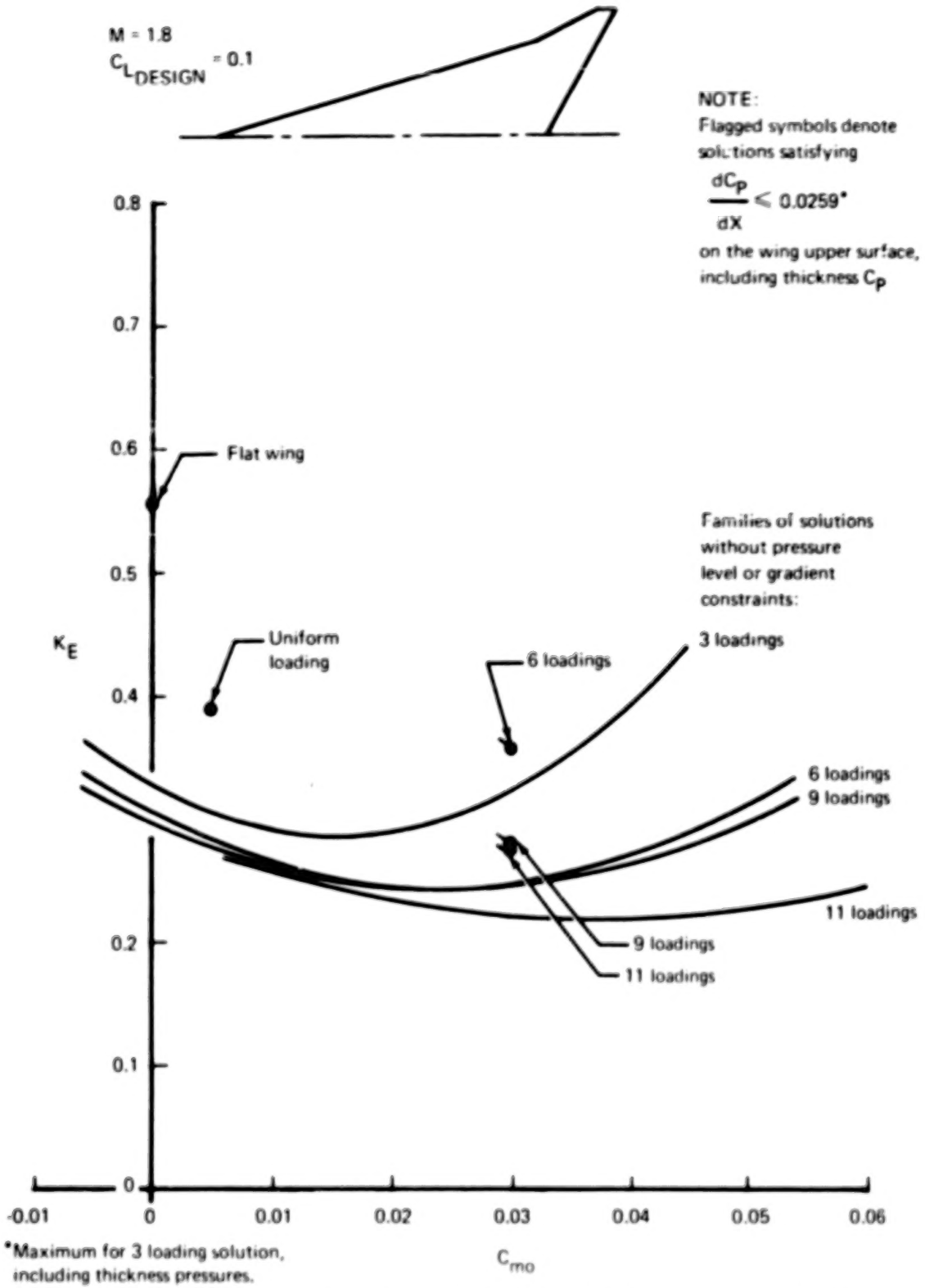

FIGURE 4.4-6.–WING DESIGN STUDY: CONSTRAINTS ON BOTH C_{mo} AND UPPER SURFACE PRESSURE GRADIENT

unstable (probable endless loop) if there are any negative eigenvalues, or if the number of zero eigenvalues exceeds the number of imposed constraints. The number of imposed constraints is equal to (if used) one each for total lift and pitching moment, plus the number of fixed configuration-dependent loadings, plus the number of Z constraints, plus the number of pressure coefficient level and gradient constraints. If the eigenvalue test proves unstable, the program halts and an error message is printed. The optimization requested must then be changed to permit a solution. (A discussion of such changes is given in the User's Manual, Part 2.)

Lift Analysis Case

Loading for a given camber surface. - Since the $\bar{R}$ function for the field point element is zero (the element generates no downwash or upwash upon itself), equation (27) can be rearranged to solve for the lifting pressure coefficient in terms of the field point slope and upstream influences:

$$\Delta C_p\,(L^*,N^*) = -\frac{4}{\beta}\frac{dz_c}{dx}\,(L^*,N^*) \qquad (33)$$

$$+\frac{1}{\pi}\sum_{\tau}\bar{R}(L^*-L,N^*-N)\;A(L,N)\;B(L,N)\;C(L,N)\;\Delta C_p(L,N)$$

Therefore, the lifting pressure distribution, ΔC_p, can be determined for a wing of arbitrary surface shape provided the calculations are performed in the proper sequence. The order of calculation of $\Delta C_p(L^*,N^*)$ is from apex aft, and from the centerline to the right-hand wing tip for each L* row. In this fashion, all pressure coefficients within the Mach forecone from any element will have been previously obtained and no unknown pressure coefficients arise in the summation. The element fractions A, B, and C are as defined for equation (27).

Theoretically $\Delta C_p(L^*, N^*)$ defined by equation (33) is the pressure coefficient at the aft mid-point of the L*, N* element. The average pressure coefficient for the element, needed in subsequent calculations, is calculated by one of two alternative methods:

1) An approximate average pressure coefficient is interpolated from the aft mid-point ΔC_p value and the ΔC_p value of the element immediately ahead. (No interpolation is performed if L*, N* is a leading edge element). This is the method used in the original formulation of the computer program. However, it was found that oscillations in the ΔC_p values occurred near the wing leading edge. So, a 9 point smoothing equation was applied after unsmoothed pressures were computed for the entire wing, which essentially

removed the oscillations and brought the smoothed pressure distribution into good agreement with established results from other theoretical methods.

The smoothing equation is of the form

$$\overline{\Delta C_p}(L^*) = \frac{\begin{array}{l} 0.2A(L^*-4)\Delta C_p(L^*-4) + 0.4A(L^*-3)\Delta C_p(L^*-3) + 0.6A(L^*-2)\Delta C_p(L^*-2) \\ + 0.8A(L^*-1)\Delta C_p(L^*-1) + A(L^*)\Delta C_p(L^*) + 0.8A(L^*+1)\Delta C_p(L^*+1) \\ + 0.6A(L^*+2)\Delta C_p(L^*+2) + 0.4A(L^*+3)\Delta C_p(L^*+3) + 0.2A(L^*+4)\Delta C_p(L^*+4) \end{array}}{\begin{array}{l} 0.2A(L^*-4) + 0.4A(L^*-3) + 0.6A(L^*-2) + 0.8A(L^*-1) + A(L^*) + 0.8A(L^*+1) \\ + 0.6A(L^*+2) + 0.4A(L^*+3) + 0.2A(L^*+4) \end{array}} \tag{34}$$

where the A values account for element fractions. A is zero if the corresponding element is ahead of the wing leading edge, or aft of trailing edge in the case of a subsonic trailing edge. The supersonic trailing edge solution is treated as a special case, and the trailing edge is extended four elements to provide pressure coefficient data to fill out the smoothing equation.

2) The other average ΔC_p method is an alternate technique, which uses an aft element sensing approach. This method involves solving for preliminary ΔC_p results for a given L*, N* element and the element immediately aft, then following it up with a second calculation to refine the preliminary results. The procedure is detailed in reference 12, but is summarized below and in figure 4.4-7.

   a) Calculate preliminary ΔC_p values for a given L* = constant row. Designate as $\Delta C_{p,a}(L^*,N^*)$.

   b) Calculate preliminary ΔC_p values for the element row immediately aft = L*+1, using $\Delta C_{p,a}$ values. Designate as $\Delta C_{p,b}(L^*,N^*)$.

   c) Finalize ΔC_p values for the original L* = constant row from one of the two following equations. For leading edge elements:

$$\Delta C_p(L^*,N^*) = \frac{1}{2}\left[1 + \frac{A(L^*,N^*)}{1 + A(L^*,N^*)}\right]\Delta C_{p,a}(L^*,N^*) + \frac{1}{2}\left[\frac{A(L^*,N^*)}{1 + A(L^*,N^*)}\right]\Delta C_{p,b}(L^*,N^*) \tag{35}$$

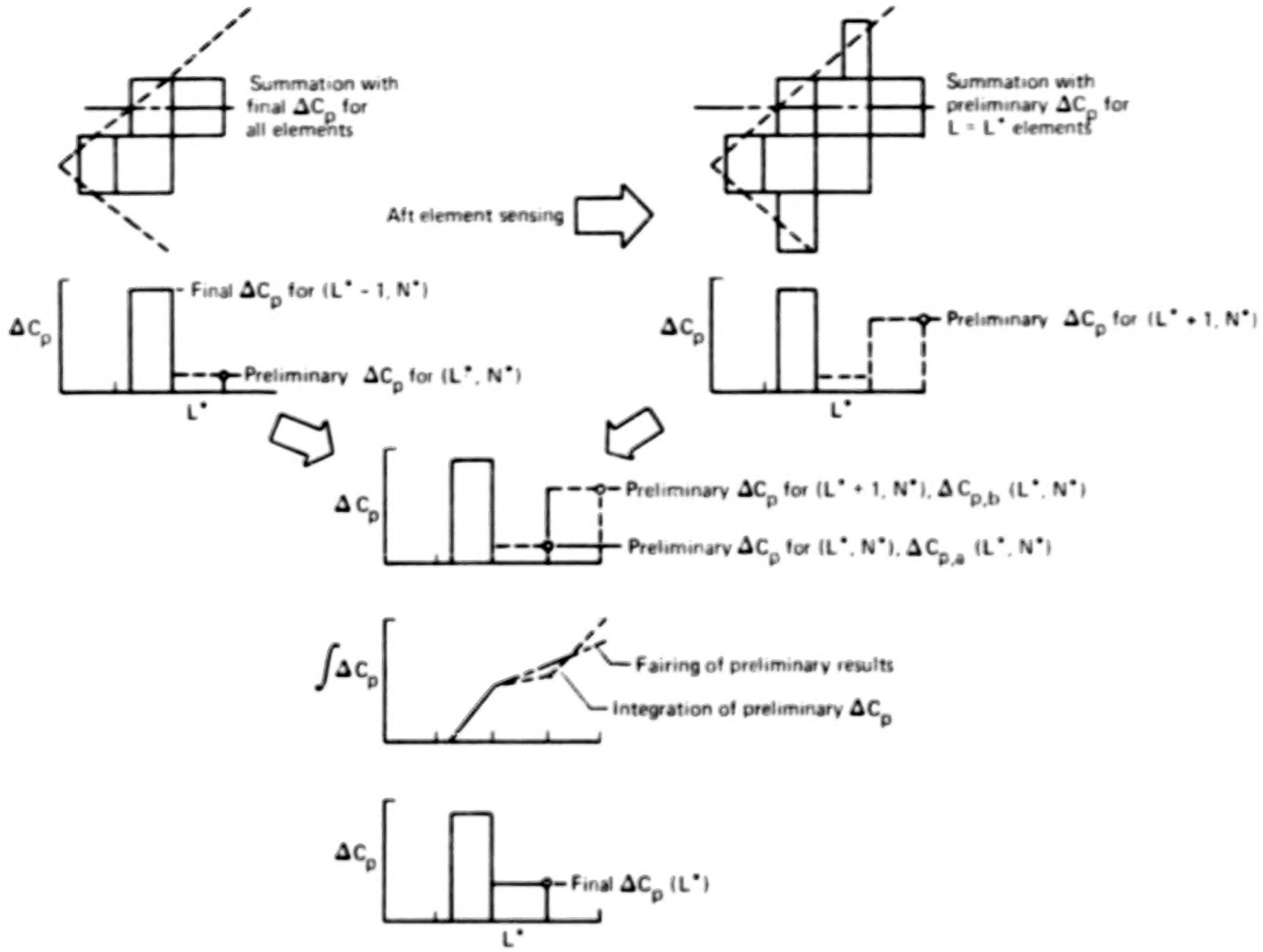
Summation with final ΔC_p for all elements
Aft element sensing
Summation with preliminary ΔC_p for $L = L^*$ elements
ΔC_p
Final ΔC_p for $(L^* - 1, N^*)$
Preliminary ΔC_p for (L^*, N^*)
L^*
ΔC_p
Preliminary ΔC_p for $(L^* + 1, N^*)$
L^*
ΔC_p
Preliminary ΔC_p for $(L^* + 1, N^*)$, $\Delta C_{p,b}$ (L^*, N^*)
Preliminary ΔC_p for (L^*, N^*), $\Delta C_{p,a}$ (L^*, N^*)
$\int \Delta C_p$
Fairing of preliminary results
Integration of preliminary ΔC_p
ΔC_p
Final ΔC_p (L^*)
L^*

FIGURE 4.4.7.–APPLICATION OF AFT-ELEMENT SMOOTHING TECHNIQUE (FROM REF. 12)

For all other elements:

$$\Delta C_p = \frac{3}{4}\,\Delta C_{p,a}(L^*,N^*) + \frac{1}{4}\,\Delta C_{p,b}(L^*,N^*) \tag{36}$$

The aft element sensing technique produces a substantial reduction in pressure coefficient oscillation. In cambered wing test cases run with the method, however, some oscillation was found to persist. Therefore, a 3 term smoothing equation was added (after all wing pressures are calculated), of the form:

$$\overline{\Delta C_p}(L^*) = \frac{0.5A(L^*-1)\Delta C_p(L^*-1) + \Delta C_p(L^*) + 0.5A(L^*+1)\Delta C_p(L^*+1)}{0.5A(L^*-1) + 1.0 + 0.5A(L^*+1)} \tag{37}$$

In the computer program one of the two alternate smoothing methods is selected by an input code. Both produce essentially the same answers . When the pressure limiting option is used (discussed later), the aft-sensing smoothing technique is automatically selected.

For the analysis solution, the pressure coefficients for all elements must be calculated. The force coefficients are, therefore, calculated from direct summations of local pressures applied to each element, rather than employing a spanwise integration as in the design case. Lengthwise and spanwise lift distributions are obtained by summing the lift in the corresponding element rows.

Leading edge suction force. - The drag summation may be obtained either with or without the leading edge suction force included (as requested by input codes). Both the maximum theoretical leading edge suction or the attainable leading edge suction force defined by Carlson in references 18 and 19 may be calculated. The referenced reports contain detail description of the methods involved, which are summarized here.

The magnitude of the theoretical leading edge thrust developed by a thin lifting wing is dependent upon the upwash in the vicinity of the leading edge. This upwash determines the character of the associated pressure distribution. For a flat lifting wing with a subsonic leading edge, the pressure distribution near the leading edge is peaky, with the lifting pressure at the leading edge theoretically approaching infinity. The theoretical leading edge thrust is related to the limiting value at the leading edge of the parameter

$$\lim_{x' \to 0} \left(\Delta C_p \sqrt{x'}\right) = \left(\Delta C_p \sqrt{x'}\right)_0 \tag{38}$$

and the thrust per unit distance in the spanwise direction is

$$t = \frac{\pi q}{8} \tan \Lambda \sqrt{1 - \beta^2 \cot^2 \Lambda} \left(\Delta C_p \sqrt{x'}\right)_o^2 \tag{39}$$

The total theoretical thrust for the wing becomes

$$C_T = \int_o^{b/2} c_t \, dy = \int_o^{b/2} \frac{\pi}{8} \frac{b}{S} \tan \Lambda \sqrt{1 - \beta^2 \cot^2 \Lambda} \left(\Delta C_p \sqrt{x'}\right)_o^2 \tag{40}$$

The central problem in calculating the leading edge thrust involves the evaluation of $\left(\Delta C_p \sqrt{x'}\right)_o^2$. It is complicated by the fact (typical of panel aerodynamic methods) that the calculated pressure distributions are appproximately correct but vary from "exact theory" values and are most inaccurate near the leading edge. In reference 18, Carlson performed a detail analysis of the nature of the errors associated with the presssure distributions near the leading edge for the "Mach-box" numerical method. An adjustment parameter was developed (a shift in the x' location of the calculated pressure near the leading edge as a function of wing sweepback and Mach number) which significantly improved the pressure distribution details near the leading edge, with attendant improvement in the value of $\left(\Delta C_p \sqrt{x'}\right)_o$.

The solution for $\left(\Delta C_p \sqrt{x'}\right)_o$ is obtained by a least squares fit of $\Delta C_p \sqrt{x'}$ versus x', using the fitting function shown below:

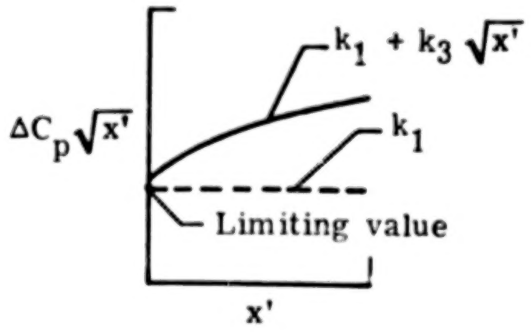

Since it is known that the flat wing pressure distribution near the leading edge displays a square root singularity, the function

$$\Delta C_p \sqrt{x'} = k_1 + k_2 x' \tag{41}$$

is used for the flat wing solution. Wings input as a cambered surface are

analyzed with the more general expression

$$\Delta C_p\sqrt{x'} = k_1 + k_3\sqrt{x'} \qquad (42)$$

All wings, flat or cambered, could have been treated with the cambered-wing fitting function, but flat wings were considered to be a special case because of some improvement in results and relatively minor programming complications.

Leading edge sectional thrust values are computed for all spanwise rows of the wing grid system for a series of wing angles of attack.

The sectional thrust values are resolved into drag or lift components according to assumptions of fully attached flow, fully separated (vortex) flow, or the attainable thrust definition of reference 19. The components associated with the fully attached or separated (Polhamus analogy) flow assumptions are illustrated in figure 4.4-8 for a typical leading edge segment having a local angle of attack of $\alpha - \delta$. The sectional data are integrated spanwise to get the total wing data for output in the force coefficient summaries.

Attainable leading edge suction. - Carlson, in reference 19, further developed the leading edge suction solution through the concept of an attainable leading edge thrust. Based on a study of airfoil data and utilizing simple sweep theory, reference 19 derives an empirical estimate of attached flow and vortex flow components. The principal factors of importance were found to be wing leading edge normal Mach number and wing airfoil normal section parameters (leading edge radius, maximum thickness and position of maximum thickness). From these parameters and sectional Reynolds number, a factor K_T relating the theoretical sectional thrust coefficient to the attainable attached-flow-type thrust coefficient is computed. The difference between the attached flow thrust coefficient and the theoretical sectional thrust coefficient is then treated as a vortex lift component, with associated drag and lift coefficient components. The attainable thrust force coefficient components for a typical wing leading edge segment are illustrated in figure 4.4-9. The attainable lift and drag sectional coefficients are also integrated spanwise and printed in the wing force coefficient summaries.

It should be noted that the theoretical leading edge suction force is an approximate calculation due to the panel representation of the wing and corresponding pressure coefficient dependency. Particularly in the case of a cambered wing, the calculated leading edge thrust forces typically involve a small but significant inaccuracy and should be used with appreciation for possible error.

Typical drag polars with the different leading edge suction options are illustrated in figure 4.4-10.

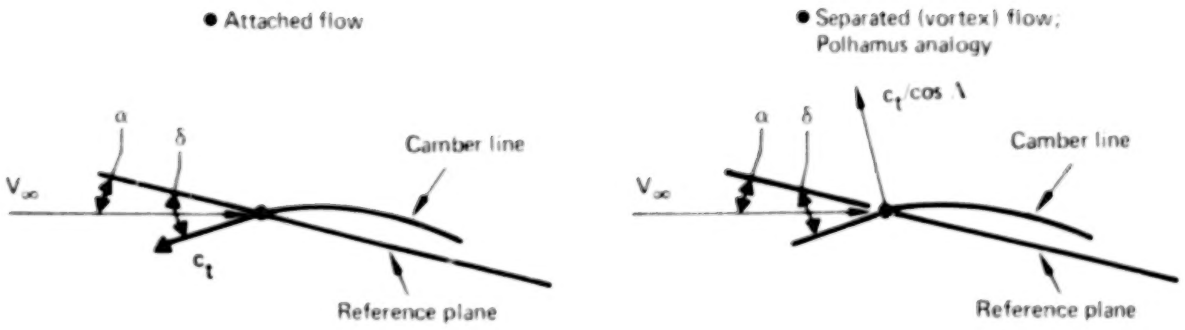

$$c_\ell = c_t \sin(\alpha - \delta)$$

$$c_d = -c_t \cos(\alpha - \delta)$$

$$c_\ell = \frac{c_t}{\cos \Lambda} \cos(\alpha - \delta) \text{ sign } (C_{p_{x=0}})$$

$$c_d = \frac{c_t}{\cos \Lambda} \sin(\alpha - \delta) \text{ sign } (C_{p_{x=0}})$$

FIGURE 4.4-8.—THEORETICAL LEADING-EDGE SUCTION LIFT AND DRAG COMPONENTS

- Attainable suction sensitive to–
  - Airfoil geometry
  - Normal Mach number
  - Reynolds number

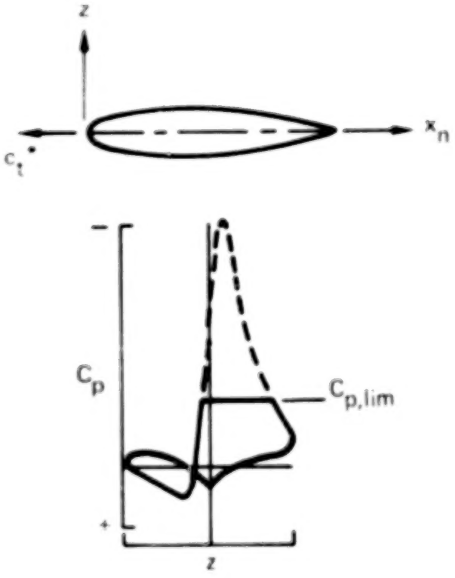

- Attainable thrust factor, $K_T = \dfrac{c_t^*}{c_t}$

$$c_n = \frac{c_t}{\cos \Lambda} \sin (\cos^{-1} K_T - \delta)$$

$$c_a = -c_t \cos (\cos^{-1} K_T - \delta)$$

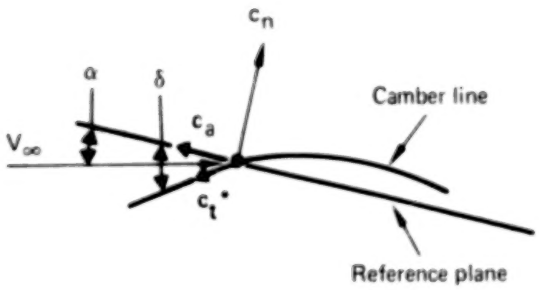

If $K_T = 1.0$, attached flow
$K_T = 0.$, Polhamus analogy

FIGURE 4.4-9.–ATTAINABLE LEADING-EDGE SUCTION (CARLSON)

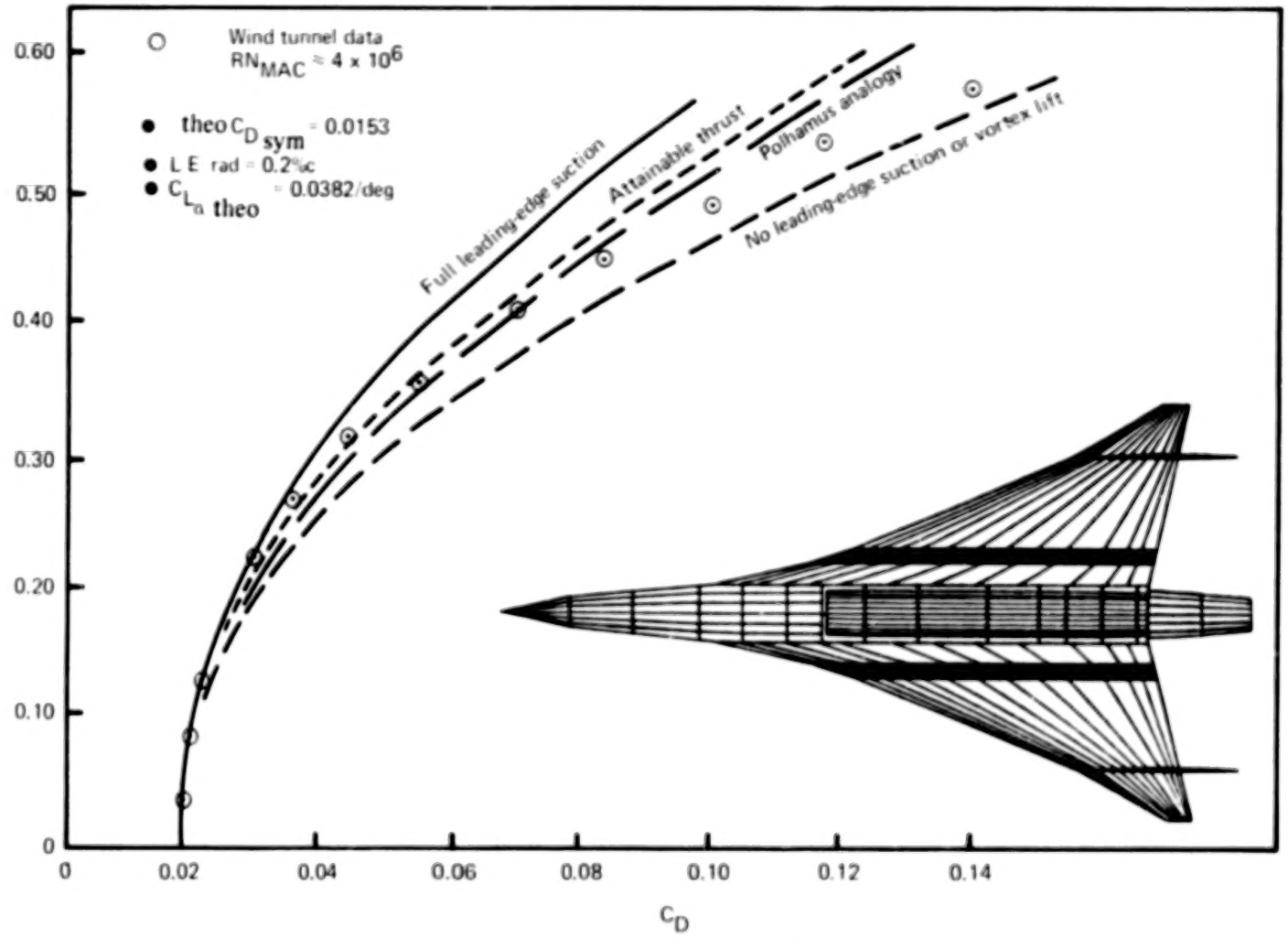

FIGURE 4.4-10.–LEADING EDGE SUCTION EFFECTS

Analysis of complete configuration. - The preceding discussion describes the theory used in the lifting pressure calculations for a wing camber surface at a selected angle of attack. The analysis program may also be used to calculate lifting pressure distributions and force coefficients for complete configurations over a range of angles of attack, adding in the effects of fuselage, nacelle, canard, and/or horizontal tail, as applicable.

The program actually carries two solutions along: one for the configuration at its input angle of attack, the other the incremental solution per degree angle of attack (called the flat wing solution). The interference terms associated with the two solutions acting on the other surface shape are also calculated. The summation of these effects into the drag polar and other force coefficients is performed by superposition, as described on page 70.

Calculation of the complete configuration lifting pressure solution involves up to 7 principal tasks:

- Isolated fuselage upwash field
- Nacelle pressure field acting on wing
- Pressure field due to asymmetrical fuselage volume
- Wing/canard solution in presence of fuselage upwash field. Effects of the wing pressure field acting on nacelles are also calculated
- Fuselage lift distribution in presence of wing downwash field
- Horizontal tail solution in presence of fuselage and wing flow fields.
- Superposition of solutions

The calculation logic of these tasks is described in the following sections:

Isolated fuselage upwash field. - Two alternate solutions for the fuselage upwash field are provided, selected by an input code. One is a slender body solution which is valid for a pointed body of circular cross-section shape. The second is a general slender body solution of arbitrary cross-section.

Fuselage of circular cross-section. - The fuselage upwash (or downwash) field in the plane of the wing, canard, or horizontal tail is obtained from slender body theory. The fuselage must have a pointed nose and cannot have discontinuities in cross sectional area (e.g., a step in longitudinal area distributions).

From reference 15, the velocity potential of a slender body of revolution, shown in figure 4.4-11, is:

$$\frac{1}{U}\phi(x,r,\theta) = \frac{1}{2\pi}\frac{dA(x)}{dx}\ln\frac{\beta r}{2} - \frac{1}{2\pi}\frac{\partial}{\partial x}\int_0^x \frac{dA(x)}{dx}\ln|x-x_1|dx_1 + [a+c(x)]R^2(x)\frac{\cos\theta}{r} \qquad (43)$$

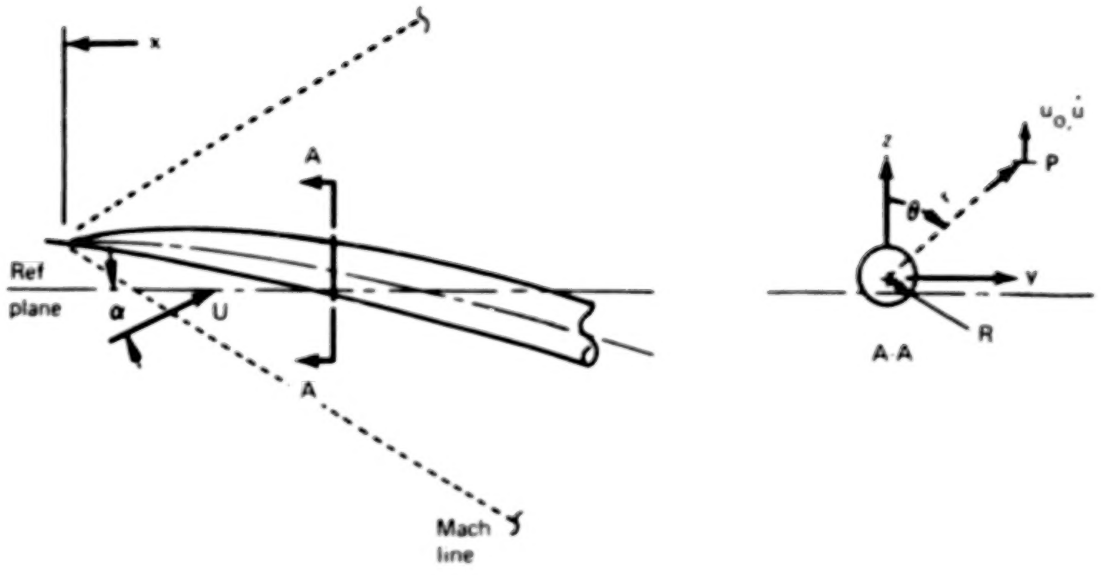

Upwash propagates along Mach lines.
Upwash at arbitrary point P is

$$\frac{w_o}{U} = u_o = \frac{1}{2\pi} \frac{dA(x)}{dx} \frac{z}{r^2} - \epsilon(x) \frac{R^2(x)}{r^2} \left(\frac{z^2 - y^2}{r^2} \right)$$

$$\frac{\dot{w}}{U} = \dot{u} = -\frac{R^2(x)}{r^2} \left(\frac{z^2 - y^2}{r^2} \right)$$

Where:

- u_o = upwash at input fuselage incidence ($\alpha = 0$)
- $\dot{u}$ = upwash increment per unit α
- $A(x)$, $R(x)$ = Fuselage cross sectional area, radius
- $\epsilon(x)$ = Fuselage incidence due to camber (relative to reference plane)
- z, y, r = location of point at which upwash is calculated
- α = angle of attack of reference plane
- U = free stream velocity

FIGURE 4.4-11.–FUSELAGE UPWASH CALCULATION (CIRCULAR CROSS SECTION)

The nondimensional radial velocity component is

$$\frac{1}{U}\phi_r = \frac{1}{2\pi r}\frac{dA(x)}{dx} - \frac{a+\epsilon(x)}{r^2}R^2(x)\cos\theta \tag{44}$$

and the tangential component is

$$\frac{1}{Ur}\phi_\theta = -[a+\epsilon(x)]\frac{R^2(x)}{r^2}\sin\theta \tag{45}$$

The vertical velocity component (upwash angle) is

$$\frac{w}{U} = \frac{1}{U}\phi_r\cos\theta - \frac{1}{Ur}\phi_\theta\sin\theta \tag{46}$$

Substituting for ϕ_r and ϕ_θ and converting to Cartesian coordinates gives

$$\frac{w}{U} = \frac{1}{2\pi}\frac{dA(x)}{dx}\frac{z}{r^2} - [a+\epsilon(x)]\frac{R^2(x)}{r^2}\left(\frac{z^2-y^2}{r^2}\right) \tag{47}$$

When the fuselage is at input incidence, the fuselage upwash is

$$u_0 = \frac{1}{2\pi}\frac{dA(x)}{dx}\frac{z}{r^2} - \epsilon(x)\frac{R^2(x)}{r^2}\left(\frac{z^2-y^2}{r^2}\right) \tag{48}$$

and the incremental upwash per degree angle of attack increase is

$$\dot{u} = \frac{d\,w/u}{da} = -\frac{R^2(x)}{r^2}\left(\frac{z^2-y^2}{r^2}\right) \tag{49}$$

Slender body theory assumes that the upwash field propagates normal to the body centerline. In the program, options are provided for the upwash field to be propagated either normal to the body centerline or along Mach lines (i.e., according to the characteristics of supersonic flow).

Fuselage of arbitrary cross-section. - In cases where the fuselage cross-section is significantly different from circular, or where the fuselage nose is open, or where discontinuities in longitudinal area distribution occur, an alternative fuselage solution may be selected. The cross-sectional shape for this option is input as sets of Y and Z coordinates at a series of longitudinal (X) stations.

The method used for the arbitrary cross-section fuselage solution has been referred to as general slender body theory. The computer program employed was developed by Bonner at Rockwell-International and was adapted for use in the present application. A description of the analysis is given in the Appendix and summarized here.

The perturbation velocity components due to the fuselage are obtained by a linear combination of two solutions:

- An axisymmetric solution (non-lifting) due to the thickness distribution of the equivalent body of revolution. The numerical method employs linearly varying line sources and sinks. Discontinuities in the area distribution (defined in the input definition) are treated by step perturbation functions.

- A cross-flow solution to account for fuselage angle of attack and cross-sectional shape. The method of conformal mapping of the known solutions for a circular contour is used for this analysis. Discontinuities in the fuselage longitudinal area distribution are treated by step perturbation functions.

The cross-flow solution is obtained through the conformal transformation solution of Theodorsen and Garrick (reference 20). The method is quite general, requiring principally that the cross-section contour must be simply connected and describable by a single valued function in polar coordinates about the centroid of the section.

Static pressures on the surface of the fuselage are computed and integrated over the surface contours to get isolated fuselage lift, drag, and pitching moment. Upwash flow angles in the plane of the wing are computed for the fuselage input angle of attack and per degree additional angle of attack and used in the wing/canard/tail solutions, as described on page 66.

Nacelle pressure field acting on wing. - The pressure field caused by the nacelles on the wing is calculated by the Whitham solution, as described in Section 4.3. The nacelles are assumed to be bodies of revolution, and the pressure signature due to each nacelle is calculated for a series of spanwise stations from wing root to tip. The composite pressure signature at a given spanwise station is the sum of the individual nacelle signatures, with all pressure coefficients doubled to account for reflection from the wing. Either "wrap" or "glance" nacelles may be used, as discussed in Section 4.3.

Pressure field due to asymmetric fuselage volume. - Another term in the superposition approach is associated with the growth in fuselage area above and below the wing. If the area growth is asymmetric (e.g., a low wing configuration), a differential pressure across the wing plane is created, which is additive to the effect created by the fuselage upwash field.

An approximate method of computing the asymmetric fuselage pressure field is employed, using the area distributions shown in figure 4.4-12. To the actual forebody area distribution is added the growth in fuselage area in the wing region relative to the area at the leading edge of the wing-fuselage intersection. This is done for both the below- and above-wing area distributions. Pressure signatures for both body representations are computed using the Whitham technique at a series of spanwise stations, doubled to account for reflection from the wing, and differenced to get the lifting pressure distribution due to asymmetric fuselage volume.

If the wing trailing edge is subsonic, the pressure fields above or below the wing revert to that corresponding to the actual fuselage area distribution in the region aft of a Mach line from the trailing edge of the wing-fuselage intersection.

Use of the asymmetric fuselage calculation is controlled by an input code in the computer program. If the asymmetric calculation is not requested, the fuselage pressure field corresponding to a mid-wing arrangement is calculated, so that there will always be a thickness pressure field due to the fuselage, if present, for use in limiting pressure calculations (discussed later).

Wing/Canard Solution in Presence of Fuselage and Nacelles

The wing or canard lifting pressure solution in the presence of fuselage and/or nacelles is performed as described for the isolated wing, with the following alterations:

- The local surface angles of attack are increased by the fuselage upwash values for the purposes of computing pressure coefficients. (To compute drag, the pressure coefficient is applied to the local surface slopes, only).

- In the region of the wing covered by the fuselage, the wing slopes are zeroed. This reflects the fact that the wing lift distribution in this region is of the "carry-over" type, only. (To compute drag, the carry- over lift is applied to the fuselage camber line shape.)

- The canard pressure distributions are computed in the same fashion as the wing pressure distribution, with the canard also creating a downwash (or upwash) field for the wing.

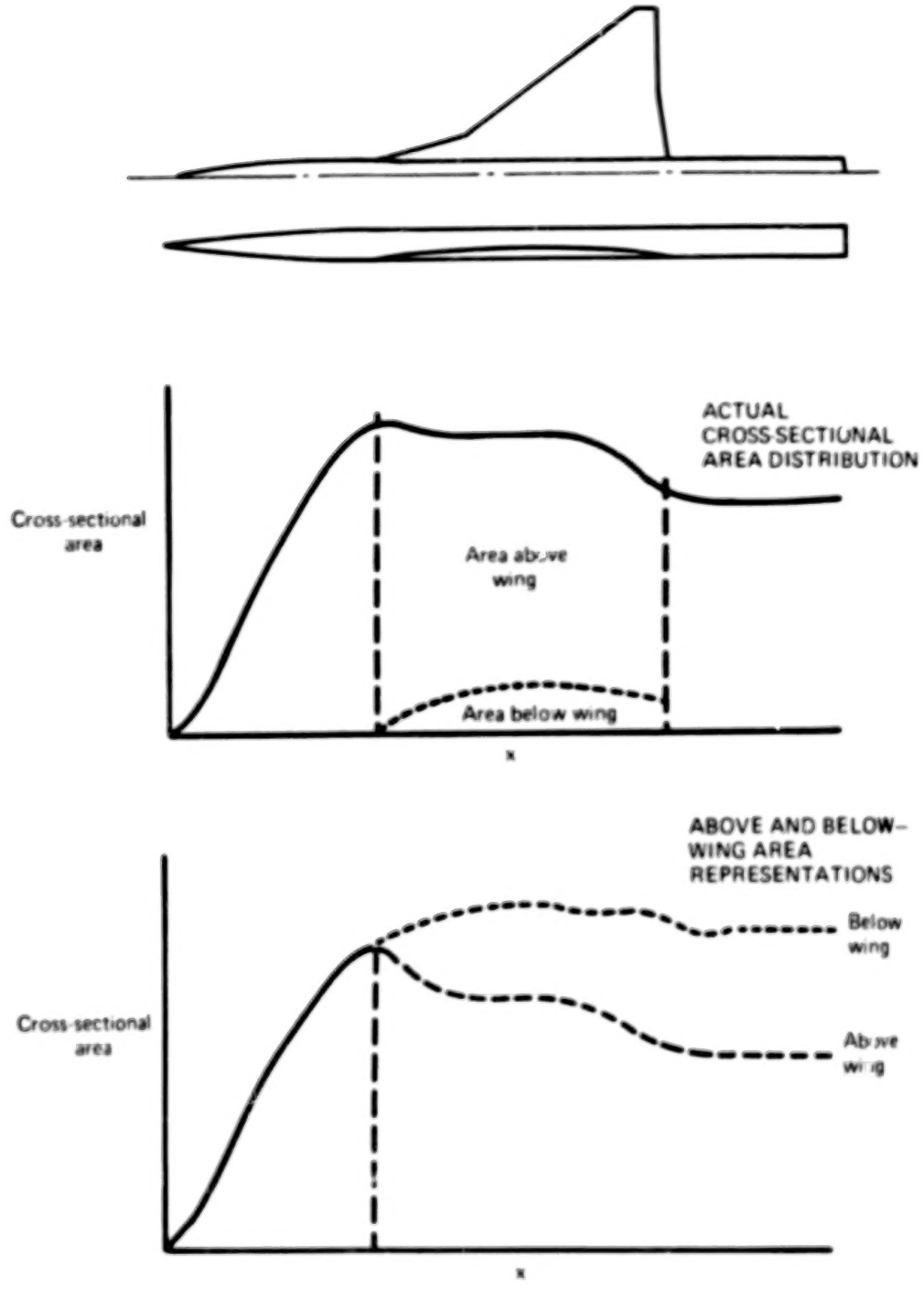

FIGURE 4.4-12.– FUSELAGE AREA REPRESENTATION FOR ASYMMETRIC FUSELAGE BUOYANCY FIELD

The nacelle or asymmetric fuselage volume pressure fields are superimposed upon the wing elements to obtain the effect of the nacelles or fuselage asymmetry on the wing. If nacelles are present, the buoyancy drag of the wing lifting pressures acting on the nacelle area distribution is also calculated. This term is obtained by transferring local wing pressures aft along Mach lines to act upon the nacelle area growth, in a fashion paralleling the wing-thickness-on-nacelle term of the near-field wave drag program.

Fuselage force coefficients in presence of wing. - Two different fuselage force coefficient solutions may be obtained in the program, corresponding to the circular cross-section or arbitrary cross-section solutions described previously.

Fuselage of circular cross-section. - From slender body theory, the fuselage lift distribution is given by

$$q \cdot R(x) = \frac{dA(x)}{dx}[\alpha + \varepsilon(x)] + A(x) \frac{d}{dx}[\varepsilon(x)] \qquad (50)$$

using the notation of figure 4.4-11.

The first term of the equation is the slender body term associated with a straight body at angle of attack; the second term is due to the curvature change associated with body camber.

In computing the fuselage lift distribution, the downwash (or upwash) from the wing/canard is included in the local angle of attack term, $\varepsilon(x)$. For drag computations, the lift is applied only to the physical fuselage attitude.

Fuselage force coefficients (lift, drag, and pitching moment) are calculated from the slender body lift distribution and converted to a wing reference area basis for summation into the complete configuration characteristics.

Fuselage of arbitrary cross-section. - Static pressures on the surface of the fuselage are computed and integrated over the surface contours to get fuselage lift, drag, and pitching moment. In computing the surface presssures, the downwash (or upwash) from the wing/canard is included in the local angle of attack term.

For the circular cross-section fuselage, the fuselage "camber drag" is computed by integrating the fuselage lift along the fuselage mean line, as noted above. For the arbitrary cross-section fuselage, there is no such meaningful Z reference line. For consistency in drag bookkeeping (and a direct comparison in case the cross-section is circular), the fuselage lift

along the Z centroid line is computed and printed. In addition, the integrated fuselage lift, drag, and pitching moment from the surface pressures are calculated for a series of fuselage angles of attack. The drag in this case consists of both drag due to thickness and drag due to angle of attack. An example of the fuselage data printout is given in Part 4 (Test Cases).

Horizontal tail solution. - The horizontal tail lifting pressure distribution is calculated in the presence of the fuselage upwash field and wing/canard downwash field. The solution employs the same logic of partitioning the tail into exposed and carry-over regions used in the wing and canard pressure computations.

Since the horizontal tail is assumed to be aft of the wing, the fuselage and wing/canard upwash (or downwash) field is first calculated, then the tail lift distribution and force coefficients are computed for the desired tail angles of attack. These are summed into the wing/fuselage, etc., solution for each tail angle, resulting in a set of force coefficients for each tail setting in the same fashion as wind tunnel data are obtained.

Calculation of the wing/canard downwash field is performed by extending the wing grid system aft to include the horizontal tail. With all pressure coefficients on the wing or canard previously established, the effect of the wing/canard on the horizontal tail is obtained from

$$\Delta_{W,C} = \sum_{\tau}^{\text{Wing}} \bar{R}\,(L^* - L, N^* - N)\,A\,(L, N)\,B(L, N)\,C(L, N)\,\Delta C_p\,(L, N) + \sum_{\tau}^{\text{Canard}} \bar{R}\,(L^* - L, N^* - N)\,A(L, N)\,B(L, N)\,C(L, N)\,\Delta C_p\,(L, N) \tag{51}$$

in which the wing, canard, and tail are all assumed to be located in essentially the same plane.

Calculations of the horizontal tail lifting pressures are then performed using the analysis form of the lifting pressure equation

$$\Delta C_p\,(L^*, N^*) = -\frac{4}{\beta}\frac{dz}{dx}\,(L^*, N^*) + \frac{1}{\pi}\sum_{\tau}^{\text{Tail}} \bar{R}\,(L^* - L, N^* - N)\,A(L, N)\,B(L, N)\,C(L, N)\,\Delta C_p\,(L, N) + \Delta_{W,C} \tag{52}$$

with the wing/canard term added to the summation of upstream effects. As in the wing/canard pressure solution, the fuselage upwash is added to the

physical tail slope for the purposes of computing lifting pressures, but removed for the calculation of the drag term. The carry-over lift of the horizontal tail is applied to the fuselage camber line to obtain the drag interference of the tail on the fuselage.

The effect of wing downwash on the horizontal tail lifting pressures is significant. The data of figure 4.4-13 show the theoretical drag and pitching moment increments at constant total lift for a typical configuration, with and without wing downwash included. (Comparisons of the theoretical calculations with experimental data are presented in the User's Manual, Part 2.)

Canard or horizontal tail downwash shift. - The lift analysis program contains a feature to shift the downwash field of wing or canard in the horizontal plane. The basic theoretical solution assumes the downwash field moves directly aft, instead of following the fuselage contour, as illustrated in figure 4.4-14. The shift feature can have significant influence on the calculated interference characteristics, as shown in figure 4.4-15. Program options allow for:

- No shift
- Shift according to the side-of-fuselage span stations of wing, canard, or tail.
- Shift according to an input dimension.

Superposition of Solutions

The arrangement of terms in the superposition of the complete configuration force coefficients is:

$$C_L = \Sigma C_{L_{\alpha=0}} + \alpha \Sigma \Delta C_L \tag{53}$$

$$C_m = \Sigma C_{m_{\alpha=0}} + \alpha \Sigma \Delta C_m \tag{54}$$

$$C_D = \Sigma C_{D_{\alpha=0}} + K_1 (C_L - C_{L_{\alpha=0}}) + K_2 (C_L - C_{L_{\alpha=0}})^2 \tag{55}$$

where the lift, drag, and pitching moment coefficients at $\alpha = 0$ correspond to

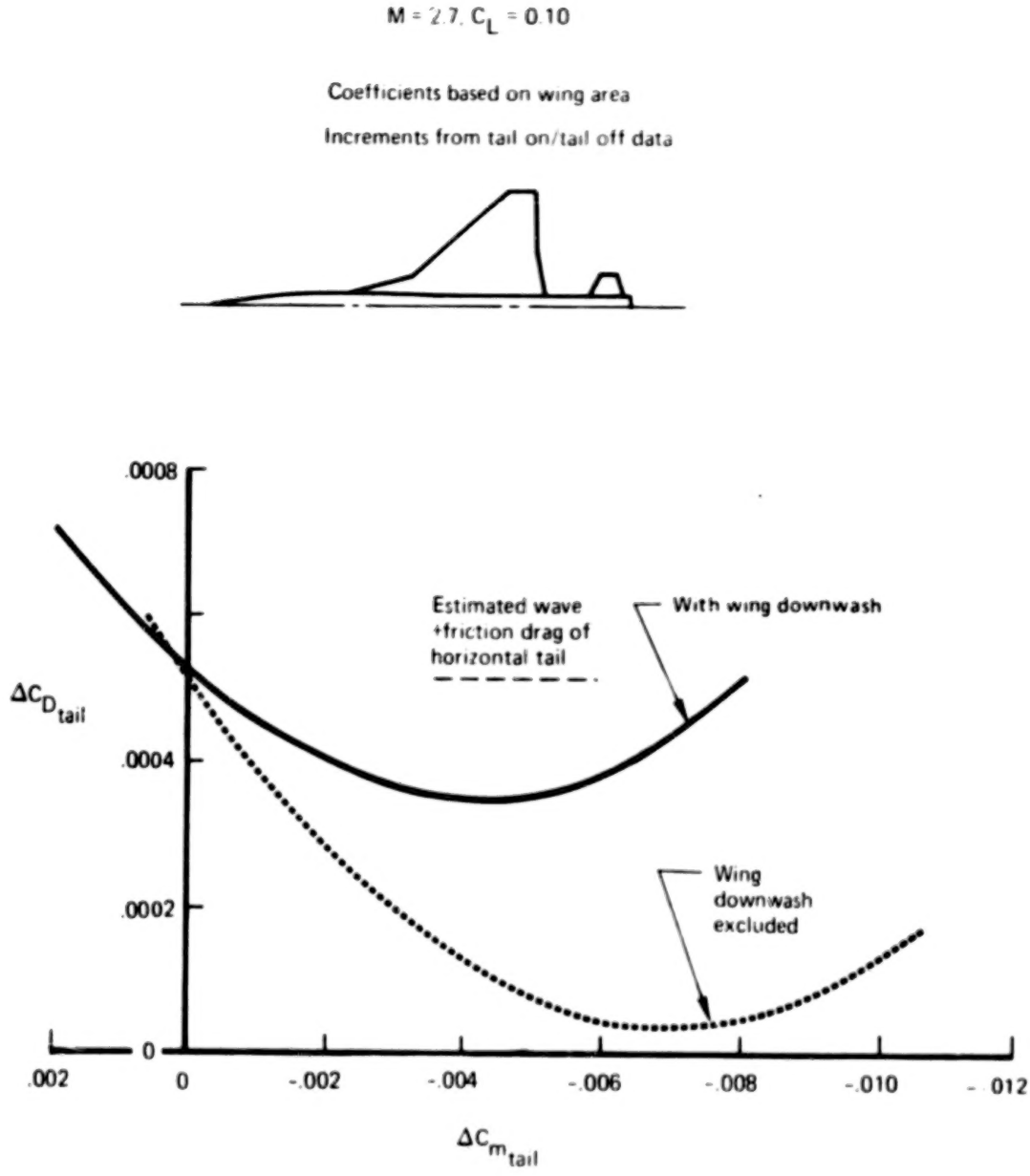

FIGURE 4.4-13.–EFFECT OF WING DOWNWASH ON TAIL (THEORETICAL ESTIMATE)

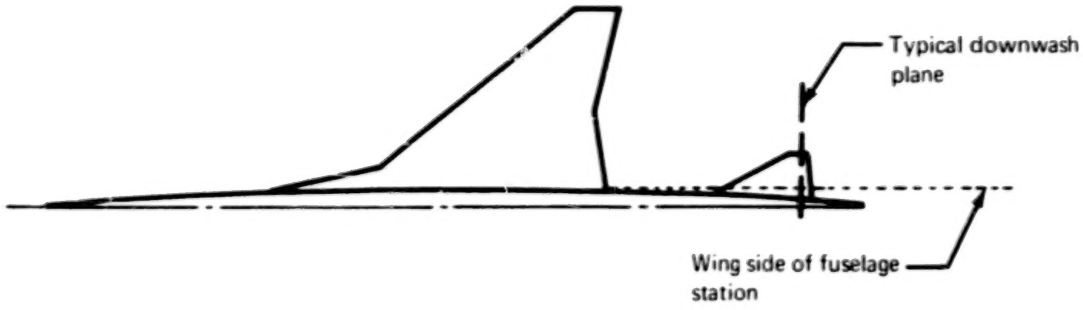

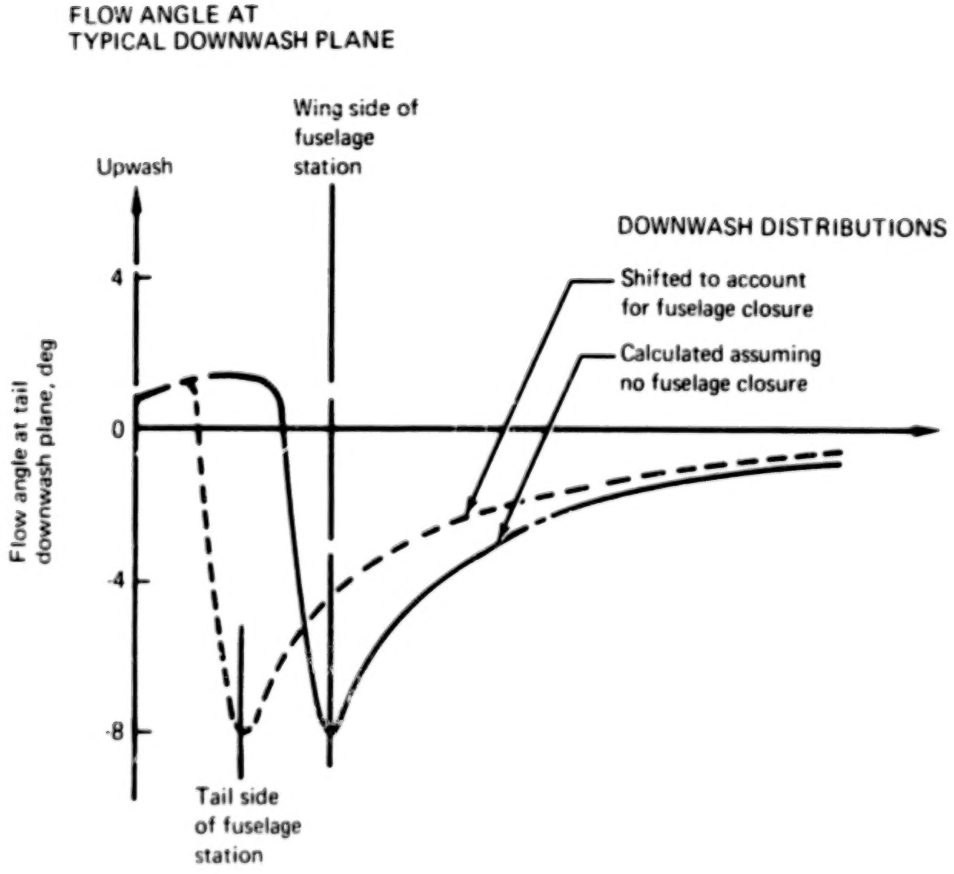

FIGURE 4.4-14.– DOWNWASH PATH CORRECTION

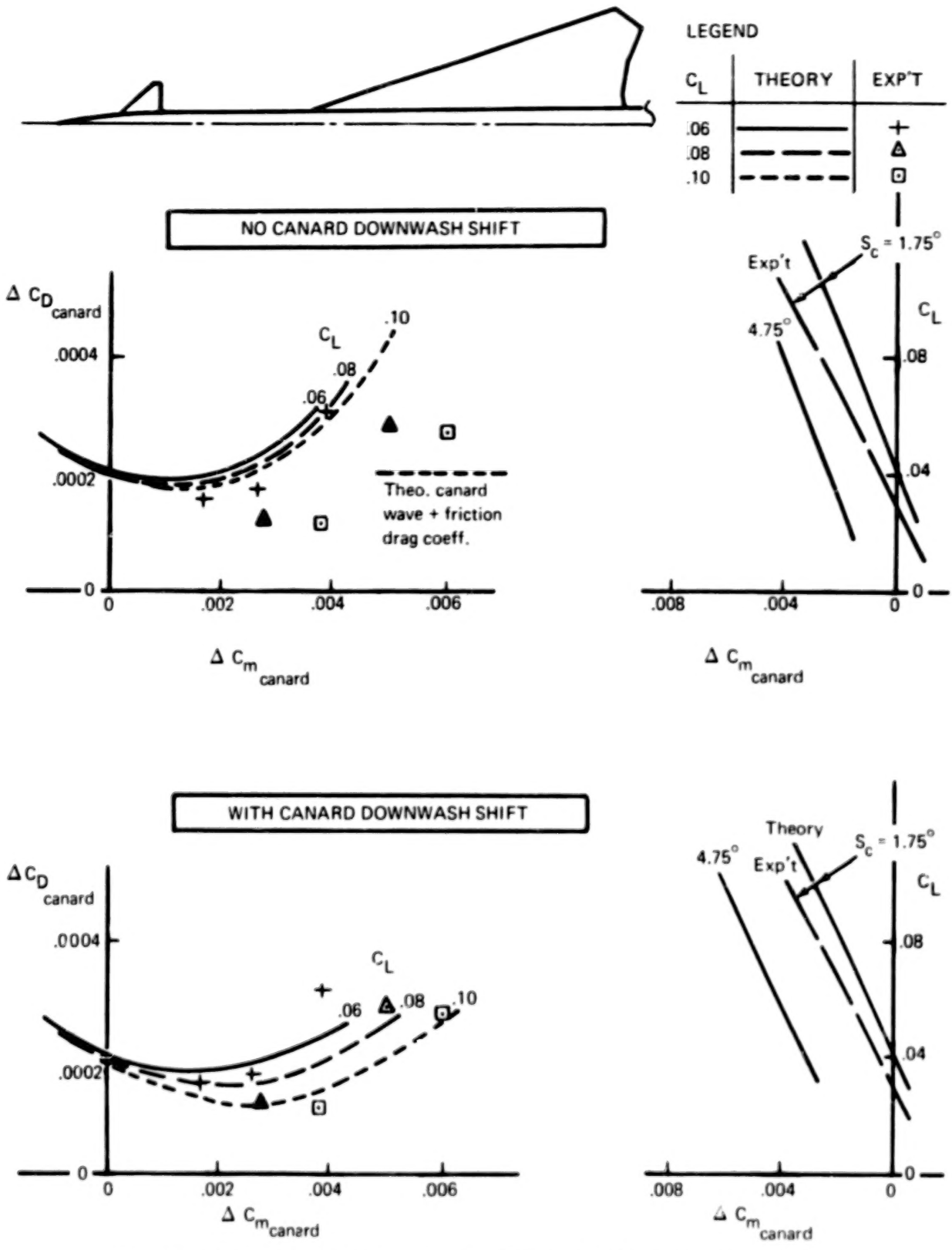

FIGURE 4.4-15.–EFFECT OF CANARD DOWNWASH SHIFT ~ M = 2.7

the individual fuselage, wing, tail, etc., solutions at input configuration incidence, and the ΔC_L and ΔC_m coefficients correspond to the incremental (flat wing) solutions per degree angle of attack.

The drag coefficient equation includes the interference terms between the solution at input incidence and the incremental solution per degree. With subscripts C and F denoting input incidence and the flat wing terms, respectively, the drag coefficient equation is:

$$C_D = C_{D_C} + (C_{D_{FOC}} + C_{D_{COF}}) \frac{\alpha}{\alpha_F} + \frac{\alpha}{\alpha_F} C_{L_F} \alpha \tag{56}$$

$$\text{or } C_D = C_{D_C} + \frac{(C_{D_{FOC}} + C_{D_{COF}})}{C_{L_F}} (C_L - C_{L_C}) + \frac{0.01745 (C_L - C_{L_C})^2}{C_{L_F}} \tag{57}$$

where α = configuration angle of attack

α_F = flat wing incidence, .01745 radian

$$C_{L_C} = \frac{1}{S} \Sigma \Delta C_{P_C} A_E \qquad C_{D_C} = \frac{1}{S} \Sigma \Delta C_{P_C} A_E \alpha_C$$

$$C_{L_F} = \frac{1}{S} \Sigma \Delta C_{P_F} A_E \qquad C_{D_F} = \alpha_F C_{L_F}$$

with A_E = local element area corresponding to ΔC_{P_C}

S = reference area

α_C = local element slope

$C_{D_{FOC}} = \frac{1}{S} \Sigma \Delta C_{P_F} A_E \alpha_C$ — interference drag of flat wing pressures acting on cambered wing slopes, per degree.

$C_{D_{COF}} = \alpha_F C_{L_C}$ — interference drag of cambered wing pressures acting on flat wing incidence, per degree.

with the summations carried out over the wing planform.

Therefore, for each of the solutions involved in the superposition, it is necessary to calculate both an input incidence solution, a flat wing solution, and the interference drag terms between the two solutions. All of the force coefficients are referred to an input area, moment center, and moment reference length in the summations.

Limiting pressure solution. - Linear theory imposes no restrictions on the allowable wing pressure coefficients. Particularly in the case of subsonic leading edge wings, large upper surface pressure coefficients may be computed near the outboard wing leading edge that exceed (are more negative than) pressure coefficients corresponding to a vacuum. These pressure coefficients can occur at moderate wing angles of attack, due to the strength of the upwash generated by the inboard wing.

Several investigators have examined experimental data to define the minimum attainable upper surface pressure coefficients. One such correlation is shown in figure 4.4-16 (from reference 16), which indicates a physical pressure coefficient limit of approximately .8 vacuum. The mechanism of this limiting is associated with local leading edge flow separation. However, the phenomenon may be approximated in the wing analysis program by limiting the calculated linear theory pressure coefficients to a specified fraction of vacuum Cp.

In the analysis program, pressure limiting is an optional feature, controlled by an input code. If limiting is requested, then a set of configuration angles of attack is required for the solution, since superposition will not apply after limiting occurs. Also, a definition of the wing thickness pressures is required (transferred over from the near field wave drag program module), since it is the sum of lifting plus thickness pressures that is limited, rather than the lifting pressure alone.

Pressure coefficients, as calculated, are separated into upper and lower surface values. Thickness pressures (wing plus fuselage) are added and the upper surface pressure coefficient tested against the limit pressure coefficient. If the limit is exceeded, the calculated lifting pressure coefficient is adjusted to a level which causes the total upper surface pressure coefficient to match the limit value.

Comparisons of the "limiter" calculations with measured force and pressure coefficient data are presented in figures 4.4-17 through 4.4-21 for 2 arrow wings of reference 1. Both were 70^{o} sweptback wings, having 3 percent biconvex airfoils, and wing design lift coefficients of 0 (flat) and .08.

The basic thickness pressure comparison is shown in figure 4.4-17. Comparisons of upper and lower surface pressure coefficients at lifting conditions of C_L = .13 and .25 are shown in figures 4.4-18 and 4.4-19. In the case of the flat wing (figure 4.4-18), several fractions of vacuum pressure coefficient are illustrated; the design C_L = .08 wing data are shown for .7 vacuum limiting only.

The limiter feature exhibits considerable improvement in the detail pressure coefficient comparisons over unlimited linear theory as C_L increases.

Force coefficient comparisons for the two wings are shown in figures 4.4-20 and 4.4-21. Pressure limiting at approximately .7 vacuum improves the comparisons appreciably at the higher C_L values.

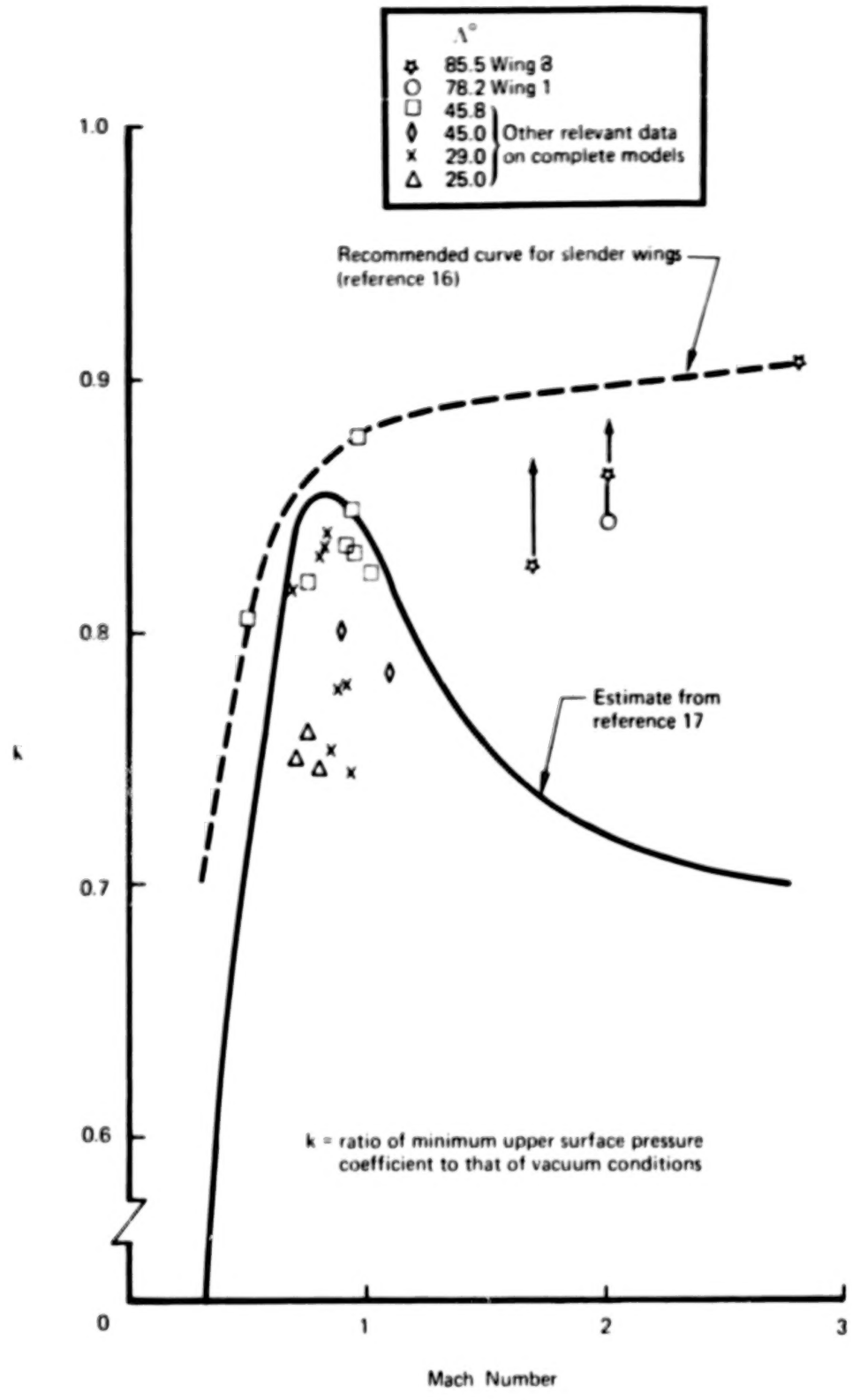

FIGURE 4.4-16.–MINIMUM ATTAINABLE PRESSURE COEFFICIENTS (FROM REF. 16)

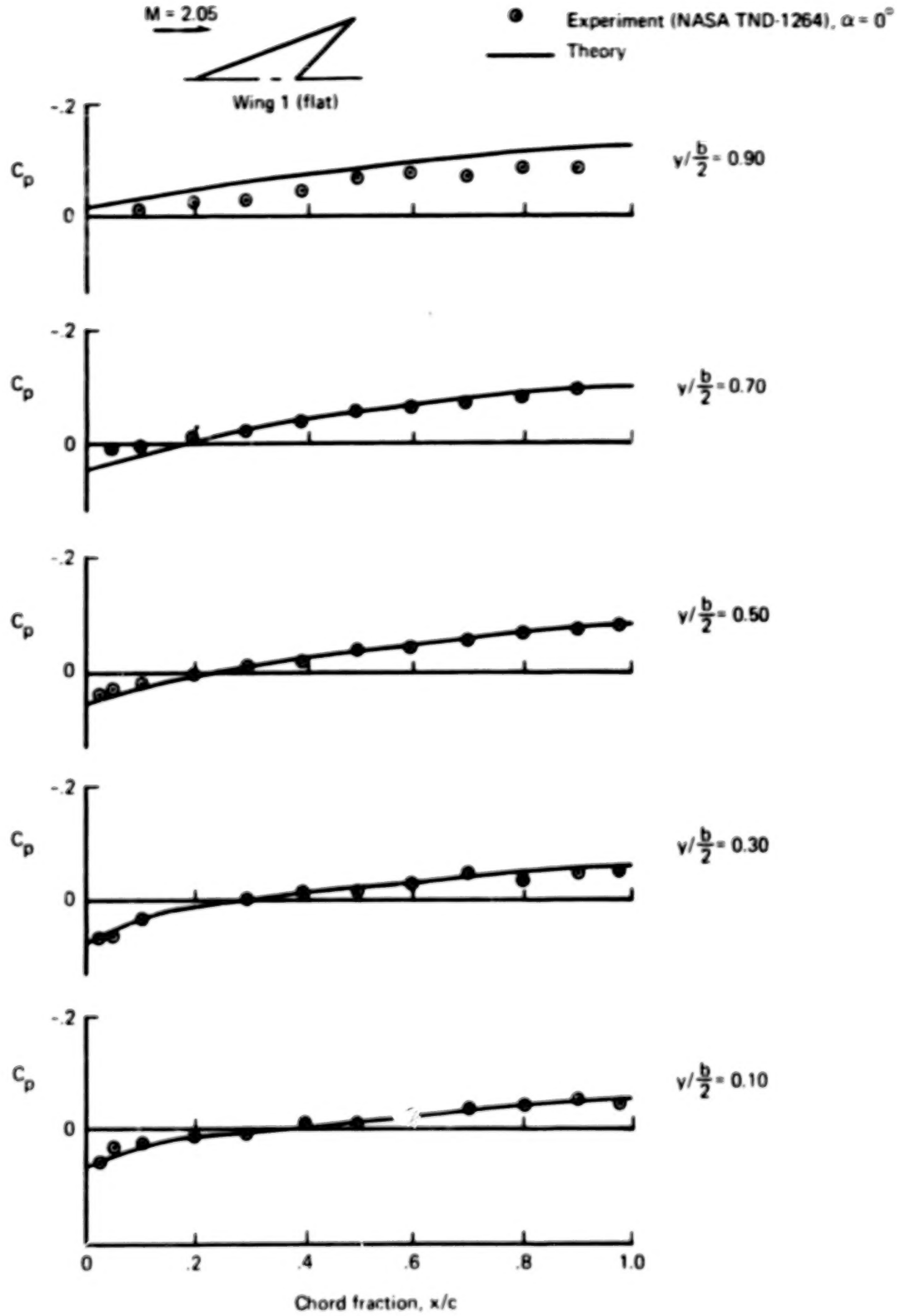

FIGURE 4.4-17.– THICKNESS PRESSURE COMPARISON (C_p DUE TO THICKNESS ONLY)

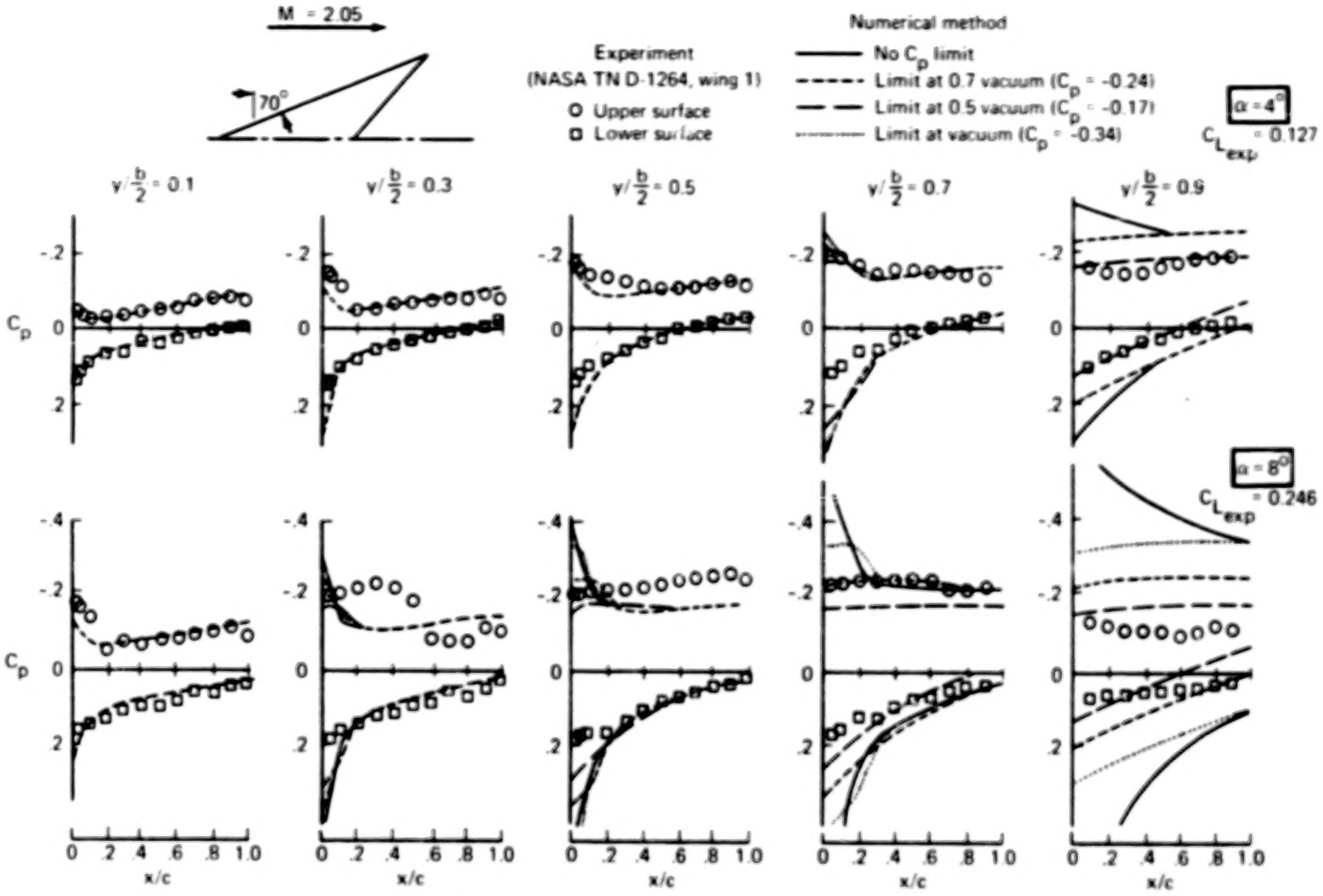

FIGURE 4.4-18.–PRESSURE COEFFICIENT COMPARISON, WING 1 (FLAT WING)

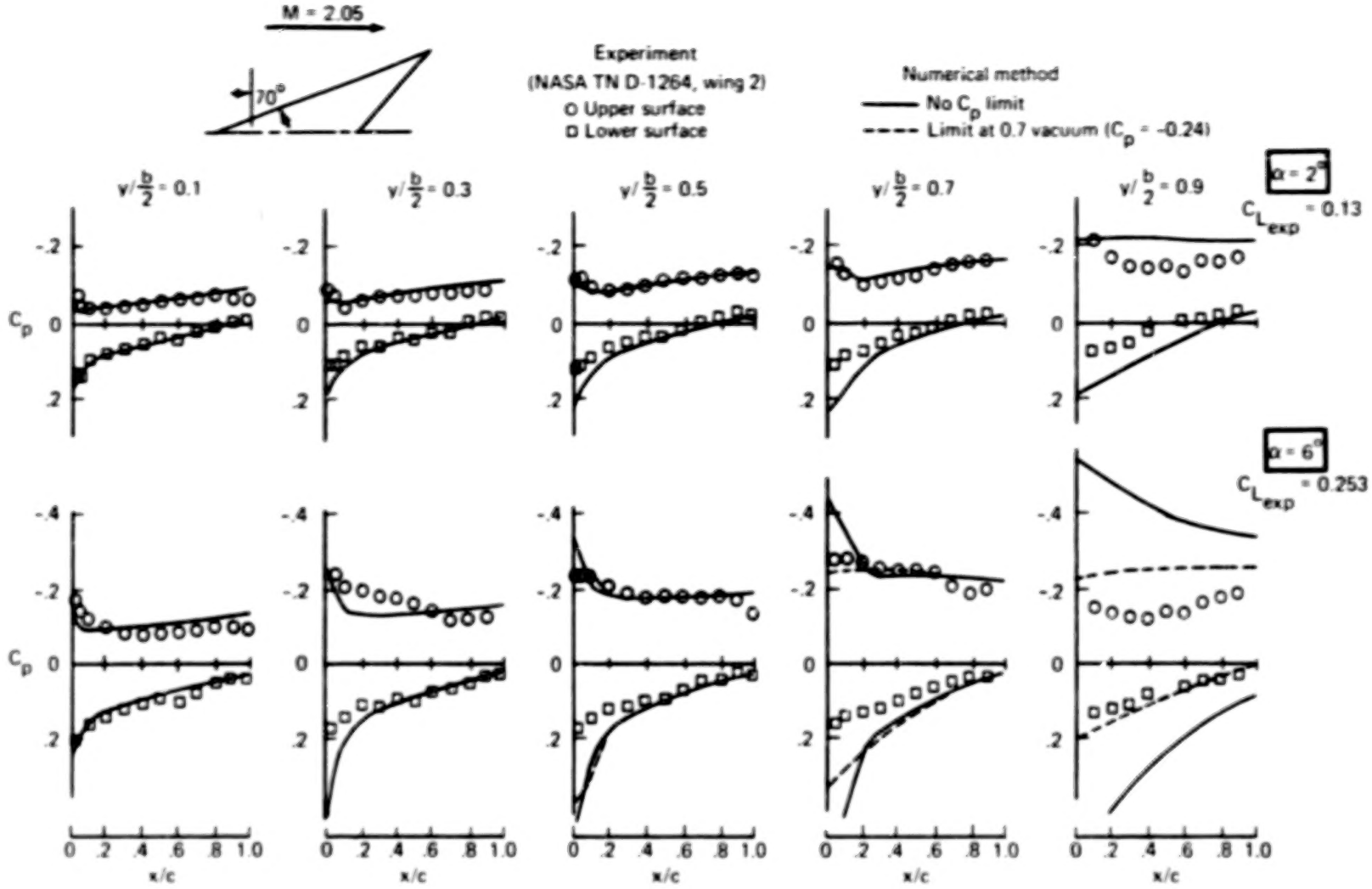

FIGURE 4.4-19.—PRESSURE COEFFICIENT COMPARISON, WING 2 (TWISTED AND CAMBERED WING, DESIGN C_L = .08)

BLANK PAGE

BLANK PAGE

CONTENTS

		Page	
1.0	SUMMARY	1	1/A6
2.0	INTRODUCTION	3	1/A8
3.0	SYMBOLS	5	1/A10
4.0	DISCUSSION	9	1/A14
	4.1 Skin Friction Drag	12	1/B4
	4.2 Far-Field Wave Drag	13	1/B5
	4.3 Near-Field Wave Drag	15	1/B7
	4.4 Drag-Due-to-Lift	[illegible]	1/D3
5.0	INTERACTIVE GRAPHICS	83	2/A7
	APPENDIX (General Slender Body Theory)	85	2/A10
	REFERENCES	97	2/B8

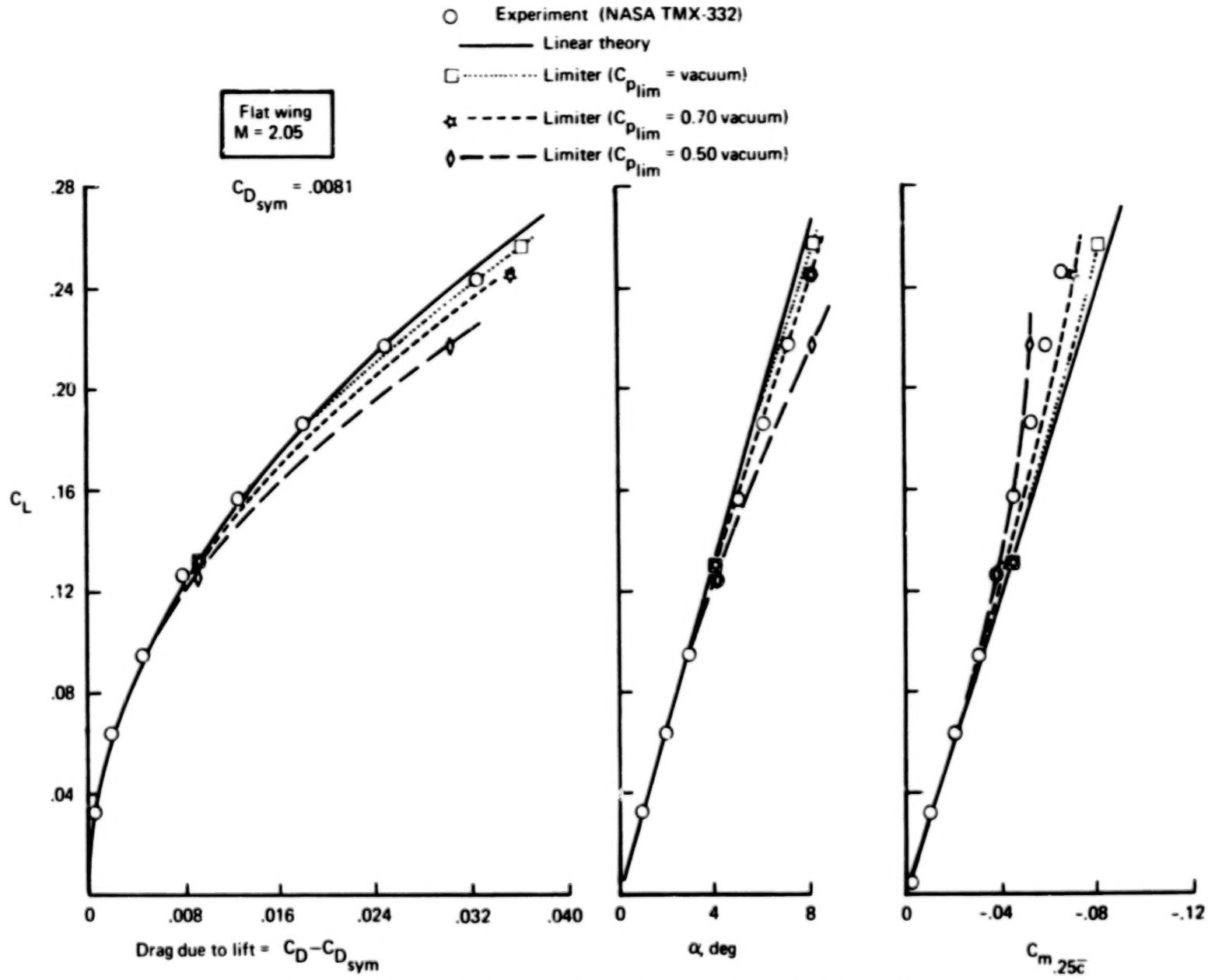

FIGURE 4.4-20.—TEST-THEORY COMPARISON, WING 1 (FLAT WING)

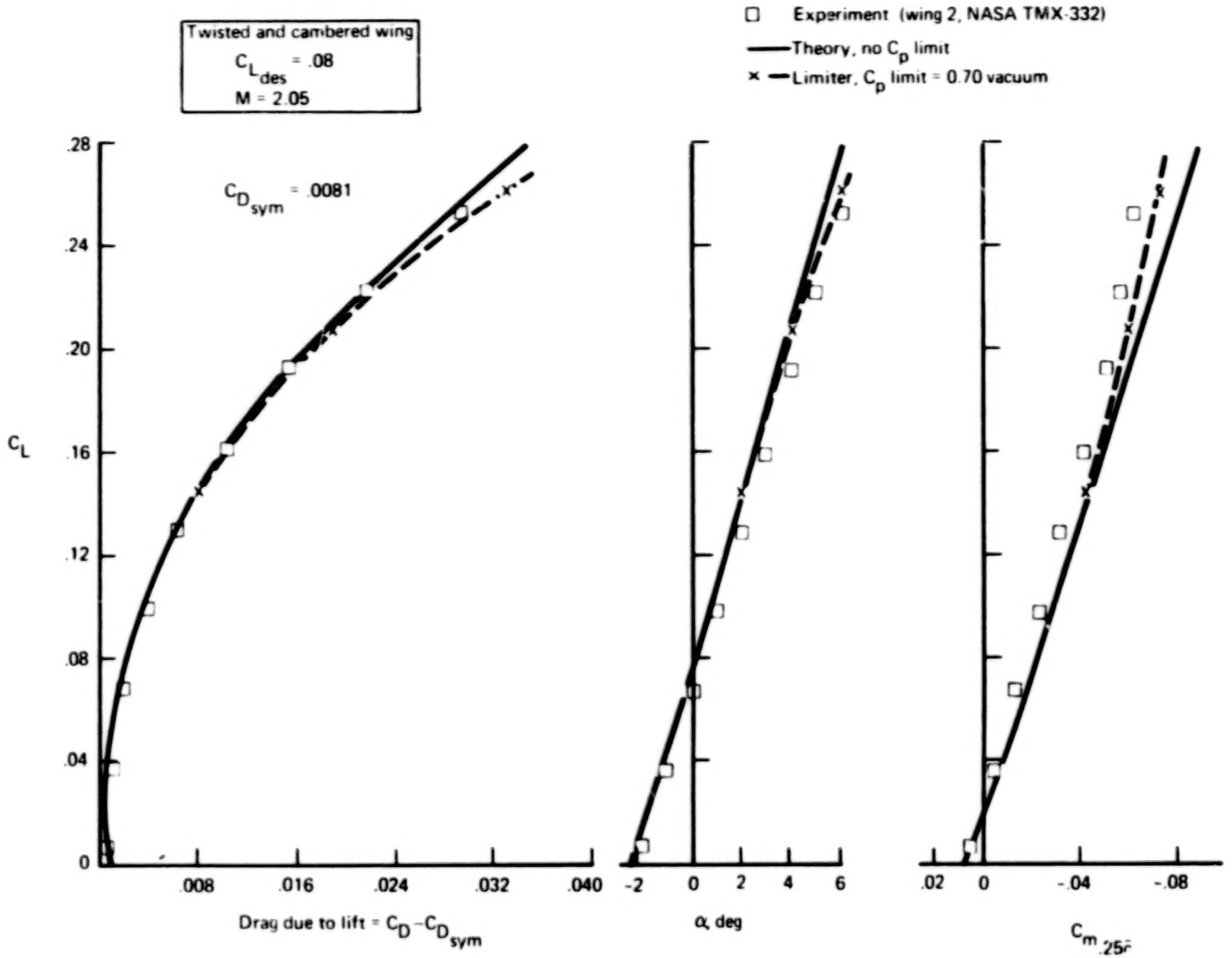

FIGURE 4.4-21.–TEST–THEORY COMPARISON, WING 2 ($C_{L_{des}}$ = 0.08)

5.0 INTERACTIVE GRAPHICS

Interactive graphics for use with the design and analysis system are optional, employing the NASA-LRC cathode ray tube (CRT) display and associated software. Use of the graphics option is requested by an executive control card (described in User's Manual, Part 2).

The principal uses of the graphics routines in the design and analysis system are to display the configuration, edit input geometry, and to display and/or alter the basic program calculations. Limited capability to redirect the system calculation sequence is available from the CRT console during program execution.

The CRT display and program coding for the interactive graphics setup are based on the NASA-LRC system. However, all display portions of the coding are subroutined or overlaid from the basic programs, so that the system could be readily converted to other CRT arrangements.

Details of the interactive graphics portion of the design and analysis system are given in (User's Manual, Part 2).

APPENDIX

General Slender Body Theory

The solution for a fuselage of arbitrary cross-sectional shape employs a computer program developed by E. Bonner at the Los Angeles Aircraft Division of Rockwell International. The computer program is described in detail in Rockwell report NA-74-687, which is excerpted here to supplement the theory description on page 65 of this report. Nomenclature in this section, which is taken from the Rockwell report, is presented on page 93.

Theoretical approach. - The approach used has been referred to in the literature as general slender body theory. The solution is based on limiting (slender body) solutions to the three dimensional non-linear potential small perturbation equations of motion.

$$[1 - M_\infty^2 - (r+1) M_\infty^2 \phi_x / U_\infty] \phi_{xx} + \phi_{yy} + \phi_{zz} = 0. \tag{1}$$

with bounding conditions

$$\frac{\partial \phi}{\partial n} = 0 \text{ on } \tilde{S}$$

The perturbation velocity potential on the surface and in the neighborhood of a slender three-dimensional system satisfying equation (1) is in the form

$$\phi(x, y, z, M_\infty) = \phi_2(y, z; x) + g(x, M_\infty) \tag{2}$$

for $\sqrt{M_\infty^2 - 1}\, \frac{r}{x} << 1$

ϕ_2 is the solution of Laplace's equation

$$(\phi_2)_{yy} + (\phi_2)_{zz} = 0 \tag{2a}$$

satisfying three dimensional boundary conditions in the YZ plane at the axial station X and g is a contribution dependent on Mach number and the equivalent body of revolution but not on the shape of the contour. The crossflow solution ϕ_2 is in general comprised of the following three terms:

$$\phi_2(y, z, x) = \phi_{2,t} + \phi_{2,\alpha} + \phi_{2,\beta} \tag{3}$$

where $\phi_{2,t}$ is the two dimensional incompressible flow solution for expansion

or contraction of the section (thickness problem) and $\phi_{2,\alpha}$ and $\phi_{2,\beta}$ are the solutions for angle of attack or sideslip, respectively. The method of conformal mapping of the known solutions for a circular contour is used for this analysis.

The solutions for a non-lifting body of revolution are used to establish the function g appearing in equation 2:

$$g(x, M_\infty) = \lim_{r \to 0} [\, \phi_B(x, r, M_\infty) - \phi_{2,B}(y, z; x) \,] \tag{4}$$

where $\phi_{2,B} = U_\infty / 2\pi \; S'(x) \ln r$ and ϕ_B are the crossflow thickness and total thickness solution, respectively. The latter term is established from the more simple problem of compressible axisymmetric flow

$$[\, 1 - M_\infty^2 - M_\infty^2 \tfrac{\gamma+1}{U_\infty} \phi_x \,] \phi_{xx} + \phi_r / r + \phi_{rr} = 0 \tag{5}$$

The three dimensional perturbation potential is obtained from a superposition of the crossflow and axisymmetric solution.

$$\phi = \phi_{2,\alpha} + \phi_{2,\beta} - \phi_{2,B} + \phi_B \tag{6}$$

The body axes Cartesian velocity components u, v, w follow from the standard potential differentations ϕ_x, ϕ_y, and ϕ_z, respectively.

Crossflow solution. - The approach here is to transform the known complex potential solutions (ref. 21, p. 29) due to thickness and attitude for a circular contour with the center at the origin to the boundary of interest using conformal mapping theory. (The transformed boundary encompasses the class of simply connected contours which are describable by a single valued function in polar coordinates about a centered origin.)

$$W_{2,B} = r v_r \ln \sigma = \frac{U_\infty S'(x) \ln \sigma}{2\pi} \tag{7}$$

$$W_{2,\mu} = -i v_c e^{-i\mu} (\sigma - R_0^2 e^{2i\mu} / \sigma) \tag{8}$$

$$\phi_2 + i \psi_2 = W[\, \sigma(\zeta) \,] = W(\sigma) \tag{9}$$

ζ and σ are the complex variables in the physical and transformed plane, respectively, as shown in the sketch below:

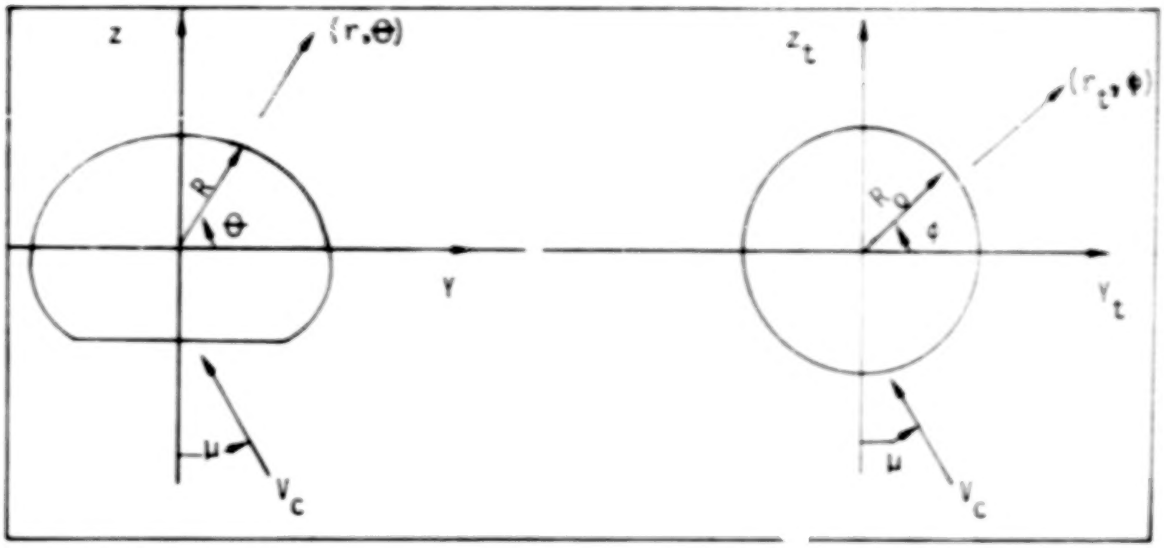

ζ Plane σ Plane

ζ and σ are related by the general series

$$\zeta = \sigma + a_0(x) + \frac{a_1(x)}{\sigma} + \frac{a_2(x)}{\sigma^2} + \ldots = \sum_{n=-1}^{\infty} \frac{a_{n(x)}}{\sigma^n} \tag{10}$$

The evaluation of the transformation constants a_n is accomplished according to the method of Theodorsen and Garrick (ref. 20) by casting the mapping into the equivalent form

$$\zeta = \sigma\, e^{\sum_{1}^{\infty} C_n / \sigma_n} \tag{11}$$

The constants C_n are related to the physical contour by the following set of integral equations:

$$C_n = A_n + i\, B_n = \frac{R_0^n}{\pi} \int_0^{2\pi} e^{in\sigma} \ln R \, d\phi \tag{12}$$

where

$$\ln R_0 = \frac{1}{2\pi}\int_0^{2\pi} \ln R \, d\phi \tag{13}$$

and

$$\phi = + \sum_{n=1}^{\infty} \left[\frac{A_n}{R_0^n} \sin n\phi - \frac{B_n}{R_0^n} \cos n\phi \right] \tag{14}$$

This set of expressions is solved by the method of successive approximations using the known function $R(\theta)$ describing the actual contour as initial data.

The original set of mapping constants a_n of equation (10) are related to the constants C_n by

$$\begin{aligned} a_0 &= C_1 \\ a_1 &= C_1 \frac{2}{2} + C_2 \\ &\vdots \\ a_{n-1} &= \frac{1}{n} \sum_{n'=1}^{n-1} n' \, a_{n-n'-1} C_{n'} + C_n \end{aligned} \tag{15}$$

Contour points in the physical plane (R_i, θ_i) are located in the transformed plane by $\sigma = R_0 e^{i\phi_i}$ where $\phi_i(\theta_i)$ is given by equation (14). Transformed field points are established by rearranging equation (10) in the following successive approximation form:

$$\sigma_{j+1} = \zeta - a_0 - \frac{a_1}{\sigma_j} - \frac{a_2}{\sigma_j^2} - \frac{a_3}{\sigma_j^3} - \cdots \tag{16}$$

$$\sigma_1 = \zeta \tag{17}$$

It has been established that the transformation procedure is satisfactory for a wider variety of "fuselage-like" contours using 25 transformation terms or less ($n \leq 25$).

The crossflow solution perturbation velocity components due to thickness and angle of attack are

$$\frac{u_{2,t}}{U_\infty} = \frac{1}{2\pi} \text{ R.P. } [S'(x) \frac{1}{\sigma} \frac{d\sigma}{dx} + S''(x) \ln \sigma]$$

$$\frac{v_{2,t}}{U_\infty} = \frac{S'(x)}{2\pi} \text{ R.P. } \frac{1}{\sigma} \frac{d\sigma}{d\zeta} \tag{18}$$

$$\frac{w_{2,t}}{U_\infty} = -\frac{S'(x)}{2\pi} \text{ I.P. } \frac{1}{\sigma} \frac{d\sigma}{d\zeta}$$

$$\frac{u_{2,\alpha}}{U_\infty \alpha(x)} = \text{I.P.} \left\{ \left[\left(\frac{R_o}{\sigma} \right)^2 + 1 \right] \frac{d\sigma}{dx} - 2R_o \frac{dR_o}{dx} \frac{1}{\sigma} \right\} + \frac{dz_o}{dx} + \frac{1}{\alpha(x)} \frac{d^2 z_o}{dx^2} \text{ I.P.} \left[\frac{R_o^2}{\sigma} - \sigma - \zeta - a_o \right]$$

$$\frac{v_{2,\alpha}}{U_\infty \alpha(x)} = \text{I.P.} \left[\left(\frac{R_o}{\sigma} \right)^2 + 1 \right] \frac{d\sigma}{d\zeta} \tag{19}$$

$$\frac{w_{2,\alpha}}{U_\infty \alpha(x)} = \text{R.P.} \left[\left(\frac{R_o}{\sigma} \right)^2 + 1 \right] \frac{d\sigma}{d\zeta} - 1$$

where $\alpha(x) = \alpha - dz_o/dx$

Axisymmetric solution. - The linearized thickness solution is numerically evaluated by the superposition of K linearly varying finite line sources and sinks.

$$\Phi_B(x, r, M_\infty) = -\int_{-\infty}^{x-\beta r} \frac{f(\xi) d\xi}{\sqrt{(x-\xi)^2 - \beta^2 r^2}} \tag{20}$$

where

$$f(\xi) = \sum_{k=1}^{k} a_k \ (\xi - \xi_k) \quad : \quad \xi_k \leq \xi \leq ? \tag{21}$$

thus

$$\phi_B (x, r, M_\infty) = \sum_{k=1}^{k} \phi_k \ (x, r, M_\infty) \tag{22}$$

and

$$\phi_k (x, r, M_\infty) = \int_{x_k}^{x - Br} \frac{- a_k \ (\xi - x_k) \ d\xi}{\sqrt{(x - \xi)^2 - \beta^2 r^2}} \tag{23}$$

The unit velocity components in cylindrical coordinates

$$\begin{aligned} u_k (x,4) &= \partial\phi_k / \partial x \\ v_k (x,r) &= \partial\phi_k / \partial r \end{aligned} \tag{24}$$

are given by

$$\begin{aligned} u_k (x,r) &= - \cosh^{-1} \frac{x - x_k}{\beta r} \rightarrow - \ln \frac{2}{\beta} \frac{x - x_k}{r} \\ v_k (x,r) &= \beta \sqrt{\left(\frac{x - x_k}{\beta r}\right)^2 - 1} \rightarrow \frac{x - x_k}{r} \end{aligned} \tag{25}$$

The axisymmetric solution velocities are obtained from the sum of the individual line contributions

$$u_B(x,r) = \sum_{k=1}^{K} a_k \; u_k(x,r) = \frac{\partial \Phi_B}{\partial x}$$

$$v_B(x,r) = \sum_{k=1}^{K} a_k \; v_k(x,r) = \frac{\partial \Phi_B}{\partial r} \qquad (26)$$

The unknown line source constraints, a_K, are established by satisfying the flow tangency condition at the surface of the body through solving the associated set of simultaneous equations.

Complete solution. - The total perturbation velocity components are obtained by a linear combination of the crossflow and axisymmetric solutions.

$$\frac{u}{U_\infty} = \frac{u_{2,t}}{U_\infty} + \frac{u_{2,\alpha}\,\alpha(x)}{\alpha(x)\,U_\infty} + \frac{u_{2,\beta}\,\beta}{\beta U_\infty} - \frac{S''(x)\,\ln R}{2\pi} + \frac{u_B(x,r)}{U_\infty}$$

$$= \frac{\partial \Phi}{\partial x} - 1$$

$$\frac{v}{U_\infty} = \frac{v_{2,t}}{U_\infty} + \frac{v_{2,\alpha}\,\alpha(x)}{\alpha(x)\,U_\infty} + \frac{v_{2,\beta}\,\beta}{\beta U_\infty} - \frac{S'(x)\,\cos\theta}{2\pi\;\;R} + \frac{v_B(x,r)\,\cos\theta}{U_\infty} \qquad (27)$$

$$= \frac{\partial \phi}{\partial y} + \beta$$

$$\frac{w}{U_\infty} = \frac{w_{2,t}}{U_\infty} + \frac{w_{2,\alpha}}{\alpha(x)U_\infty} + \frac{w_{2,\beta}\,\beta}{\beta U_\infty} - \frac{S'(x)\,\sin\theta}{2\pi\;\;R} + \frac{v_B(x,r)\sin\theta}{U_\infty}$$

$$= \frac{\partial \phi}{\partial z} - \alpha$$

Where the last term on the right hand side is the equivalent body of revolution surface result.

The static pressure coefficient is established from these velocities using the body axis small perturbation form of Bernoulli's equation:

$$C_p = -2\left[\frac{u}{U_\infty} - \frac{v\,\beta}{U_\infty} + \frac{w\quad \alpha(x)}{U_\infty}\right] - \left(\frac{v}{U_\infty}\right)^2 - \left(\frac{w}{U_\infty}\right)^2 \qquad (28)$$

NOMENCLATURE

a_k	k^{th} line source coefficient, equation (23)
a_n	Conformal transformation complex constants, equations (10), (15)
c_n	Conformal transformation complex constants, equation (12)
C_p	Static pressure coefficient
$f(\xi)$	Source strength per unit length
g	Equation (4)
I.P.	Imaginary part
M	Freestream Mach number
R	Radius of equivalent body
R.P.	Real part
R_o	Contour radius in transformed plane, equation (13) and figure on page 87
S	Equivalent body cross sectional area
S'	$\frac{dS}{dx}$
$\tilde{S}$	Arbitrary surface
u, v, w	Body axis longitudinal, lateral, and vertical perturbation velocities
u_B, v_B	Equivalent body axial and radial perturbation velocities, equation (29)
u_k, v_k	k^{th} line source unit axial and radial perturbation velocity, equations (27), (28)
u_2	$= \frac{\partial \phi_2}{\partial x} = \text{R.P.} \frac{\partial w}{\partial x}$
v_2	$= \frac{\partial \phi_2}{\partial y} = \text{R.P.} \frac{\partial w}{\partial \sigma} \frac{d\sigma}{d\zeta}$
w_2	$= \frac{\partial \phi_2}{\partial z} = -\text{I.P.} \frac{dw}{d\sigma} \frac{d\sigma}{d\zeta}$
$u_{2,t}$, $v_{2,t}$, $w_{2,t}$	Crossflow perturbation velocities due to thickness (growth)

$u_{2,\alpha}$, $v_{2,\alpha}$, $w_{2,\alpha}$	Cross flow perturbation velocities due to angle of attack (vertical translation)
$u_{2,\beta}$, $v_{2,\beta}$, $w_{2,\beta}$	Crossflow perturbation velocities due to sideslip (lateral translation)
U_∞	Freestream velocity
V_c	Cross flow velocity, $U_\infty \sqrt{\alpha^2(x) + \beta^2}$
W	Physical plane complex potential, $\phi_2 + i\psi_2$
$W_{2,B}$	Transformed plane complex potential due to thickness
$W_{2,\mu}$	Transformed plane complex potential due to attitude
x, r, θ	Physical plane cylindrical coordinate system
x, r_i, ϕ	Transformed plane cylindrical coordinate system
x, y, z	Right-hand body axis Cartesian coordinate system
x_k	k^{th} line source origin
$\frac{d\zeta}{d\sigma}$	mapping derivative (equation (18)) $= 1 - \frac{1}{\sigma} \sum_{\eta=1}^{\infty} \eta \frac{a_\eta}{\sigma^\eta}$
$\frac{d\sigma}{dx}$	mapping derivative (equation (18)) $= -\frac{d\sigma}{d\zeta} \sum_{\eta=0}^{\infty} \frac{1}{\sigma_\eta} \frac{da_\eta}{dx}$
z_0	z location of conformal centroid, I.P. a_0
α	Angle of attack
$\alpha(x)$	$\alpha - dz_0/dx$
β	$\sqrt{M^2 - 1}$ or sideslip angle
γ	Ratio of specific heat
ζ	Complex variable in physical plane, $y + iz$
μ	See figure on page 87
ξ	Dummy axial variable
σ	Complex variable in transformed plane, $y_t + iz_t$

ϕ	Total perturbation velocity potential*
ϕ_B	Axisymmetric perturbation potential
ϕ_2	Crossflow potential
$\phi_{2,B}$	$\phi_{2,t}$ for circular contour, equation (7)
$\phi_{2,t}$	Crossflow perturbation potential due to thickness
$\phi_{2,\alpha}$	Crossflow perturbation potential due to angle of attack
$\phi_{2,\beta}$	Crossflow perturbation potential due to sideslip
Φ	Total velocity potential, $U_\infty [x - \beta y + \alpha z] + \phi$
$\longrightarrow$	Limiting (slender body) result

SUBSCRIPTS:

B	Equivalent body
C	Centroid of contour
k	k^{th} line source
x, y, z, r	∂/∂_x, ∂/∂_y, ∂/∂_z, ∂/∂_r
xx, yy, zz, rr	$\partial^2/\partial x^2$, $\partial^2/\partial y^2$, $\partial^2/\partial x^2$, $\partial^2/\partial r^2$

* All potentials are dimensional.

BLANK PAGE

BLANK PAGE

REFERENCES

1. Carlson, Harry W.; and Harris, Roy V., Jr.: A Unified System of Supersonic Aerodynamic Analysis. NASA SP-228, 1970, pp. 639-658.

2. Sommer, Simon C.; and Short, Barbara J.: Free-Flight Measurements of Turbulent-Boundary-Layer Skin Friction in the Presence of Severe Aerodynamic Heating at Mach Numbers From 2.8 to 7.0. NACA TN 3391, 1955.

3. Harris, Roy V., Jr.: An Analysis and Correlation of Aircraft Wave Drag. NASA TM X-947, 1964.

4. Von Kármán, Th.: The Problem of Resistance in Compressible Fluids. R. Accad. d'Italia, Cl. Sci. Fis., Mat. e Nat., vol. XIII, 1935, pp. 210-265.

5. Sheppard, L. M.: Methods for Determining the Wave Drag of Non-Lifting Wing Body Combinations. ARC Technical Report R&M No. 3077, 1958.

6. Lighthill, M. J.: Supersonic Flow Past Slender Bodies of Revolution, the Slope of Whose Meridian Section is Discontinuous. Quarterly J. Mech. & Appl. Math., vol. I, pt. 1, Mar. 1948, pp. 90-102.

7. Whitham, G. B.: The Flow Pattern of a Supersonic Projectile. Commun. Pure & Appl. Math., vol. V, no. 3, Aug. 1952, pp. 301-348.

8. Middleton, Wilbur D.; and Carlson, Harry W.: A Numerical Method for Calculating Near-Field Sonic-Boom Pressure Signatures. NASA TN D-3082, 1965.

9. Carlson, Harry W.; and Middleton, Wilbur D.: A Numerical Method for the Design of Camber Surfaces of Supersonic Wings With Arbitrary Planforms. NASA TN D-2341, 1964.

10. Middleton, Wilbur D.; and Carlson, Harry W.: A Numerical Method for Calculating the Flat-Plate Pressure Distributions on Supersonic Wings of Arbitrary Planform. NASA TN D-2570, 1965.

11. Sorrells, Russell B.; and Miller, David S.: Numerical Method for Design of Minimum-Drag Supersonic Wing Camber With Constraints on Pitching Moment and Surface Deformation. NASA TN D-7097, 1972.

12. Carlson, Harry W.; and Miller, David S.: Numerical Methods for the Design and Analysis of Wings at Supersonic Speeds. NASA TN D-7713, 1974.

13. Lomax, Howard; Heaslet, Max A.; and Fuller, Franklyn B.: Integrals and Integral Equations in Linearized Wing Theory. NACA Rep. 1054, 1951.

14. Grant, Frederick C.: The Proper Combination of Lift Loadings for Least Drag on a Supersonic Wing. NACA Rep. 1275, 1956.

15. Sears, W. R., ed.: General Theory of High Speed Aerodynamics. Princeton Univ. Press, 1954.

16. Fellows, K. A.; and Carter, E. C.: Results and Analysis on Two Isolated Slender Wings and Slender Wing-Body Combinations at Supersonic Speeds. Part 1 - Analysis. ARC C.P. 1131, 1970.

17. Rolf, E. F.: Note on the Maximum Attainable Suction on a Body in an Airstream. ARC 16062, 1953.

18. Carlson, Harry W.; and Mack, Robert J.: Estimation of Leading-Edge Thrust for Supersonic Wings of Arbitrary Planform. NASA TP-1270, 1978.

19. Carlson, Harry W.; Mack, Robert J.; and Barger, Raymond L.: Estimation of Attainable Leading-Edge Thrust for Wings at Subsonic and Supersonic Speeds. NASA TP-1500, 1979.

20. Theodorsen, T.; and Garrick, I. E.: General Potential Theory of Arbitrary Wing Sections. NACA Rep. 452, 1933.

21. Neilsen, J. N.: Missile Aerodynamics. McGraw-Hill Book Company, 1960.

1 Report No.	2 Government Accession No	3 Recipient's Catalog No
NASA CR-3351		

4 Title and Subtitle	5 Report Date
A SYSTEM FOR AERODYNAMIC DESIGN AND ANALYSIS OF SUPERSONIC AIRCRAFT PART 1 - GENERAL DESCRIPTION AND THEORETICAL DEVELOPMENT	December 1980
	6 Performing Organization Code

7 Author(s)	8 Performing Organization Report No
W. D. Middleton and J. L. Lundry	D6-41840-1
	10 Work Unit No

9 Performing Organization Name and Address	11 Contract or Grant No
Boeing Commercial Airplane Company P.O. Box 3707 Seattle, Washington 98124	NAS1-15534

12 Sponsoring Agency Name and Address	13 Type of Report and Period Covered
National Aeronautics and Space Administration Washington, DC 20546	Contractor Report September 1978-August 1980
	14 Sponsoring Agency Code

15 Supplementary Notes

Langley Technical Monitor: B. L. Shrout
Part 1 of final report

16 Abstract

An integrated system of computer programs has been developed for the design and analysis of supersonic configurations. The system uses linearized theory methods for the calculation of surface pressures and supersonic area rule concepts in combination with linearized theory for calculation of aerodynamic force coefficients. Interactive graphics are optional at the user's request.

The description of the design and analysis system is broken into four parts, covered in four separate documents:

Part 1 - General Description and Theoretical Development (NASA CR-3351)
Part 2 - User's Manual (NASA CR-3352)
Part 3 - Computer Program Description (NASA CR-3353)
Part 4 - Test Cases (NASA CR-3354).

This part contains a general description of the program and a description of the theory used.

These four documents supersede NASA contractor reports CR-2715, CR-2716, and CR-2717, which described an earlier version of the system.

17 Key Words (Suggested by Author(s))	18 Distribution Statement
Wing design Configuration analysis Wave drag Pressure distribution	Unclassified - Unlimited Subject Category 02

19 Security Classif. (of this report)	20 Security Classif. (of this page)	21 No. of Pages	22 Price
Unclassified	Unclassified	100	A05

For sale by the National Technical Information Service, Springfield, Virginia 22161

NASA-Langley, 1980

END

March 2, 1981